DISSERTATION

ENGINEERING NANOSTRUCTURED POLYSACCHARIDE-BASED POLYELECTROLYTE COMPLEXES

Submitted by

Soheil Boddohi

Department of Chemical and Biological Engineering

In Partial Fulfillment of the Requirements

For the Degree of Doctor of Philosophy

Colorado State University

Fort Collins, Colorado

Fall 2009

COLORADO STATE UNIVERSITY

November 6, 2009

WE HEREBY RECOMMEND THAT THE DISSERTATION PREPARED UNDER OUR SUPERVISION BY SOHEIL BODDOHI ENTITLED "ENGINEERING NANOSTRUCTURED POLYSACCHARIDE-BASED POLYELECTROLYTE COMPLEXES" BE ACCEPTED AS FULFILLING IN PART REQUIRMENTS FOR THE DEGREE OF DOCTOR OF PHILOSOPHY.

Committee on Graduate Work

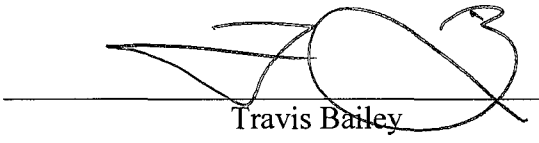

Travis Bailey

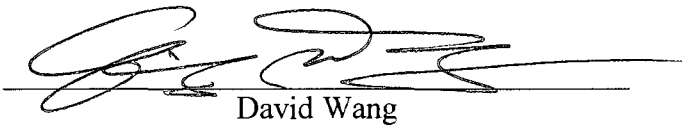

David Wang

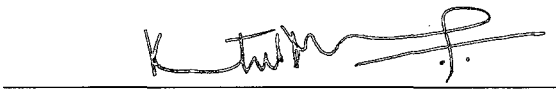

Ketul Popat

Adviser: Matt J. Kipper

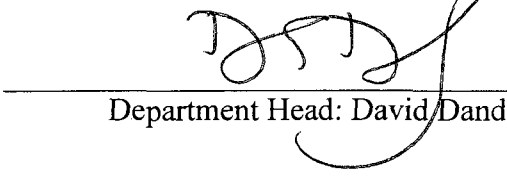

Department Head: David Dandy

ABSTRACT OF DISSERTATION

ENGINEERING NANOSTRUCTURED POLYSACCHARIDE-BASED POLYELECTROLYTE COMPLEXES

The overall goal of this dissertation is to demonstrate how the structure and composition of polysaccharide-based materials might be tuned at the nanometer length scale. Nanostructured biomaterials are promising candidates for biomedical engineering applications. Among all biomaterials, polysaccharides have shown great potential because of their many biochemical functions and their complex nanoscale structure in biological contexts. The nanoscale structure of polysaccharides is an important property that controls their biochemical and biological functions, in a variety of tissues. Therefore, in this dissertation, the nanoscale assembly of polysaccharides-based polyelectrolytes using polyelectrolyte multilayers (PEMs), polyelectrolyte complex nanoparticles (PCNs), and combinations of these two nanostructures was investigated. These new nanostructured surface coatings are being further developed by the Kipper research group as means of stabilizing and delivering therapeutic proteins, and as bioactive surface coatings for stem cell engineering. Thus the ability to tune their structure and composition is an important contribution of the current work.

The polysaccharides used in this work were chitosan, heparin, and hyaluronan. These three polysaccharides are biodegradable, biocompatible, and non-toxic. Chitosan, a weak polycation, has shown great potential in biomedical applications. Chitosan carries amine groups, and its charge density is determined by the protonation of the amine groups in

aqueous solutions. Heparin and hyaluronan are glycosaminoglycans (GAGs), and they are polyelectrolytes, carrying sulfate and carboxylate anionic substituents. They have been used in a variety of biomedical applications ranging from drug delivery to cell and tissue engineering. In this work, different nanostructured features have been fabricated and characterized based on these three polysaccharides. This work demonstrates the ability to tune the structure and composition of polysaccharide assemblies at the nanoscale by controlling the conditions under which the polyelectrolytes are complexed.

The formation of PEMs using these polylelectrolytes was studied via *in situ* Fourier-transform surface plasmon resonance (FT-SPR). Multilayer assembly was characterized as a function of both pH and ionic strength of buffer both with *in situ* and *ex situ* techniques. Both chitosan-heparin and chitosan-hyaluronan multilayers were electrostatically deposited on a gold surfaces for up to ten layers. X-ray photoelectron spectroscopy (XPS) and polarization-modulation infra-red reflection absorption spectroscopy (PM-IRRAS) were used to characterize the chemistry and composition of the multilayer thin films.

The physical properties of chitosan, heparin, and hyaluronan in solution at different pH and ionic strength of buffer were also characterized and discussed in this work. The conformation in solution for these three polyelectrolytes was studied using gel permeation chromatography. Molecular weight distribution, hydrodynamic radius, Mark-Houwink parameters, and intrinsic viscosity were measured for each macromolecule.

The formation of PCNs using these three polyelectrolytes was also investigated in this work. PCNs have shown promising potential for the stabilization and delivery of several therapeutic agents, and have also been used in tissue engineering studies. A procedure

was developed to form nanoparticles using chitosan, heparin, and hyaluronan. PCNs were complexed by combining polyelectrolyte solutions at different charge mixing ratios to promote the complexation of oppositely charged polyelectrolytes in solution. The size distributions and compositions of PCNs can be altered by changing the charge mixing ratios of the two constituent polyelectrolytes. Positively charged PCNs contain chitosan in excess, and negatively charged PCNs have either heparin or hyaluronan in excess. Formation of PCNs was best accomplished by one-shot addition of polyelectrolytes in pH 5.0, 0.1 M buffer. The variations in PCN size, zeta potential, and morphology with charge mixing ratio were studied for both positively charged and negatively charged PCNs made from each of the two polyelectrolyte combinations.

Finally, this work describes how PCNs can be combined with PEMs by electrostatically adsorbing PCNs during PEM deposition. The topography and composition of these polysaccharide-based, PCN-containing, PEM surface coatings can be tuned at the nanoscale. PCNs were adsorbed to oppositely charged PEMs, and were also embedded within PEMs. Nanostructured surface coatings were characterized on both modified gold substrates and tissue-culture polystyrene surfaces. The formation of these surface coatings was monitored by *in situ* quartz crystal microbalance with dissipation experiments. Surface topography was characterized by scanning electron microscopy and atomic force microscopy. Surface chemistry was confirmed by both PM-IRRAS and XPS. We demonstrate that PEM thickness can be controlled with nanometer resolution by altering the deposition conditions (buffer pH, molarity, number of layers). We demonstrate that PCNs were colloidally stable and homogeneously distributed when adsorbed on or in the PEMs. The combination of PCNs and PEMs can be used to tune the

nanoscale topographical features and composition of polysaccharide-based ultra thin films.

Soheil Boddohi
Department of Chemical and Biological Engineering
Colorado State University
Fort Collins, CO, 80523
Fall 2009

ACKNOWLEDGEMENTS

I would like to acknowledge my advisor Dr. Matt J. Kipper and my committee members Dr. Travis Bailey, Dr. David Wang, and Dr. Ketul Popat for their support and friendship, and all experiences and knowledge acquired during my Ph.D. work at Colorado State University. I also like to give special thanks to my great advisor, Dr. Matt J. Kipper, for his eternal help, patience, and support from the beginning of my graduate work at Colorado State University. He educated me with his limitless source of information and knowledge. It has been an honor to work with him.

I would also like to thank Dr. Sandeep Kohli and Dr. Patrick McCurdy in Central Instrumentation Facilities (CIF) at Colorado State University who patiently and eagerly trained me on many instruments. I would also like to thank Dr. Patrick Johnson at University of Wyoming and Dr. Ellen Fisher, Dr. Nancy Levinger, and Dr. Amy Prieto at Colorado State University for giving me this opportunity to use their instruments during my graduate work.

I would like to thank Clair Lavelle and Marilyn Gross for their patience and making sure that all of my paper works have been accurately done on time. I would also like to thank all members of Dr. Kipper's group, for their assistance and patience during these years of my graduate work.

Finally, I would like to give very special thanks to my parents and my sister who encouraged and bared with me through every step of my education. I would also like to thank my father for his great support and guidance through every step of my life. I would also like to thank my mother, who always scarified best of everything for me. At last, I would like to thank my sister for her infinite support and kindness.

Table of Contents

List of Figures

List of Tables

Chapter 1

Introduction and Objectives

1.1 Why Engineering Nanostructured Materials?

For several years, engineers have been trying to develop polymeric materials to mimic the biochemical and biomechanical properties of human tissue under physiological conditions. The combination of nanotechnology and biotechnology creates a wealth of opportunities for materials scientists to engineer biomaterials that mimic the structure and function of biological tissues. Biological tissues are composed of a complex mixture of materials (including proteins, polysaccharides, and small molecular weight molecules) that are organized at a variety of length scales, including the nanometer length scale. It is the hierarchical organization of materials that provides the foundation for the biochemical and biomechanical function of tissues. For example proteoglycans, which are proteins containing negatively charged glycosaminoglycans (GAG), are found in connective tissues. They exhibit complex nanostructure and participate in organizing other materials at nanoscale in extracellular matrices.

In order to exploit their nanoscale structure and their potential for future biomedical applications, characterization of the physical and chemical properties of the nanoscale biologically-derived polymers is required. The ability to control their assembly at the nanometer length scale will provide new platforms for evaluating biological responses to engineered nanostructures. Engineering size, composition, and morphology of polymers

at the nanometer length scale can be a novel approach to designing functional biomaterials.[1-3]

1.1.1 Polysaccharides and Polysaccharide-Based Polyelectrolytes

Polysaccharides are polymeric carbohydrates, many of which exhibit specific biochemical and biomechanical functions.[4] In their biological contexts, many polysaccharides are organized at the nanometer length scale, and this organization is an essential determinant of their biological functions.[4, 5] Among all polysaccharides, GAGs are becoming increasingly important in biologically relevant applications. They have a rich biochemistry, which includes the ability to specifically bind and activate growth factors, enzymes, and other members of the extracellular matrix.[6] GAGs have become target molecules for development of new therapies ranging from vaccines to cancer treatment.[5]

Many biologically derived polysaccharides are also polyelectrolytes. Polyelectrolytes are polymers that carry electrolyte residues on their repeating units. They can be positively charged polyions, such as chitosan, which has amino groups, or negatively charged polyions such as heparin and hyaluronan, which carry sulfate and carboxylate groups respectively. Polysaccharide-based polyelectrolytes, which are generally biologically derived, have shown promise in applications ranging from drug delivery to tissue engineering.[4, 5, 7, 8] In order to tune the biological functions of these materials, their polyelectrolyte nature can be used to control electrostatic interactions between charged residues, resulting in the formation of nanoscale complexes of two oppositely charged

macromolecules. This electrostatic complexation can then be controlled to develop nanoscale polysaccharide-based assemblies.

1.1.2 Polyelectrolytes Used in this Work

In this chapter, a brief overview of the polysaccharides used for rest of the dissertation is given. A more detailed discussion of their physical chemistry and biological function is provided in Chapter 2. These polysaccharides are shown in Figure 1.1.

The polycation chitosan (Figure 1.1a) is mainly produced from partial *N*-deacetylation of chitin. The main structural parameter of chitosan is the degree of acetylation (DA). Chitosan has a pKa of 6.46 to 7.32 and it is insoluble in most solvents but is soluble in aqueous weak organic acids such as acetic acid.[9] Chitosan has some outstanding biological properties such as antimicrobial activity, biodegradability and biocompatibility for tissue culture applications. Chitosan promotes cell adhesion and migration.[10, 11] Chitosan has also been shown to be a good candidate for biological applications such as drug delivery[12], tissue engineering[13, 14], and cell adhesion[15].

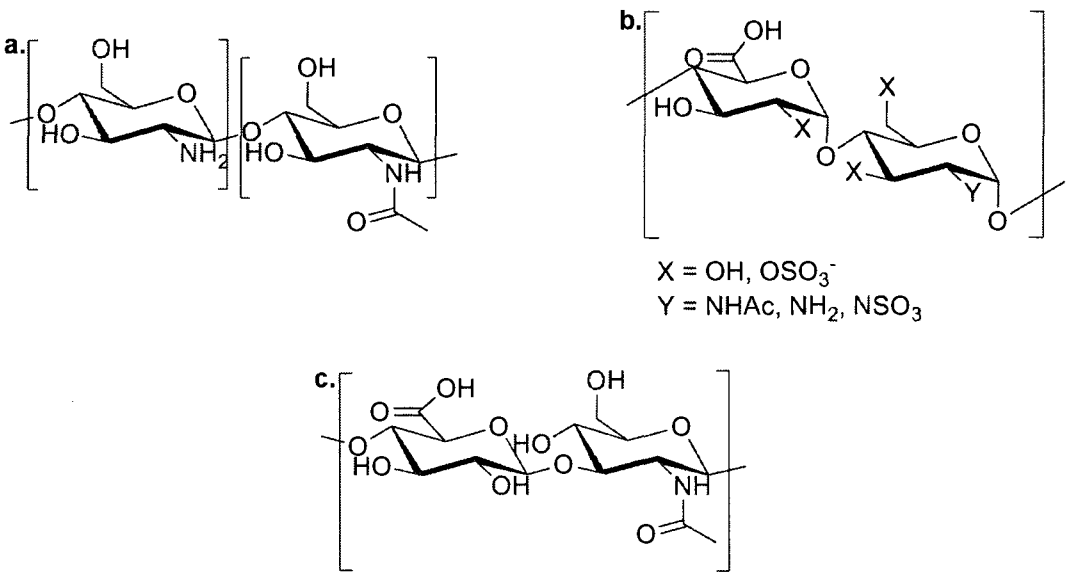

Figure 1.1. Chemical structure of chitosan (a), heparin (b), and hyaluronan (c).

Heparin (Figure 1.1b) is a biologically derived polyanion, which has the highest negative charge density among all biological polyanions.[6] Heparin has an average molecular weight of 12 to 15 kDa. Heparin has been used in the clinic as an antithrombotic, anti-adhesive, and anticoagulant agent.[16, 17 18] Heparin has the ability to bind to different proteins such as enzymes, growth factors, and extra cellular matrix proteins.[19] Heparin can activate many growth factors such as fibroblast growth factors (FGF) and some members of the transforming growth factor beta superfamily (TGFβ).[20-22] TGFβ growth factors can control proliferation and differentiation of different cell types including endothelial cells, fibroblasts, vascular smooth muscle cells, and epithelial cells.[22-24] Heparin is also structurally similar to the other sulfated glycosaminoglycans. It is therefore a good model for other biologically active polysaccharides.

Hyaluronan (Figure 1.1c) is a non-sulfated glycosaminoglycan that behaves as a weak polyanion. It is composed of alternating D-glucuronic acid and *N* acetyl-D-glucosamine residues. It carries one carboxylate group per disaccharide, with a pKa of 2.9. The average molecular weight of hyaluronan is 10 to 10000 kDa.[25] Hyaluronan is found in many skeletal and connective tissues. Hyaluronan has been shown to be effective at promoting cell migration and proliferation.[26, 27]

1.2 Research Objectives

As mentioned earlier, the overall goal of this dissertation is to demonstrate how the structure and composition of polysaccharide-based materials might be tuned at the nanometer length scale. The polyelectrolyte nature of polysaccharides is used to assemble new materials with nano architecture for biomedical engineering applications. To achieve this goal, the relationships between polysaccharides' physical chemistry and self assembly must be studied to develop new polysaccharide-based nanostructured bioactive materials.

The overall goal of this dissertation is achieved by the following objectives:

Objective 1. Engineer polysaccahride-based polyelectrolyte multilayers (PEMs) using chitosan, heparin, and hyaluronan by varying the processing conditions.

Objective 2. Experimental investigation of the solution behavior of polysaccharides.

Objective 3. Develop a method to make polysaccharide-based polyelectrolyte complex nanoparticles (PCNs) at different charge mixing ratios with two different polycation-polyanion pairs: chitosan-heparin (chi-hep) and chitosan-hyaluronan (chi-ha).

Objective 4. Tailor morphology and composition of different surface coatings using PEMs and PCNs.

1.3 Organization of the Dissertation

Chapter 2 is a review describing the current state of engineering nanoassemblies of polysaccharides, with a focus on tailoring their properties for biomedical applications. In this chapter, several relevant polysaccharides are discussed, and their unique properties for biochemical and biomedical applications are introduced. An important group of polysaccharides called GAGs is highlighted, and their potential application as nanoscale biomaterials is discussed. This chapter also focuses on the use of the polyelectrolyte nature of polysaccharides as a powerful tool to control their nanoscale assembly. Specifically, PEMs, PCNs, nanofibers, and complex combinations of these structures is reviewed. Finally, this chapter provides some perspectives on the application of these polysaccharide based nanomaterials for biomedical applications such as drug delivery and tissue engineering.

In Chapter 3, the complexation of the chi-hep polycation-polyanion pair at surfaces is studied. Ten-layer PEMs were assembled at different values of pH and ionic strength of the buffer solution. *In situ* Fourier-transform surface plasmon resonance (FT-SPR) was used to monitor PEM formation. The novel contribution of this chapter is a detailed understanding of the physical chemistry of these PEMs, provided by a detailed study of the PEM formation under different conditions. PEM thickness and refractive index of chi-hep system were measured *ex situ* by spectroscopy ellipsometry. Ellipsometry is a sensitive optical technique for determining properties of surfaces and thin films. Surface

chemistry and composition of the PEMs were evaluated with polarization modulation infra-red reflection absorption spectroscopy (PM-IRRAS) and X-ray photoelectron spectroscopy (XPS). Results are completely interpreted in this chapter.

Characterization of the polyelectrolytes in solution is presented in Chapter 4. The goal here was to discern how the solution conditions affect the conformation of chitosan, heparin, and hayluronan in solution as the solution properties may affect the formation of interpolyelectrolyte complexes at surfaces. The results obtained are related to the final properties of the polyelectrolyte multilayer surface coatings obtained for the chi-hep system (reported in Chapter 3) and the chi-ha system (reported in Chapter 4). To achieve this goal, gel permeation chromatography (GPC) coupled with laser light scattering and viscometry instruments was used to measure the molecular weight distributions and the intrinsic viscosity and hydrodynamic radii of each of the polyelectrolytes under different solution conditions. These results are reported in Chapter 4.

Under the appropriate conditions, oppositely charged polyelectrolyte pairs can complex in solution to form nanoparticles. In Chapter 5, the formation of chi-hep and chi-ha PCNs is described. A reproducible procedure was developed for the complexation of these polyelectrolytes at different charge mixing ratios. This work demonstrates that control over the size distribution and composition of the PCNs can be obtained by altering the charge mixing ratios. PCNs were all characterized by dynamic light scattering (DLS) to obtain their hydrodynamic radii. Stability of the PCNs was also evaluated by zeta potential measurements, and results are interpreted in detail in Chapter 5. The morphology of the particles adsorbed to surfaces was also investigated by scanning electron microscopy (SEM). SEM confirmed that particles can be adsorbed

discretely or aggregated depending upon the stability and composition of the particles. Since particles were deposited on uncharged surface, they did not homogeneously cover the surface in all conditions.

Finally Chapter 6 demonstrates one method whereby a combination of different types of polyelectrolyte complexation can be used to make more complex nanoscale assemblies. Here, chi-haPEMs are combined with chi-hep PCNs on both gold and polystyrene surfaces. Eight different types of surface coatings were characterized by quartz crystal microbalance with dissipation (QCM-D). Six-layer and seven-layer (negatively charged and positively charged) multilayers with like-charged PCNs adsorbed, multilayers with oppositely charged PCNs adsorbed, and PEMs with PCNs incorporated as sub-terminal layers are all characterized. The morphology of the PCN-containing PEMs was also investigated by SEM and atomic force microscopy (AFM). Results confirm that PCNs can adsorb to charged surfaces discretely and homogeneously even as a sub-terminal layer. Composition of the PEM-PCN systems was also analyzed by XPS, and results confirm that morphological features observed in AFM and SEM correspond to adsorption of the PCNs.

In Chapter 7, it is concluded that engineering these nanoscale surface coatings can lead to better control over composition, morphology, and size of the nanoscale features. These nanostructured polymers have a potential to be used in biochemical and biomedical applications. The work presented in this dissertation enables the tuning of nanoscale features of polysaccharide-based surface coatings. This will enable the biological activities of these materials that arise from their nanoscale organization to be tuned. Future work with these materials will include the study of protein adsorption and stability

on different surfaces and investigation of mammalian cell responses to different types nanostructures. It is hypothesized that cells will respond differently based on the nanoscale organization of the biochemical moieties, such as encapsulated proteins and the polysaccharides that bind them.

1.4 References

1. Couchman, J. R., Syndecans: Proteoglycan regulators of cell-surface microdomains? *Nature Reviews Molecular Cell Biology* **2003,** 4, (12), 926-937.
2. Nakato, H.; Kimata, K., Heparan sulfate fine structure and specificity of proteoglycan functions. *Biochimica Et Biophysica Acta-General Subjects* **2002,** 1573, (3), 312-318.
3. Lin, X. H.; Perrimon, N. In *Role of heparan sulfate proteoglycans in cell-cell signaling in Drosophila*, 2000; 2000; pp 303-307.
4. Suh, J. K. F.; Matthew, H. W. T., Application of chitosan-based polysaccharide biomaterials in cartilage tissue engineering: a review. *Biomaterials* **2000,** 21, (24), 2589-2598.
5. Dove, A., The bittersweet promise of glycobiology. *Nature Biotechnology* **2001,** 19, (10), 913-917.
6. Salmivirta, M.; Lidholt, K.; Lindahl, U., Heparin sulfate: A piece of information. *Faseb Journal* **1996,** 10, (11), 1270-1279.
7. Janes, K. A.; Fresneau, M. P.; Marazuela, A.; Fabra, A.; Alonso, M. J., Chitosan nanoparticles as delivery systems for doxorubicin. *Journal of Controlled Release* **2001,** 73, (2-3), 255-267.
8. Janes, K. A.; Calvo, P.; Alonso, M. J., Polysaccharide colloidal particles as delivery systems for macromolecules. *Advanced Drug Delivery Reviews* **2001,** 47, (1), 83-97.
9. Sorlier, P.; Denuziere, A.; Viton, C.; Domard, A., Relation between the degree of acetylation and the electrostatic properties of chitin and chitosan. *Biomacromolecules* **2001,** 2, (3), 765-772.
10. Rabea, E. I.; Badawy, M. E. T.; Stevens, C. V.; Smagghe, G.; Steurbaut, W., Chitosan as antimicrobial agent: Applications and mode of action. *Biomacromolecules* **2003,** 4, (6), 1457-1465.
11. Li, J. L.; Pan, J. L.; Zhang, L. G.; Guo, X. J.; Yu, Y. T., Culture of primary rat hepatocytes within porous chitosan scaffolds. *Journal of Biomedical Materials Research Part A* **2003,** 67A, (3), 938-943.
12. Sashiwa, H.; Aiba, S. I., Chemically modified chitin and chitosan as biomaterials. *Progress in Polymer Science* **2004,** 29, (9), 887-908.
13. Gingras, M.; Paradis, I.; Berthod, F., Nerve regeneration in a collagen-chitosan tissue-engineered skin transplanted on nude mice. *Biomaterials* **2003,** 24, (9), 1653-1661.
14. Wang, Y. C.; Lin, M. C.; Wang, D. M.; Hsieh, H. J., Fabrication of a novel porous PGA-chitosan hybrid matrix for tissue engineering. *Biomaterials* **2003,** 24, (6), 1047-1057.
15. Mao, J. S.; Liu, H. F.; Yin, Y. J.; Yao, K. D., The properties of chitosan-gelatin membranes and scaffolds modified with hyaluronic acid by different methods. *Biomaterials* **2003,** 24, (9), 1621-1629.
16. Rusnati, M.; Oreste, P.; Zoppetti, G.; Presta, M., Biotechnological engineering of heparin/heparan sulphate: A novel area of multi-target drug discovery. *Current Pharmaceutical Design* **2005,** 11, (19), 2489-2499.
17. Fu, J. H.; Ji, J.; Yuan, W. Y.; Shen, J. C., Construction of anti-adhesive and antibacterial multilayer films via layer-by-layer assembly of heparin and chitosan. *Biomaterials* **2005,** 26, (33), 6684-6692.

18. Liu, J.; Pedersen, L. C., Anticoagulant heparan sulfate: structural specificity and biosynthesis. *Applied Microbiology and Biotechnology* **2007,** 74, (2), 263-272.
19. Borset, M.; Hjertner, O.; Yaccoby, S.; Epstein, J.; Sanderson, R. D., Syndecan-1 is targeted to the uropods of polarized myeloma cells where it promotes adhesion and sequesters heparin-binding proteins. *Blood* **2000,** 96, (7), 2528-2536.
20. Guimond, S.; Maccarana, M.; Olwin, B. B.; Lindahl, U.; Rapraeger, A. C., Activating and inhibitory heparin sequences for FGF-2 (basic FGF) - distinct requirements for FGF-1, FGF-2, and FGF-4. *Journal of Biological Chemistry* **1993,** 268, (32), 23906-23914.
21. Loo, B. M.; Kreuger, J.; Jalkanen, M.; Lindahl, U.; Salmivirta, M., Binding of heparin/heparan sulfate to fibroblast growth factor receptor 4. *Journal of Biological Chemistry* **2001,** 276, (20), 16868-16876.
22. Rider, C. C. In *Heparin/heparan sulphate binding in the TGF-beta cytokine superfamily*, 2006; 2006; pp 458-460.
23. Chen, X. L.; Chen, Z. S.; Ding, Z.; Dong, C.; Guo, H.; Gong, N. Q., Antisense extracellular signal-regulated kinase-2 gene therapy inhibits platelet-derived growth factor-induced proliferation, migration and transforming growth factor-beta(1) expression in vascular smooth muscle cells and attenuates transplant vasculopathy. *Transplant International* **2008,** 21, (1), 30-38.
24. Oberringer, M.; Meins, C.; Bubel, M.; Pohlemann, T., In vitro wounding: effects of hypoxia and transforming growth factor beta(1) on proliferation, migration and myofibroblastic differentiation in an endothelial cell-fibroblast co-culture model. *Journal of Molecular Histology* **2008,** 39, (1), 37-47.
25. Lapcik, L.; De Smedt, S.; Demeester, J.; Chabrecek, P., Hyaluronan: Preparation, structure, properties, and applications. *Chemical Reviews* **1998,** 98, (8), 2663-2684.
26. Huang, L.; Cheng, Y. Y.; Koo, P. L.; Lee, K. M.; Qin, L.; Cheng, J. C. Y.; Kumta, S. M., The effect of hyaluronan on osteoblast proliferation and differentiation in rat calvarial-derived cell cultures. *Journal of Biomedical Materials Research Part A* **2003,** 66A, (4), 880-884.
27. Goueffic, Y.; Guilluy, C.; Guerin, P.; Patra, P.; Pacaud, P.; Loirand, G., Hyaluronan induces vascular smooth muscle cell migration through RHAMM-mediated PI3K-dependent Rac activation. *Cardiovascular Research* **2006,** 72, (2), 339-348.

Chapter 2

Engineering Nanoassemblies of Polysaccharides

- **S. Boddohi**, M.J. Kipper,"Engineering nanoassembly of polysaccharides." *Advanced Materials*, 2009 (submitted).

2.1 Introduction

Polysaccharides are a class of biological macromolecules that play important roles in a vast repertoire of biochemical and biomechanical functions. Glycomics, which is the study of structure-function relationships of complex carbohydrates, is an emerging field that is recently producing a wealth of knowledge about the activity of this important class of biological macromolecules. This presents an opportunity for engineers and materials scientists developing biomaterials to capitalize on, by incorporating these carbohydrate chemistries into biologically active materials. Thus, saccharide-based chemistries have attracted the attention of biomaterials researchers as a class of materials with enormous potential in diverse areas including protein interactions, cell and tissue engineering, vaccine delivery, and cancer treatment.[2-5] Furthermore, in their native biological contexts, many polysaccharides are found organized into complex assemblies with nanoscale structures (e.g. virus capsids, bacterial cell walls, the eukaryotic cell glycocalyx, and extracellular structures such as the aggrecan aggregate in mammalian tissues). For example, Figure 2.1 shows a transmission electron micrograph of the endothelial glycocalyx from a normal blood vessel, and an atomic force micrograph of the

proteoglycan aggrecan. Both of these represent biological assemblies of polysaccharides with nanoscale organization that determines their biochemical and biomechanical function. Thus, in order to realize their full biochemical and biomechanical potential, biomaterials scientists are exploring ways to engineer polysaccharide nanostructure.

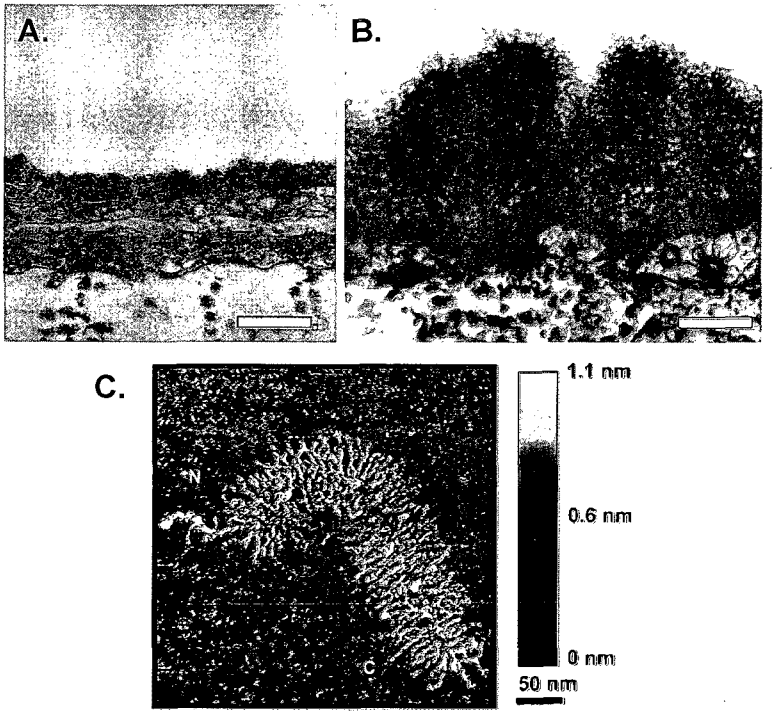

Figure 2.1. Micrographs of biologically derived polysaccharide nanoassemblies. Normal vessel (A), whereas (B) has been subjected to mild thermal injury and has become inflamed. Both micrographs show the lumen (top), glycocalyx (centrally placed), endothelial cells (below the glycocalyx), and the collagenous extracellular matrix (lower area). Scale bars are 180 nm in both (A) and (B). Reprinted from Journal of Structural Biology, 136, J. M. Squire *et al.*, Quasi-Periodic Substructure in the Microvessel Endothelial Glycocalyx: A Possible Explanation for Molecular Filtering, 239-255, copyright (2003), with permission from Elsevier. High resolution AFM image of fetal epiphyseal aggrecan (C). Scale bar is 50 nm. Reprinted from Journal of Structural Biology, 143, L. Ng, *et al.*, Individual Cartilage Aggrecan Macromolecules and their Constituent Glycosaminoglycans Visualized via Atomic Force Microscopy, 242-257, copyright (2003), with permission from Elsevier.

This review briefly summarizes the structure and function of polysaccharides commonly used in biomaterials, then discusses recent advances in engineering their nanoscale assembly for biomedical materials. The references cited in this review are selected for those interested in both the physical chemistry and nanoscale assembly of polysaccharides, and in how polysaccharide nanostructures can be used to tune the response of biological systems (e.g. cells and tissues) to these materials.

2.2 Polysaccharides Used as Biomaterials

Among the several classes of polymeric materials that have become important tools for the biomaterials scientist, polysaccharides possess unique properties that have recently been used in drug delivery (including the delivery of genes and therapeutic proteins), as scaffold materials for cell and tissue engineering studies, and as coatings for implants and prostheses.[6-12] At the molecular level, polysaccharides are unique from both synthetic polymers and other biologically derived polymers. While synthetic polymers are generally composed of a single monomer or a small number of monomers, some polysaccharides contain a much larger number of monomer chemistries. Several common pendent groups, multiple valency of monomers, and the steriospecificity of the glycosidic bonds linking them all contribute to polysaccharide sequence variability. Furthermore, their biological synthesis can result in a heterogenous mixture of sequences. This is illustrated by the complex mechanism of heparan sulfate biosynthesis, which is a combination of sequential and simultaneous statistical steps.[13, 14] This is far different from the prescribed, template-driven process that guides the synthesis of other biological polymers, like protein and DNA. Thus, a single polysaccharide may perform many

sequence-dependent biochemical functions by possessing a diversity of biochemically active sequences. This is both a blessing and a curse for the biomaterials scientist. Biomaterials scientists can benefit from the ability to introduce multiple biochemical functions with the use of a single polymer. However, this may be done at the expense of precise control over the degree to which a particular functional group will be introduced and even which additional functionalities may be introduced in the process.

To overcome this challenge and to advance the development of tools for glycomics research, significant efforts have been extended toward the production of defined saccharide sequences. The synthesis of defined polysaccharide sequences is difficult because of the multiple valency of the monomer groups and the chirality of the glycosidic linkages between them. The challenges associated with the synthesis of defined saccharide sequences and advances in synthetic sterioselective chemistries and protection strategies have been recently reviewed by Seeberger.[15] Enzymatic synthesis has also been developed for the controlled polymerization of polysaccharides.[16] However, for the present, the vast majority of research in the application of polysaccharides in biomaterials relies on polysaccharides produced by microbes or derived from animal tissues, which are harvested, purified, and in some cases, chemically modified. These naturally derived polysaccharides generally contain the full range of biological functionality (whether they be known or unknown) exhibited by the polysaccharides in their native contexts.

2.2.1 Glycosaminoglycans

The most important polysaccharides in mammalian tissues are the glycosaminoglycans (GAGs). These include chondroitin sulfate, dermatan sulfate,

keratan sulfate, heparan sulfate, heparin, and hyaluronan.[17] The GAGs are all based on disaccharide repeating units containing a hexuronic acid (or a hexose in the case of keratan sulfate) and a hexoseamine. The basic structures are shown in Table 2.1. All of the GAGs are polyelectrolytes, containing functional groups including carboxylate, amino, sulfate, and *N*-sulfonate substituents. GAGs are usually fully charged polyanions at physiological conditions.[18] Thus electrostatic interactions are important for determining both their physical chemistry and their biochemical function. In the tissues in which they are found, these polysaccharides have important biochemical and biomechanical function. They also serve to regulate the nanoscale organization of other components of the extracellular matrix (ECM).

Table 2.1. Chemical structure glycosaminoglycans discussed in this review.

Glycosaminoglycan	Chemical structures
Heparin and Heparan sulfate	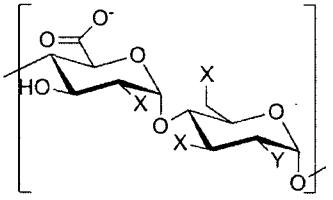 X = OH, OSO_3^- Y = NHAc, NH_2, $NHSO_3^-$
Hyaluronan	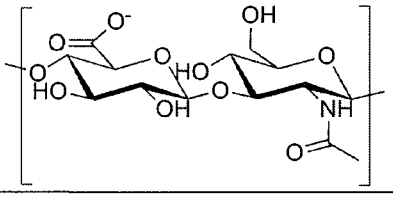
Chondroitin 4-sulfate	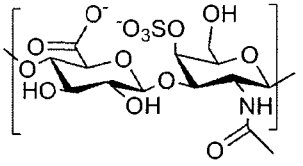
Chondroitin 6- sulfate	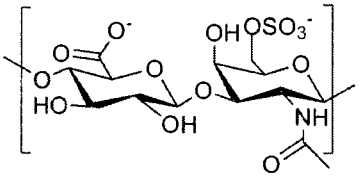
Keratan sulfate	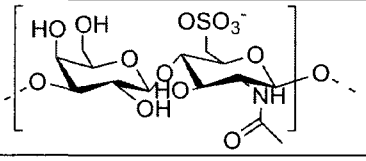
Dermatan sulfate	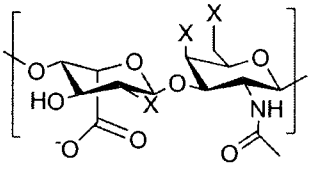 X=OH, OSO_3^-

The sulfated GAGs (chondroitin sulfate, dermatan sulfate, karatan sulfate, heparan sulfate, and heparin) have high sequence variability that enables them to bind many proteins[19] with varying levels of specificity or promiscuity. These include growth factors,

growth factor receptors, chemokines, enzymes, enzyme inhibitors, and other structural components of the extracellular matrix, such as collagen.[14, 20-22] The biochemical diversity confers function in several physiological phenomena including cell migration, morphogenesis, and differentiation,[19] which might be exploited for biomedical applications such as tissue engineering.

Chondroitin sulfate is the most prevalent glycosaminoglycan, found in the glycocalyx (the polysaccharide coating on all eukaryotic cells) and the extracellular matrix (ECM) in tissues including those of the central nervous system,[23] skeletal system,[6, 24] and connective tissues.[25] Chondroitin sulfate can bind and activate growth factors such as basic fibroblast growth factor (FGF-2)[26], FGF-7[21], platelet-derived growth factor (PDGF),[27, 28] and transforming growth factor β1 (TGFβ-1).[29] Chondroitin sulfate also binds the important fibrillar forms of collagen I and II altering the fibrillogenesis process.[20] The structurally similar GAG dermatan sulfate is important in blood vessels, where it binds strongly to heparin cofactor II in a mechanism that inhibits the blood coagulation cascade.[21] Dermatan sulfate is also found in skin. Keratan sulfate is found in the brain, cartilage, and cornea,[30] and has a higher variability of charge density than the other GAGs.[31]

Heparin is a GAG which behaves as a strong polyanion. In fact, heparin has the highest charge density of any biologically derived polyanion.[14] Heparin is normally found in intracellular granules, but is structurally similar to heparan sulfate, which is found in the glycocalyx and ECM of many tissues.[11, 14, 18, 32, 33] Heparan sulfate differs from heparin in that it has regions which are less sulfated. Heparin and heparan sulfate consist of at least ten different monosaccharide building blocks that can be combined into a large

number of different saccharide sequences.[34] They can interact with many proteins (termed "heparin binding proteins")[35] from different protein families. These include enzymes like thrombin and platelet factor 4,[14] growth factors, such as members of the FGF family and TGFβ superfamily, growth factor receptors, such as FGF receptor 4,[36] and ECM proteins, such as collagen, and lipid-binding proteins.[35, 37-39] Additionally, heparin binding can enhance the biological activity of growth factors[40], by stabilizing them with respect to degradation[41] and forming a ternary complex between heparin, the growth factor, and the growth factor receptor on a cell surface.[42] Heparin binding to members of the FGF family has been particularly well-studied. FGF-heparin binding occurs via a sequence of trisulfated disaccharide units but depends upon just a single O-sulfate group and one or two N-sulfate groups.[14] Transforming growth factor-betas (TGFβ) comprise another growth factor superfamily that binds to heparin and heparan sulfate. TGFβ growth factors control the proliferation, differentiation, and migration of many cell types. Rider and Lyon showed that not all members of the TGFβ superfamily can bind to heparin.[43, 44] Bone morphogenetic proteins (BMPs) are a group of growth factors belonging to TGFβ superfamily, and are important in regulating bone and cartilage anabolism and catabolism. BMP-2 and BMP-4 both have heparin binding sites.[45]

Hyaluronan is the only glycosaminoglycan that does not contain sulfate substituents. It is generally found in the ECM, with a relatively high molecular weight. But its molecular weight can range from 10 to 10000 kDa.[17] It has one carboxylic acid substituent per disaccharide repeat unit, making it a relatively weak polyanion with a pK_a near 2.9.[17] Hyaluronan forms aqueous solutions, behaving as a random coil polymer with

a very large hydrodynamic diameter. Hyaluronan binds some important proteoglycans that carry the sulfated GAGs,[23] and thus plays in important role in organizing the structure and composition of the ECM.[14] Hyaluronan also acts as the ligand for the cell surface receptor CD44.[46]

By binding these many different types of proteins via specific saccharide sequences GAGs activate or inhibit growth factors,[38, 47] act as ligands for cell surface receptors,[48] organize the ECM, and potentiate enzyme activity.[49-51] Potentiation of antithrombin III activity, for example, makes heparin useful as an anticoagulant.

2.2.2 Other Polysaccharides Used as Biomedical Materials

Some other polysaccharides that are important as biomedical materials are summarized in Table 2.2. These polymers have less complex sequence variability than the sulfated GAGs. Dextran is a water-soluble α-1,6 poly(glucose) containing α-1,4 branches, that is produced by some bacteria. This microbial polysaccharide has a molecular weight ranging from 10 kDa to 1000 kDa. Dextran is the only polysaccharide shown in Tables 2.1 and 2.2 that does not behave as a polyelectrolyte. Alginate is an anionic block copolymer of β-1,4 linked D-manuronic acid and α-1,4 linked L-guluronic acid, produced by algae. Thus it is a weak polyanion containing one carboxylate moiety per saccharide unit.

Chitin is a polysaccharide produced by arthropods and is a major byproduct of the shellfish industry. It is a copolymer of β-1,4 linked D-glucosamine and *N*-acetyl D-glucosamine, with a high degree of acetylation. Its high degree of acetylation makes it generally less water soluble than the other polysaccharides, though it is soluble in strong

acids. Chitosan is derived from the structurally similar polymer, chitin, by the partial *N*-deacetylation of the *N*-acetyl D-glucosamine residues. It therefore has the same basic structure as chitin, except for the ratio of the two monomers. Deacetylation improves the water solubility, making chitosan soluble in dilute organic acids like acetic acid and formic acid.[52] Chitosan has many properties that make it an attractive biomaterial. It is biodegradable, and its enzymatic degradation can be tuned by altering the degree of deacetylation.[53] Chitin and chitosan are the only two polysaccharides shown in Tables 2.1 and 2 that behave as polycations. Their polyelectrolyte properties enable them to interact with polyanions, including the GAGs, DNA, and RNA, leading to the formation of polyelectrolyte complexes.[54, 55] These complexes can then be used for the delivery of therapeutic agents.[10, 56]

Table 2.2. Polysaccharides from non-mammalian sources discussed in this review.

Polysaccharide	Chemical structure
Chitin and chitosan	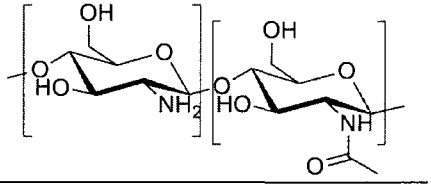
Alginate	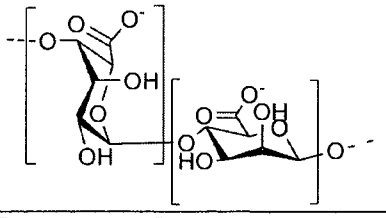
Dextran	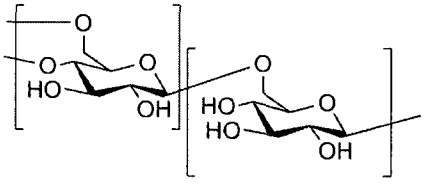

2.3 Biomedical Applications of Polysaccharides

Each of the polysaccharides introduced in the preceding section has been used as a biomedical material. Here we briefly review how the biochemistry of each of these polysaccharides has been exploited for biomedical applications.

The GAGs have been used extensively to modify surfaces for cell and tissue engineering and for blood-contacting materials.[57] Heparin has been used clinically for many years as an anticoagulant. Its anticoagulant activity also makes heparin a particularly promising candidate for use as a coating on materials to improve their hemocompatibility.[57] Heparin can also affect cell differentiation and migration by interacting with growth factors and their receptors.[36] Its ability to bind and activate growth factors involved in mesenchymal stem cell differentiation suggests that heparin would be a promising candidate for bone and cartilage tissue engineering. Kim *et al.* and Ito *et al.* showed that surface-bound heparin can influence platelet adhesion and activation.[58, 59] Bacterial adhesion has also been shown to be reduced by activating surfaces with heparin.[57] Hyaluronan and chondroitin sulfate have been used as coatings to reduce platelet adhesion in small diameter vascular grafts.[60] Hyaluronan has been used for some time as a surgical aid in ophthalmology and as a viscosupplement for the treatment of joint diseases.[61] Hyaluronan has also been used in pharmaceutical and tissue engineering applications. Introduction of sulfate groups into hyaluronan can impart similar heparin-like biochemical function into sulfated hyaluronan.[57, 62] Dextran has also been studied in various three-dimensional constructs, including hydrogels, for cell culture and tissue regeneration.[63, 64] Dextran hydrogels have been shown to be cytophilic with

respect to fibroblast cells.[64] Mehvar recently reviewed the use of different molecular weights of dextran for the delivery of therapeutic agents including drugs and proteins.[65] Alginate can readily form hydrogels by complexing with low molecular weight divalent cations. Alginate has been used in nanoparticles and hydrogels for protein and drug delivery applications. [66, 67] For example, it has been studied as a vehicle for growth factor delivery for vascular tissue engineering.[68] Alginate formulations have also been developed for encapsulation and delivery of cells.[69, 70]

Chitin is biodegradable, is generally considered to be non-toxic, and has demonstrated significant potential as a biomaterial for tissue engineering applications.[71-73] Similar to chitosan, chitin also has shown the ability to bind to some proteins and DNA.[74] Nanostructured chitin-based materials have been shown to promote the growth and differentiation of human cells.[75] Chitosan has been used in the formation of porous scaffolds for tissue engineering.[76] The structure and feature size of chitosan scaffolds can also influence the cell adhesion and response to materials. Chitosan supports the growth of a variety of types of mammalian cells.[6, 7, 76] It has shown promise for engineering a variety of tissues including blood vessels[77, 78], liver[79, 80], skin[81], bone[82-85], and cartilage.[6, 86, 87] Chitosan also exhibits antimicrobial activity.[54, 88] Antibacterial and antifungal activities have been demonstrated for films[89], coatings[90], fibers[7], hydrogels[91] and other composites containing chitosan[92].

Despite their being derived from non-mammalian sources, chitin and chitosan can have significant biochemical activity with respect to mammalian cells and tissues. Chitosan, for example, enhances the wound healing process and angiogenesis.[93] Chitosan can promote the migration of fibroblasts,[81, 94] via stimulation of growth factor (TGFβ-1,

PDGF[95]) and interleukin[93, 96] (leukotriene B_4, Il-1, and Il-8) production.[97] Muzzarelli recently reviewed the use of chitin and chitosan in wound healing applications.[98] This review describes several mechanisms whereby chitosan may modulate the production and activity of matrix metaloproteinases, which are key enzymes acting during inflammation, wound healing, and tumor metastasis.[98] In general, tissue healing near chitosan-based implants is characterized by initial inflammation with infiltration by neutrophils, followed by proliferation and a waning of the inflammation response, leading to good tissue integration and lack of chronic inflammation.[6] This biochemical activity of chitin and chitosan has lead to the success of a number of commercially available chitin-based and chitosan-based wound dressings.[98]

2.4 Biologically-Derived Nanoassemblies of Polysaccharides

Studies in structural biology have revealed that biological structures are characterized by the assembly of macromolecules at a hierarchy of length scales, and that this assembly is essential to the biological function of many tissues. In mammalian tissues, the sulfated glycosaminoglycans shown in Table 2.1 are most often found as proteoglycans – proteins modified with GAG side chains.[18] These proteoglycans impart their biochemical and biomechanical function to the tissues in which they are found. These functions include acting as cell surface receptors, guiding cell differentiation, mediating cell-cell signaling, and imparting mechanical strength to tissues.[11, 32, 99-104] Furthermore, they exhibit nanoscale organization and are also responsible for organizing other materials at the nanometer length scale in the ECM. This nanoscale assembly forms the foundation upon which additional assembly at larger length scales is also achieved. In the sections below,

we describe two important examples of the nanoscale assembly of polysaccharides and demonstrate how this nanoscale assembly influences their biochemical and biomechanical function.

2.4.1 The Glycocalyx

The glycocalyx is a biological nanoassembly that was first identified nearly a half century ago with electron microscopy.[105] The glycocalyx is a group of glycoproteins that are present on the surface of almost all eukaryotic cells. In transmission electron micrographs, the glycocalyx appears as a polymer brush structure (Figure 2.1A and 2.1B). The glycocalyx is particularly important in epithelia and endothelia, where it forms a nanostructured thin film that defines both the physical chemistry and the biochemistry of the surfaces.[106] One important function of the glycocalyx is to provide receptors for cell adhesion. For example, it is through the glycoproteins in the epithelial glycocalyx that the adhesion of platelets to damaged tissue is governed. In blood vessels the endothelial glycocalyx forms a nanostructured thin film lining the luminal surface. In blood vessels the glycocalyx defines the interactions of all blood components, including thrombocytes, with the blood vessel lumen, and is essential to preventing thrombosis. This endothelial glycocalyx consists primarily of heparan sulfate and hyluronan.[107]

The glycocalyx has been shown to play an important role in human pathophysiology. The nanoscale dimensions of this polysaccharide brush have been studied in detail to in order to evaluate its relation to risk factors for cardiovascular disease.[107, 108] The mean thickness of the vascular endothelial glycocalyx is in the range of 400 to 600 nm.[107, 109] Huxley *et al.* studied the dynamic properties of the glycocalyx in coronary arterioles in

the presence of different enzymes (pronase and heparinase), to determine how enzyme degradation of the glycocalyx influences the solute permeability and protein flux.[108] Henry *et al.* also studied the effect of hyaluronan removal from the endothelial surface to evaluate how its presence influences the permeability and structural properties of the glycocalyx.[110] Their results demonstrated that reduction of the glycocalyx density and thickness, by treatment with the hyaluronidase enzyme, increases the penetration of macromolecules into the glycocalyx.[110] These are examples of studies demonstrating that the nanoscale organization of the glycocalyx structure is clearly a significant determinant of tissue function. The glycocalyx also plays important roles in cell recognition and cell-cell communication both in eukaryotic and prokaryotic cells.[111]

2.4.2 Aggrecan and the Aggrecan Aggregate

Among the proteoglycans, aggrecan is the largest. Aggrecan is a protein that contains over 100 glycosaminoglycan side chains.[112, 113] In fact, the majority of the weight of aggrecan is the chondroitin sulfate, keratan sulfate, and oligosaccharide side chains, which are spaced only about 4 to 5 nm apart along the core protein. [33, 101, 113, 114] The strong electrostatic repulsion among the GAG chains causes aggrecan to adopt a bottle-brush structure. Ng *et al.* investigated individual cartilage aggrecan macromolecules in detail and reported the physical properties by atomic force microscopy.[115] Their characterization revealed that the contour length is in the range of 300-500 nm and varies depending upon the maturity of the source.[115] This structure is clearly seen in the atomic force micrograph shown in Figure 2.1C. The length of the individual GAG side chains attached to the core aggrecan protein was also measured, and ranges from 30-40 nm.

Aggrecan is classified as a hyaluronan-binding proteoglycan. In the ECM of articular cartilage, in the intervertebral disk, and in the vitreous humor of the eye, the proteoglycan aggrecan binds to hyaluronan, mediated by a binding protein, to form the aggrecan aggregate, illustrated schematically in Figure 2.2.[101, 113, 116] Each hyaluronan molecule can have over 100 aggrecan units bound to it, forming a densely packed, rod-like assembly with nanoscale structure.[117] The structure and dynamics of aggrecan and the aggrecan aggregate in solution have been studied in some detail by scattering and rheological techniques.[116, 118] Solutions of the aggrecan aggregate exhibit viscous, shear-thinning behavior.[116] At physiological concentrations (~ 5 wt %), aggrecan behaves as a concentrated solution, characterized by reptation, but not by entanglement of the stiff, side chain GAGs.[116] The aggrecan aggregate is extremely stiff, with a persistence length on the order of 100 nm.[116]

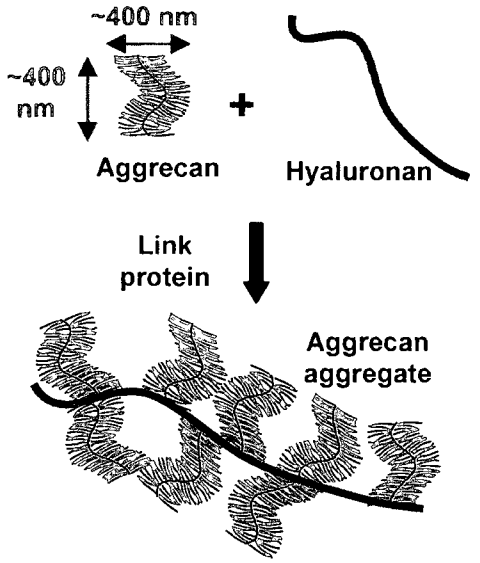

Figure 2.2. Schematic of the aggrecan aggregate showing that it is a nanostructured polysaccharide complex. The aggrecan core protein is represented in black, and the chondroitin sulfate and keratan sulfate chains are represented in red.

The biomechanics of aggrecan and the aggrecan aggregate has been the subject of extensive study by both experimental and computational approaches. [114, 119, 120 104, 121] The structure of the aggrecan aggregate confers a variety of unique properties to cartilage. The dense polyelectrolyte structure enables cartilage to maintain high water content (~70 %),[113, 117] imparting a relatively high compressive modulus[101, 118] (0.01 to 3.0 MPa[122]) and excellent tribological behavior,[118] at physiological concentrations on the order of 20-80 mg/mL.[18] Meanwhile, the tensile properties of cartilage (e.g., viscoelastic stress relaxation) arise primarily from the mechanics of fibrillar collagen.[123] Thus, the mechanical properties of articular cartilage in joints and fibrillar cartilage in intervertebral discs depend upon the nanostructure of the aggrecan aggregate. Dean *et al.* measured the forces between aggrecan macromolecules in compression by atomic force microscopy at different salt concentrations by atomic force microscopy. The objective of this work was to determine how the nanomechanical behavior of aggrecan is determined by its nanoscale structure under physiologically relevant conditions.[114] They determined, by both experimental and modeling approaches, that at physiological concentrations, the spacing between neighboring GAG moieties is near the threshold where compression causes a sharp increase in the modulus.[104, 114, 121] They estimate that the nanomechanical stiffness increases in the range of 40-80 mg/mL which is in the range of physiological concentration.[114]

Aggrecan also has a variety of important biochemical functions that play a role in the maintenance of healthy tissue. Aggrecan serves to organize other components of the ECM and may play a key role in transport of other macromolecules across the pericellular space, between chondrocytes and the ECM.[113] There is strong evidence that

aggrecan inhibits the proteolytic cleavage of collagen, another important structural component of cartilage ECM.[124] The affect of aggrecanase inhibitors on collagen degradation has been evaluated in cartilage tissue cultures, to determine whether aggrecan itself was responsible for the collagen stabilization. Aggrecanase inhibitors blocked the degradation of collagen, but only in the presence of aggrecan.[124] If aggrecan was removed first, then the addition of aggrecanase inhibitors had no effect on the collagen degradation process.[124] As mentioned previously, the chondroitin sulfate chains in aggrecan also bind and activate growth factors such as FGF2[26], FGF7[21], PDGF[27, 28], and TGFβ1[29].

2.4.3 Nanoscale Organization of other ECM Components

In other tissues, the proteoglycans have a critical role in dictating the nanoscale organization of ECM components. For example, glycosaminoglycans in blood vessels may influence the organization of structural proteins.[125] Some authors have conjectured that the GAGs in the proteoglycan versican influence the mechanical properties of blood vessels as aggrecan does in cartilage,[112, 126] while others have downplayed its significance.[125]

The small leucine-rich proteoglycans (SLRPs) are another group of proteoglycans that play essential roles in the nanoscale organization of the ECM in the tissues in which they are found. Decorin, for example, is an SLRP that helps to regulate the assembly and final size of collagen fibrils. When the decorin-mediated collagen assembly is disrupted in skin, degradation of the mechanical properties results.[127] In the cornea, decorin ensures

that collagen fibrils have a uniform (~90 nm) diameter and uniform spacing, which is essential to the transparency of the tissue.[128]

2.5 Engineering Polysaccharide Nanostructures

The examples in the sections above demonstrate that the nanoscale assembly of polysaccharides is a key determinant of their biological function. Thus, by engineering their nanoscale assembly, biomaterials scientists may capitalize on the biochemical and biomechanical potential of polysaccharides for biomedical applications. For this endeavor to be successful, the responses of proteins, body fluids, cells, and tissues to nanostructured polysaccharides must be accurately characterized, so that design principles for new biomaterials can be developed. The biological responses to different polysaccharide chemistries are often most readily characterized on flat surfaces. Ultrathin films afford the opportunity for researchers to precisely tune the chemistry, thickness, and morphology of surfaces, and can be engineered from polysaccharides via several reproducible methods.

The biological responses to nanoscale surface coatings however, are not always effective predictors of the biological response to the same chemistries presented in three dimensional nanostructures. Thus, in order to engineer nanostructured materials that afford predictive control over cell behavior, studies of cell responses to more complex nanostructures must be conducted. In the sections that follow, we will describe recent research in the development of polysaccharide nanostructures, primarily obtained through interpolyelectrolyte complexation. We will also summarize the interesting results that

begin to tell the story of how biological systems respond to the nanoscale features of these materials.

2.6 Nanoscale Polysaccharide-Based Surface Coatings

Among the several techniques available for modifying the surface chemistry of materials, the covalent attachment of self-assembled monolayers (SAMs), formation of polymer brushes, and the layer-by-layer (LBL) assembly of polyelectrolyte multilayers (PEMs) have demonstrated particular usefulness for saccharide chemistries. The covalent attachment of SAMs has been an effective strategy for studying the interactions of proteins[129-131] and cells[132] with specific monosaccharides and oligosaccharides.[133] Raynor *et al.* recently characterized the biological activity of a synthetic polymer brush containing saccharide side chains.[134] The saccharide side chains imparted resistance to cell and protein adhesion, but the addition of peptide adhesion ligands enabled cells to bind to the otherwise non-fouling surfaces.[134] Others have used thin films of polysaccharides covalently bound to surfaces to study their biochemical properties.[135]

A more common strategy for modifying surfaces with polysaccharides is through the formation of PEMs. Many of the polysaccharides of interest as biomaterials also behave as polyelectrolytes, due to pendent carboxylate, amino, sulfate, and *N*-sulfonate groups. Thus, the modification of surfaces with polysaccharides by electrostatic adsorption is an effective method for introducing polysaccharides to surfaces.

The layer-by-layer (LBL) deposition of oppositely charged polyelectrolytes to form PEMs was developed in the 1990's by Decher *et al.* [136-140] and it has been extended to many nanotechnology applications.[137, 138, 141, 142] It has become an increasingly important

method for generation of functional thin films deposited on solid substrates such as gold, glass, or silicon.[141, 142] The LBL assembly of PEMs been demonstrated to be a useful method for building nanostructured organic or inorganic thin films for biomedical applications, including biosnesors,[140, 143] and cell encapsulation,[144] and protein delivery.[145, 146] PEMs are of scientific and technological interest because of the many possible variations on their physical and chemical properties, and the ability to accurately control the assembly of materials at the nanometer length scale. PEMs are formed by adsorbing a polyelectrolyte from solution onto an oppositely charged surface. Adsorption of the polyelectrolyte leads to an inversion of the surface charge, due to excess charged groups on the adsorbing polymer.[147] The charge inversion allows the surface to be subsequently modified with an additional layer of a polyelectrolyte with a charge opposite to that of the first. The process can be iterated by sequentially exposing the surface to polyelectrolyte solutions of alternating charge. In practice, the LBL assembly can be achieved by perfusing a surface with alternating solutions either by flowing solutions across the surface or by dipping the surface in the solutions. A rinse is usually conducted between adsorption steps to remove uncomplexed polymer and achieve more uniform PEM formation. PEM assembly with both strong and weak polyelectrolytes has been extensively investigated.[148-151]

The mechanism of electrostatic LBL assembly has been attributed to the formation of a sufficiently stable interpolyelectrolyte complex at the interface. The charge density of each of the polymers and their solubility in the dipping and rinse solutions can have a strong influence on the PEM thickness and composition. For weak polyelectrolytes, the charge density on each of the polymers can be controlled by altering the solution pH. In

this case pH controls the linear charge density of an adsorbing polymer as well as the surface charge density of the previously adsorbed polymer layer. Any solution property which affects the electrostatic interactions can influence the PEM assembly, including solution pH, ionic strength,[147, 150, 152] polymer charge density,[149, 152-155] and polymer molecular weight.[156] The LBL technique has recently been extended to take advantage of additional binary attractive interactions, including hydrogen bonding[157], charge transfer[158, 159], acid base pairing[160], and covalent bonding[161]. In a detailed review, Schonhoff discussed the development of the theory of PEM formation, deposition of PEMs on colloidal templates, and the composition and transport properties of PEMs.[162] The LBL assembly of PEM can provide control over layer thickness and surface composition at the sub-nanometer length scale.[152] This technique has been used to precisely tune both the surface composition and biological function of PEMs containing biologically derived polysaccharides.[151, 163-166] Furthermore, the ability to precisely tune the composition and thickness of ultra-thin films using LBL assembly of surface coatings based on polysaccharides has enabled the detailed investigations of the interactions of proteins, biological fluids, and cells with well-defined polysaccharide-based surfaces.

Surfaces containing very hydrophilic polysaccharides, such as hyaluronan, tend to exhibit resistance to protein adsorption and cell adhesion.[135, 167] Elbert *et al.* demonstrated that the cell adhesion properties of surfaces could be dramatically modified by addition of polysaccharide-containing PEMs. Figure 2.3 shows fibroblasts growing on a fibroblast ECM-coated surface (A), a similar surface coated with a polylysine-alginate PEM (15 bilayers) (B), and gelatin coated with a polylysine-alginate PEM (15 bilayers) (C).[168] In similar experiments, they also demonstrated that addition of just two polylysine-alginate

bilayers could completely inhibit platelet adhesion to collagen coated surfaces (Figure 2.4).[168] Polysaccharides have also been combined with other proteins or polymers to promote cell adhesion or proliferation on surfaces. Osteoblast proliferation on titanium, for example, can be enhanced by chitosan-gelatin PEMs.[169]

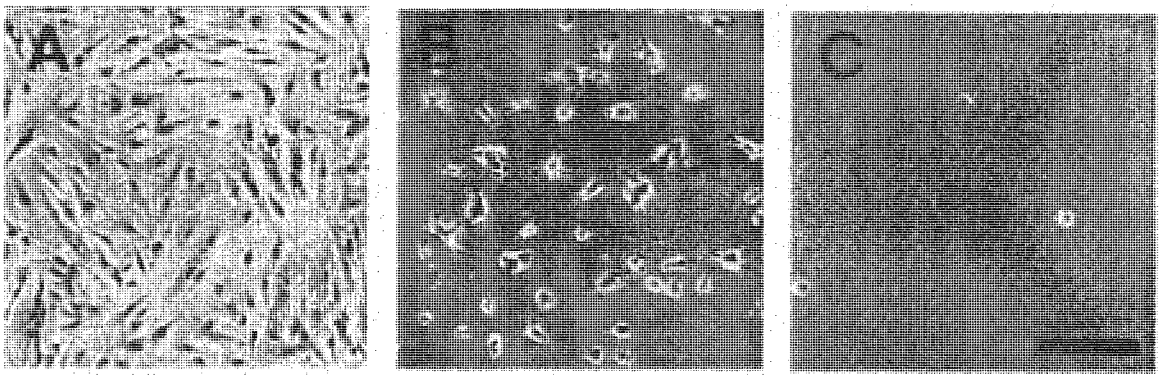

Figure 2.3. Proteinaceous surfaces were treated by polylysine-alginate PEMs. Fibroblast cells were seeded onto the treated surfaces, and cell spreading was assessed at 24 h. Photomicrographs of the following surfaces are presented: (A) fibroblast extracellular matrix treated with buffer only; (B) fibroblast extracellular matrix treated with a 15-bilayer PEM; (C) gelatin coated on tissue culture polystyrene treated with a 15-bilayers PEM. Scale bar is 200 μm. Reprinted with permission from reference 168, copyright 1999 American Chemical Society.

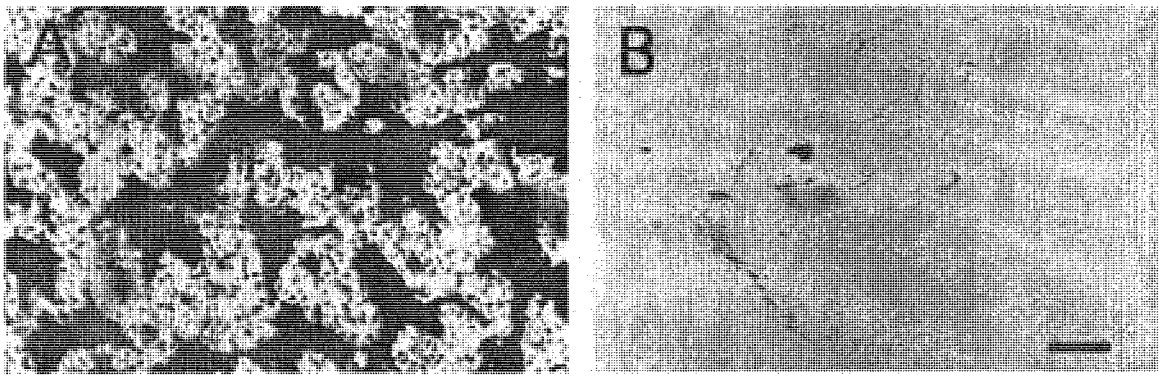

Figure 2.4. Type I collagen was adsorbed onto glass, and then treated with a PEM. The substrates were then contacted with flowing human blood for 2 min at a shear rate of 1000 s^{-1}. Adhered platelets were then stained with basic fuchsin. (A) Control, treated only with buffer. (B) Treated with a two-bilayer polylysine-alginate PEM. Scale bar is 100 μm. Reprinted with permission from reference 168, copyright 1999 American Chemical Society.

Surfaces containing sulfated polysaccharides tend to reduce platelet activation and exhibit anticoagulant activity.[170, 171] Thus, the biochemistry of sulfated polysaccharides has also been exploited to tune the interactions of cells and biological fluids with materials, through the use of PEMs. Serizawa *et al.* investigated the anticoagulant properties of dextran sulfate-chitosan PEMs and demonstrated that the terminal layer of the PEM governed the biochemical anticoagulant functionality.[170] Recently, chitosan-heparin PEMs were used to improve the endothelialization of arterial stents made from 316L stainless steel.[172] Kreke *et al.* studied the PEM formation of poly(allylamine hydrochloride)-heparin PEMs over a range of pH, and investigated protein adsorption and osteoprogenitor cell adhesion.[173] This work demonstrated that the internal nanoscale structure and composition of the PEMs influences cell and protein interactions at the surface.[173]

These studies reviewed above demonstrate that the structure and composition of thin films can be altered at the nanoscale in order to influence their biological properties. In

order to achieve predictive control over the biological responses to PEMs, it is essential to understand how these nanoscale features can be controlled. To that end, our group and others have studied in detail how the assembly of PEMs is governed by the processing conditions and the physical chemistry of the constituent polyelectrolytes.[151, 154, 174] In our work, we found that the composition and thickness of chitosan-heparin PEMs could be independently tuned by altering the ionic strength and pH of the polyelectrolyte solutions, respectively.[151]

Mammalian cells may also respond to the nanomechanics of PEMs. Schneider *et al.* measured the viscoelestic properties of polysaccharide-containing PEMs before and after cross-linking using AFM.[175] A number of recent studies have demonstrated improved cell adhesion or proliferation on polysaccharide-based PEMs that are cross-linked to increase the film rigidity.[176, 177] Nanoscale topographical features may also have a strong influence on cell behaviors such adhesion and migration. The topographical features of PEMs can be tuned by altering deposition solution properties, polymer charge density, or by incorporation of nanoparticles into PEMs.[178, 179]

Polysaccharide-based surface coatings have also been used to deliver proteins and DNA to influence cell behavior.[145, 180, 181] In the recent work by Crouzier *et al.* the release of bone morphogenetic protein-2 from polysaccharide-based PEM was demonstrated to effectively induce myocyte differentiation into osteoblasts, even after repeated cycles of cell culture on the same surface.[145] They also demonstrated that the quantity of growth factor encapsulated could be tuned by altering the PEM thickness.[145] Figure 2.5 shows that BMP-2 is distributed throughout both thick and thin PEMs. In these confocal micrographs, the PEMs are stained green and the BMP-2 is stained red. Thus the

thickness of the PEM can be tuned to alter the quantity and kinetics of protein release from the surface.[145] In this work differentiation of myocytes into osteoblasts was demonstrated in a dose-dependent manner, where the growth factor dose could be controlled by the structure of the PEMs. Quantitative studies of this type are essential for controlling the biological activity of nanostructured polysaccharides. Polysaccharide-based PEMs have also been used to regulate the release of bioactive proteins from alginate hydrogels.[182] In this work, the polysaccharide PEM coating helped to both maintain the integrity of the alginate gel, and to retard the diffusion of the growth factor from the gel matrix.[182]

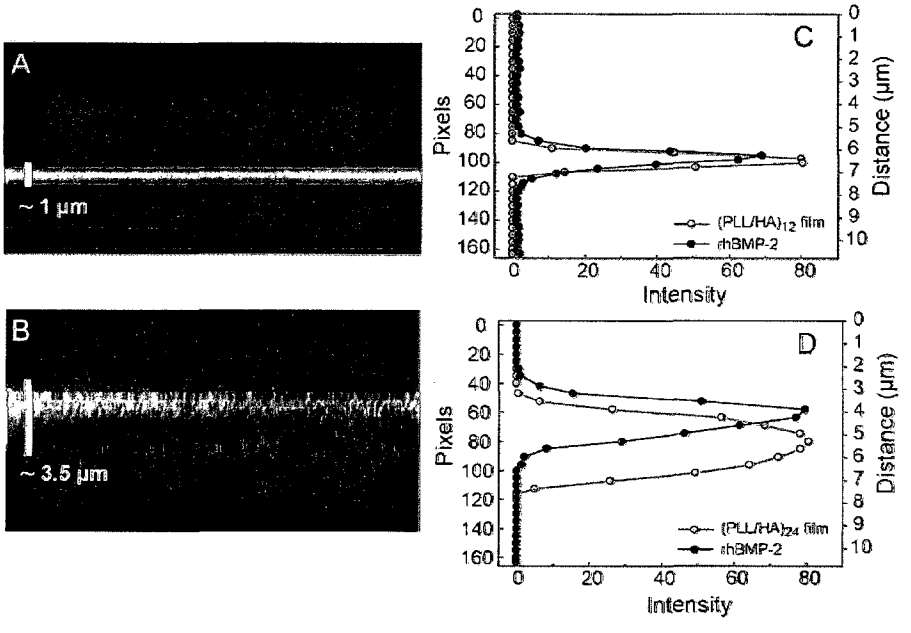

Figure 2.5. A and B: Confocal microscopy in HEPES/NaCl buffer (pH 7.4) of crosslinked polylysine-hyaluronan PEMs loaded with rhBMP-2; A) 12-bilayer PEM and B) 24-bilayer PEM. C and D: The z-intensity profiles and film thickness (left y axes) for BMP-2 (red) and for polylysine (green). T.Crouzier, *et al.*, Layer-by-layer films as a biomimetic reservoir for rhBMP-2 delivery: Controlled differentiation of myoblasts to osteoblasts. Small. 2009. 5. Copyright Wiley-VCH Verlag GmbH & Co. KGaA. Reproduced with permission.

2.7 Polysaccharide-Based Nanoparticles

In the previous section we discussed how the complexation of polyelectrolytes at surfaces has proven particularly useful for generating surface coatings with control over composition and thickness at the nanometer length scale. We also discussed some examples illustrating how this control can influence the biological responses to nanostructured polysaccharides. Polyelectrolytes can also be electrostatically complexed in solution to form polyelectrolyte complex nanoparticles (PCNs). This can be done using either oppositely charged polyelectrolytes, or a complementary polyelectrolyte-surfactant pair.[183, 184] This process is usually entropically driven by the release of counter ions and water from the hydrated polyelectrolyte molecules.[183] In some cases, van der Waals forces and dipole-charge transfer may be involved in the formation of PCNs. Several mechanisms of complexation have been described leading to different effects on PCN size and morphology. Early studies of PCN formation were conducted in the 1970s by Tsuchida, and later by both Tsuchida and Kabanov.[185-188] This work was followed by several groups characterizing the complexation of weak and strong polyelectrolytes,[188, 189] and experimental studies of PCN formation at different charge mixing ratios, buffer concentration, and pH.[183, 190] The effects of salt on PCN formation and polyelectrolyte exchange continued to be a subject of study into the 1990s.[188, 190-192]

The formation of water soluble PCNs, and control over their composition, colloidal stability, and degree of hydration is of particular interest for developing nanoparticles for biomedical application. Dautzenberg *et al.* have made significant contributions in this area. This group has studied how salt addition can affect the stability, density, and aggregation state of PCNs.[183, 190, 192] In general, their work has demonstrated that at lower

ionic strength particle flocculation is reduced. At higher ionic strength PCNs tend to aggregate, partially due to screening of electrostatic charges that otherwise stabilize PCN solutions. While polymer charge density is an important factor determining PCN stability, Dautzenberg *et al.* confirmed that charge density by itself cannot control the structure and stability of PCNs, specifically in the presence of salt.[193] This work, primarily conducted with synthetic polyelectrolytes, provides a framework for understanding the mechanisms of PCN formation, and a basis upon which to design processes for PCN formation from polysaccharides.

As early as the late 1970's, Kikuchi studied the electrostatic complexation of polysaccharides using the chitosan-heparin polyelectrolyte pair.[194-196] In this work, the sulfur content was used to assess the composition of the complexes, without further characterization.[194, 196] Since this work, the complexation of multiple polysaccharide pairs has been investigated in more detail. These including chitosan-dextran sulfate[197-199], chitosan-chondroitin sulfate[200-202], chitosan-heparin[203, 204], and chitosan-hyaluronan.[201, 202, 204] Chitosan has also been complexed with synthetic polyelectrolytes, such as poly(acrylic acid).[205, 206]

The formation, composition, size, stability, and swelling behavior of polysaccharide-based PCNs has been the subject of extensive study. For example, Domard, Delair, and co-workers have characterized the chitosan-dextran sulfate system, using different molecular weights of chitosan and dextran sulfate, and different degrees of acetylation for chitosan. They found that for particles with chitosan in excess, the molecular weight of chitosan had a strong influence on the particle size, with larger particles formed from higher molecular weight chitosan.[198] They also found that the hydrodynamic diameter of

the particles tended to decrease with increasing pH, which is consistent with the interpretation that the particles form a neutral, hydrophobic core, surrounded by a chitosan-rich, charged corona.[198] In separate publications by the same group, different complexation mechanisms were proposed depending upon the molecular weight ratio of the polyelectrolyte in excess and the polyelectrolyte in default,[197] and the differences in chain stiffness and charge group reactivity.[199] When the polyelectrolyte in excess is much lower molecular weight than the polyelectrolyte in default, a more compact morphology results, leading in some cases to flocculation of the PCNs and poor colloidal stability.[197]

When dextran sulfate was in excess, this group found that the complexes could form by either random cross-linking of chitosan chains by dextran sulfate, or by a one-to-one charge complexation of the oppositely charged groups between two polyelectrolyte chains.[199] The prevalence of the second mechanism increased with increasing stiffness of the chitosan.[199] The method of complexation also influenced the stability of the PCNs. A "one-shot" addition of the polyelectrolytes resulted in more stable particle formulations than slow titration of the polyelectrolyte solutions when the charge mixing ratios were close to 1:1.[197]

The extensive characterization of polysaccharide-based nanoparticles enables them to be engineered for specific biomedical applications. A particularly promising application of polysaccharide-based PCNs is the development of vehicles for the stabilization and delivery of a variety of therapeutic agents. Polysaccharide-based PCNs have the potential to address some of the most pressing challenges associated with polymeric drug delivery vehicles. Polymeric drug delivery vehicles must be capable of stabilizing their payload with respect to the body's natural defense mechanisms, target the drug to the desired site

of delivery, and safely release the drug with an optimized release profile.[207, 208] Rather than providing an exhaustive review, the overview offered here focuses on how the properties of polysaccharide-based PCNs have been engineered to improve their performance with respect to a few applications for which they are particularly well-suited. Polysaccharide formulations are effective at stabilizing biological macromolecules such as proteins and DNA.[8] Thus, development of polysaccharide based delivery systems for both protein-based and DNA-based drugs and vaccines has been pursued.[9, 10, 209-217]

Motwani *et al.* performed a particularly well-designed study to develop chitosan-alginate PCNs for intra-ocular drug delivery with optimal drug loading and release profiles.[212] Their study developed a predictive model for how the composition of the PCNs altered the size, zeta potential, drug loading, and release kinetics in order to perform engineering design optimization.[212] Polysaccharide PCNs have generated particular interest as vehicles for mucosal delivery of various therapeutics, due to their mucoadhesive properties. The size and zeta potential of chitosan-hyaluronan nanoparticles, for example, can be tuned by altering their composition.[213] Prego *et al.* studied a three different types of chitosan-based nanoparticle formulations for mucosal delivery, and demonstrated that all of them are capable of reducing the trans-epithelial resistance in a model tissue culture system.[218]

A number of studies elucidating the mechanisms by which polysaccharide-based PCNs interact with cells and tissues have been conducted. Chitosan-containing nanoparticles are known to facilitate mucosal drug delivery by opening tight junctions in epithelial tissues. Lin *et al.* studied the transport of chitosan-heparin PCNs in the gastric

epithelia of mice, demonstrating efficient uptake of the PCNs by epithelial cells and colocalization of PCNs to sites of *Helicobacter pylori* infection (Figure 2.6).

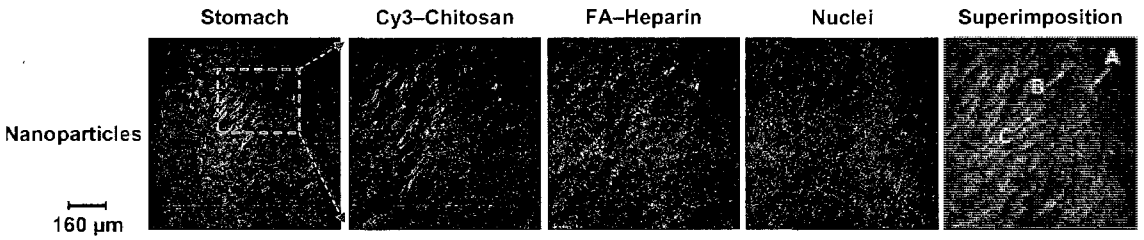

Figure 2.6. Confocal microscopy image of one of the vilii from the murine gastric epithelium, 120 minutes following oral administration of fluorescently labeled chitosan-heparin PCNs. The chitosan is stained red, the heparin is stained green, and the cell nuclei are stained blue. The superimposed image shows nanoparticles in various stages of interaction with the cells. Particles can be seen at the surface (A), interacting with the outermost layer of cells (B), and transported into the tissue (C). Reprinted from *Biomaterials*, 30, Y.-H. Lin, *et al.*, Development of pH-responsive chitosan/heparin nanoparticles for stomach-specific anti-*Helicobacter pylori* therapy, 3332-3342, copyright (2009), with permission from Elsevier.

Chitosan-cyclodextrin nanoparticles have also been demonstrated to facilitate drug delivery by opening tight junctions in cell culture models of epithelia.[214] This phenomena led to the successful *in vivo* demonstration of efficient trans-mucosal (nasal) delivery of therapeutic levels of insulin in a rabbit model.[214] This study demonstrated that both opening of tight junctions and direct transport of nanoparticles across the epithelium contribute the enhanced delivery of insulin by this carrier.[214] The interactions of endothelial cells with alginate and chondroitin sulfate-containing nanoparticles were also recently studied.[215] In this work, a combination of techniques was used to determine the mechanisms PCN uptake by endothelial cells.[215] While nonspecific binding to endothelial cells was confirmed by fluorescence assisted cell sorting, the dominant mechanism of PCN uptake was by active micropinocytosis.[215]

A large number of studies have used chitosan containing PCNs for gene delivery. One recent study of chitosan-plasmid DNA nanoparticle delivery demonstrated successful protein and antibody production in a murine model after both intramuscular and subcutaneous injection.[216] This study concluded that chitosan with low molecular weight and low degree of acetylation produced the best functional response.[216] Chitosan-based PCNs may be used in the future for development of both gene therapies and DNA vaccines.

2.8 Polysaccharide-Based Nanofibers

In the previous two sections, we discussed how polysaccharide nanostructures can be engineered with a focus on interpolyelectrolyte complexation. The few examples cited demonstrate that rational design of such systems can lead to materials with biological properties dictated by the nanoscale features. However, these simple nanostructures do not fully represent the complexity of possible nanoscale assemblies that might be developed. The formation of electrospun nanofibers is another technique that has been used to tune the nanostructure of polymeric biomaterials, including polysaccharides.[219-221] Electrospinning has been used to develop nanofibers for engineering of many tissues, including bone,[222] blood vessel,[223] and cartilage.[224] From these studies, some basic design parameters such as fiber size, alignment, and chemistry have been developed. The vast majority of this work has been done with synthetic polymers.

Electrospinning of polysaccharides can be difficult due to their limited solubility in organic solvents, and the relatively high viscosity of concentrated aqueous solutions. Nonetheless, some success has been demonstrated by using solvent combinations or

blends with synthetic polymers. Ohkawa and co-workers studied electrospinning using chitosans of different molecular weights.[225] In extensive work by Torres-Giner and co-workers chitosan-poly(lactic acid) blend nanofibers were electrospun and the effects of chitosan molecular weight and buffer solution was investigated.[226] Chitosan-poly(ethylene oxide) blend nanofibers have also been studied by a few groups. This work has shown that the blend composition and molecular weight can affect the size and shape of nanofibers.[225, 227, 228] Bhattarai and co-workers electrospun chitosan-poly(ethylene oxide) blends in different blend ratios to adjust the solution viscosity.[228] They cultured chondrocytes and osteoblasts on the nanofibers to observe the effects of nanofiber geometry on cell response.[228] Electrospinning of a cellulose-heparin blend was achieved by Viswanathan *et al.* using room-temperature ionic liquids as the solvent. [229]

While it is not yet clear exactly what features of nanofibers influence cell response, nanofibers size and mechanical properties have been correlated to biological responses. In recent work done by Subramanian *et al.*, the viability and proliferation of chondrocytes cultured on chitosan-poly(ethylene oxide) blend nanofibers was characterized as a function of nanofibers mechanical properties.[230] Noh *et al.*, compared the responses of human keratinocytes and fibroblasts to chitin nanofibers and microfibers.[75] In an *in-vitro* study, they found that over a pried of 15 days, degradation rate of chitin nanofibers was higher than for chitin microfibers due to the higher surface area to volume ratio.[75] They also demonstrated biocompatibility in a subcutaneous implantation model. Figure 2.7 shows scanning electron micrographs of human gingival fibroblasts cultured on nanofibers and microfibers, illustrating increased cell attachment and spreading on the nanofibers, both with and without collagen.[75]

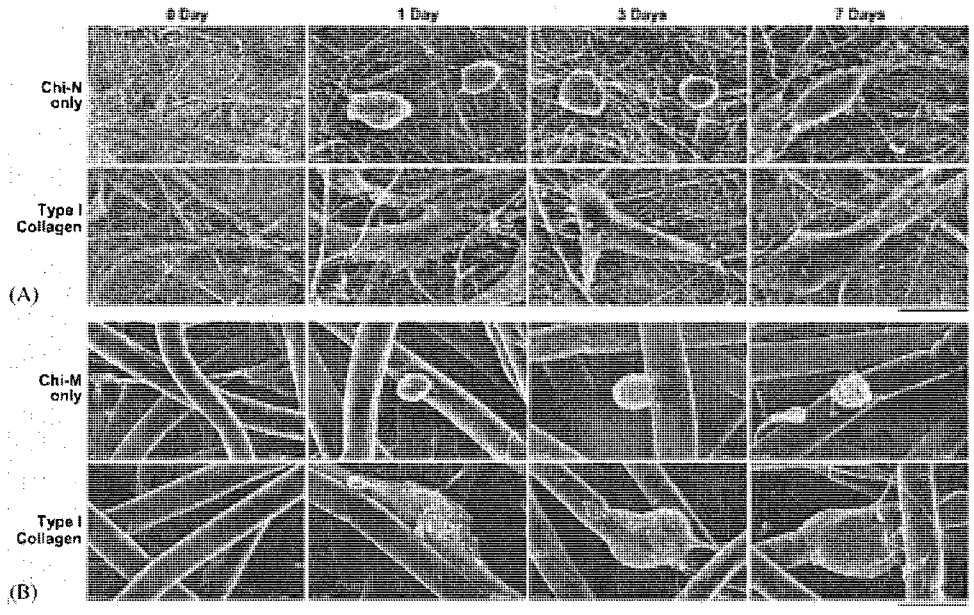

Figure 2.7. Scanning electron micrographs of human gingival fibroblasts cultured on chitin nanofibers (A) and microfibers (B) structures, with and without type I collagen coating after 0, 1, 3, and 7 days of culture. The scale bar is 20 μm. Reprinted from *Biomaterials*, 27, H. K. Noh, *et al.*, Electrospinning of chitin nanofibers: Degradation behavior and cellular response to normal human keratinocytes and fibroblasts, 11, copyright (2006), with permission from Elsevier.

Polysaccharide-based nanofibers are still under investigation by researchers interested in cell and tissue engineering, wound healing, and drug, protein, and gene delivery. The promising work done to date demonstrates that biological systems respond to the nanoscale features of these materials, and that their biochemical functions can be tuned by altering the nanostructure. This work suggests that there is a wealth of opportunities for the development of new nanostructured biomedical materials with tailored biological function.

2.9 Development of more Complex Polysaccharide-Based Nanoassemblies

The repertoire of nanoscale assemblies currently available to biomaterials scientists is certainly not limited to surface coatings, nanoparticles, and nanofibers. New synthetic approaches are being developed to generate polysaccharides with novel architectures that self assemble at the nanoscale. Lithographic techniques provide for the top-down development of arbitrary nanoscale surface features with sub-micron resolution, and biological nanoassemblies such as the aggrecan aggregate can be harvested from tissues and modified to alter their nanoscale properties. An exhaustive review of all of these strategies would require far more space than is permitted here. Nonetheless, nanoscale surface coatings, nanoparticles, and nanofibers represent the three most well-characterized methods to tune the nanostructure of polysaccharides. These three types of nanostrcutures could therefore be viewed as a set of building blocks from which more complex nanoassemblies might be developed. For example, the modification of nanofibers surfaces with polyelectrolyte multilayers, formation of nanofibers containing nanoparticles, and the incorporation of nanoparticles into PEM films has been demonstrated by a number of groups.[231-236] Most of this work has been done using synthetic polymers. The ability to engineer these three nanostructures therefore, provides a good starting point for the fabrication of more complex nanoassemblies.

We have recently investigated the decoration of surfaces with polysaccharide-containing PCNs as a means of altering surfaces with nanoscale regions of varying chemistry and surface topographical features. Figure 2.8 shows scanning electron

micrographs of chitosan-heparin PCNs adsorbed to an aluminum surface (left) and chitosan-heparin PCNs embedded within a chitosan-hyaluronan PEM (right).

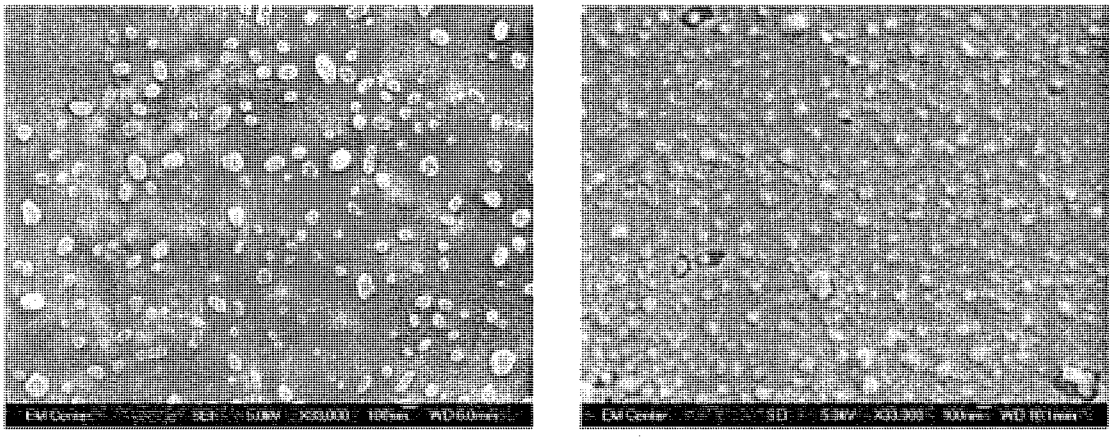

Figure 2.8. Scanning electron micrographs of positively charged chitosan-heparin PCNs adsorbed to an aluminum surface (left) and embedded within a chitosan-hyaluronan PEM (right). Adsorption within the PEM induces a more uniform surface coverage, while maintaining the PCN stability.[179, 204]

A similar approach was recently reported by Lin *et al.* to develop nanostructured surfaces for DNA delivery.[180] In this work, PCNs were first formed from the chitosan-plasmid DNA polyelectrolyte pair.[180] These PCNs were then embedded in chitosan-hyaluronan PEMs and used to transfect mammalian cells with a reporter gene (green fluorescent protein) with high transfection efficiency.[180] The ability to tune the nanostructure and chemistry of polysaccharide based nanomaterials enables the design of systems such as this one, that can be optimized by to increase the stability of the DNA and engineer the payload release profile to achieve optimum results.

2.10 Conclusion

Many important biochemical and biomechanical functions of polysaccharides are dependent upon their organization at the nanometer length scale. The strategies briefly reviewed here, and similar strategies that are under development, will enable more detailed investigations into the emergent biological properties of nanostructured polysaccharides. We already have the ability to precisely tune the structure of polysaccharides at the nanometer length scale. The next step in the development of biologically active polysaccharide nanostructures should be well-defined studies of the biological responses to these nanostructures that enable (1) elucidation of mechanisms whereby biological systems respond to the nanoscale features, and (2) the development of design principles that can guide the development of nanostructured materials for new applications as they arise.

2.11 References

1. Raman, R.; Raguram, S.; Venkataraman, G.; Paulson, J. C.; Sasisekharan, R., Glycomics: an integrated systems approach to structure-function relationships of glycans. *Nature Methods* **2005,** 2, (11), 817-824.
2. Dove, A., The bittersweet promise of glycobiology. *Nature Biotechnology* **2001,** 19, (10), 913-917.
3. Alper, J., Glycobiology - Turning sweet on cancer. *Science* **2003,** 301, (5630), 159-160.
4. Doublier, J. L.; Garnier, C.; Renard, D.; Sanchez, C., Protein-polysaccharide interactions. *Current Opinion in Colloid & Interface Science* **2000,** 5, (3-4), 202-214.
5. Turgeon, S. L.; Beaulieu, M.; Schmitt, C.; Sanchez, C., Protein-polysaccharide interactions: phase-ordering kinetics, thermodynamic and structural aspects. *Current Opinion in Colloid & Interface Science* **2003,** 8, (4-5), 401-414.
6. Suh, J. K. F.; Matthew, H. W. T., Application of chitosan-based polysaccharide biomaterials in cartilage tissue engineering: a review. *Biomaterials* **2000,** 21, (24), 2589-2598.
7. Hu, S. G.; Jou, C. H.; Yang, M. C., Surface grafting of polyester fiber with chitosan and the antibacterial activity of pathogenic bacteria. *Journal of Applied Polymer Science* **2002,** 86, (12), 2977-2983.
8. Schilli, C. M.; Zhang, M. F.; Rizzardo, E.; Thang, S. H.; Chong, Y. K.; Edwards, K.; Karlsson, G.; Muller, A. H. E., A new double-responsive block copolymer synthesized via RAFT polymerization: Poly(N-isopropylacrylamide)-block-poly(acrylic acid). *Macromolecules* **2004,** 37, (21), 7861-7866.
9. Janes, K. A.; Fresneau, M. P.; Marazuela, A.; Fabra, A.; Alonso, M. J., Chitosan nanoparticles as delivery systems for doxorubicin. *Journal of Controlled Release* **2001,** 73, (2-3), 255-267.
10. Janes, K. A.; Calvo, P.; Alonso, M. J., Polysaccharide colloidal particles as delivery systems for macromolecules. *Advanced Drug Delivery Reviews* **2001,** 47, (1), 83-97.
11. Couchman, J. R., Syndecans: Proteoglycan regulators of cell-surface microdomains? *Nature Reviews Molecular Cell Biology* **2003,** 4, (12), 926-937.
12. Oksala, O.; Salo, T.; Tammi, R.; Hakkinen, L.; Jalkanen, M.; Inki, P.; Larjava, H., Expression of proteoglycans and hyaluronan during wound-healing. *Journal of Histochemistry & Cytochemistry* **1995,** 43, (2), 125-135.
13. Peterson, S.; Frick, A.; Liu, J., Design of biologically active heparan sulfate and heparin using an enzyme-based approach. *Natural Product Reports* **2009,** 26, (5), 610-627.
14. Salmivirta, M.; Lidholt, K.; Lindahl, U., Heparan sulfate: A piece of information. *Faseb Journal* **1996,** 10, (11), 1270-1279.
15. Seeberger, P. H., Automated oligosaccharide synthesis. *Chemical Society Reviews* **2008,** 37, (1), 19-28.
16. Kobayashi, S., New developments of polysaccharide synthesis via enzymatic polymerization. *Proceedings of the Japan Academy Series B-Physical and Biological Sciences* **2007,** 83, (8), 215-247.

17. Lapcik, L.; Lapcik, L.; De Smedt, S.; Demeester, J.; Chabrecek, P., Hyaluronan: Preparation, structure, properties, and applications. *Chemical Reviews* **1998,** 98, (8), 2663-2684.
18. Comper, W. D.; Laurent, T. C., Physiological function of connective-tissue polysaccharides. *Physiological Reviews* **1978,** 58, (1), 255-315.
19. Esko, J. D.; Lindahl, U., Molecular diversity of heparan sulfate. *Journal of Clinical Investigation* **2001,** 108, (2), 169-173.
20. Douglas, T.; Heinemann, S.; Mietrach, C.; Hempel, U.; Bierbaum, S.; Scharnweber, D.; Worch, H., Interactions of collagen types I and II with chondroitin sulfates A-C and their effect on osteoblast adhesion. *Biomacromolecules* **2007,** 8, (4), 1085-1092.
21. Sasisekharan, R.; Raman, R.; Prabhakar, V., Glycomics approach to structure-function relationships of glycosaminoglycans. *Annual Review of Biomedical Engineering* **2006,** 8, 181-231.
22. Handel, T. M.; Johnson, Z.; Crown, S. E.; Lau, E. K.; Sweeney, M.; Proudfoot, A. E., Regulation of protein function by glycosaminoglycans - as exemplified by chemokines. *Annual Review of Biochemistry* **2005,** 74, 385-410.
23. Viapiano, M. S.; Matthews, R. T., From barriers to bridges: chondroitin sulfate proteoglycans in neuropathology. *Trends in Molecular Medicine* **2006,** 12, (10), 488-496.
24. Li, W. J.; Tuan, R. S., Polymeric scaffolds for cartilage tissue engineering. *Macromolecular Symposia* **2005,** 227, 65-75.
25. Arnott, S.; Guss, J. M.; Hukins, D. W. L.; Mathews, M. B., Dermatan sulfate and chondroitin 6-sulfate conformations. *Biochemical and Biophysical Research Communications* **1973,** 54, (4), 1377-1383.
26. Mi, F. L.; Shyu, S. S.; Peng, C. K.; Wu, Y. B.; Sung, H. W.; Wang, P. S.; Huang, C. C., Fabrication of chondroitin sulfate-chitosan composite artificial extracellular matrix for stabilization of fibroblast growth factor. *Journal of Biomedical Materials Research Part A* **2006,** 76A, (1), 1-15.
27. Fthenou, E.; Zafiropoulos, A.; Berdiaki, A.; Tzanakakis, G. N., Chondroitin sulfate a specifically modulates the mitogenic effects of PDGF-BB on normal fibroblasts. *Febs Journal* **2006,** 273, 265-265.
28. Fthenou, E.; Zafiropoulos, A.; Tsatsakis, A.; Stathopoulos, A.; Karamanos, N. K.; Tzanakakis, G. N., Chondroitin sulfate A chains enhance platelet derived growth factor-mediated signalling in fibrosarcoma cells. *International Journal of Biochemistry & Cell Biology* **2006,** 38, (12), 2141-2150.
29. Chou, C. H.; Cheng, W. T. K.; Lin, C. C.; Chang, C. H.; Tsai, C. C.; Lin, F. H., TGF-beta 1 immobilized tri-co-polymer for articular cartilage tissue engineering. *Journal of Biomedical Materials Research Part B-Applied Biomaterials* **2006,** 77B, (2), 338-348.
30. Funderburgh, J. L., Keratan sulfate: structure, biosynthesis, and function. *Glycobiology* **2000,** 10, (10), 951-958.
31. Funderburgh, J. L.; Funderburgh, M. L.; Mann, M. M.; Prakash, S.; Conrad, G. W., Synthesis of corneal keratan sulfate proteoglycans by bovine keratocytes in vitro. *Journal of Biological Chemistry* **1996,** 271, (49), 31431-31436.

32. Nakato, H.; Kimata, K., Heparan sulfate fine structure and specificity of proteoglycan functions. *Biochimica Et Biophysica Acta-General Subjects* **2002,** 1573, (3), 312-318.
33. Hardingham, T. E.; Fosang, A. J., Proteoglycans - many forms and many functions. *Faseb Journal* **1992,** 6, (3), 861-870.
34. Lindahl, U.; Kusche, M.; Lidholt, K.; Oscarsson, L. G., Biosynthesis of Heparin and Heparan-Sulfate. *Annals of the New York Academy of Sciences* **1989,** 556, 36-50.
35. Conrad; Edward, H., Heparin-binding proteins. In Academic press: San diego, 1998; p 3.
36. Loo, B. M.; Kreuger, J.; Jalkanen, M.; Lindahl, U.; Salmivirta, M., Binding of heparin/heparan sulfate to fibroblast growth factor receptor 4. *Journal of Biological Chemistry* **2001,** 276, (20), 16868-16876.
37. Sasaki, T.; Larsson, H.; Kreuger, J.; Salmivirta, M.; Claesson-Welsh, L.; Lindahl, U.; Hohenester, E.; Timpl, R., Structural basis and potential role of heparin/heparan sulfate binding to the angiogenesis inhibitor endostatin. *Embo Journal* **1999,** 18, (22), 6240-6248.
38. Guimond, S.; Maccarana, M.; Olwin, B. B.; Lindahl, U.; Rapraeger, A. C., Activating and Inhibitory Heparin Sequences for FGF-2 (Basic FGF) - Distinct Requirements for FGF-1, FGF-2, and FGF-4. *Journal of Biological Chemistry* **1993,** 268, (32), 23906-23914.
39. Zhao, B. H.; Katagiri, T.; Toyoda, H.; Takada, T.; Yanai, T.; Fukuda, T.; Chung, U. I.; Koike, T.; Takaoka, K.; Kamijo, R., Heparin potentiates the in vivo ectopic bone formation induced by bone morphogenetic protein-2. *Journal of Biological Chemistry* **2006,** 281, (32), 23246-23253.
40. Takada, T.; Katagiri, T.; Ifuku, M.; Morimura, N.; Kobayashi, M.; Hasegawa, K.; Ogamo, A.; Kamijo, R., Sulfated polysaccharides enhance the biological activities of bone morphogenetic proteins. *Journal of Biological Chemistry* **2003,** 278, (44), 43229-43235.
41. Blanquaert, F.; Saffar, J. L.; Colombier, M. L.; Carpentier, G.; Barritault, D.; Caruelle, J. P., Heparan-like molecules induce the repair of skull defects. *Bone* **1995,** 17, (6), 499-506.
42. Yayon, A.; Klagsbrun, M.; Esko, J. D.; Leder, P.; Ornitz, D. M., Cell-Surface, Heparin-Like Molecules Are Required for Binding of Basic Fibroblast Growth-Factor to Its High-Affinity Receptor. *Cell* **1991,** 64, (4), 841-848.
43. Rider, C. C., Heparin/heparan sulphate binding in the TGF-beta cytokine superfamily. *Biochemical Society Transactions* **2006,** 34, 458-460.
44. Lyon, M.; Rushton, G.; Gallagher, J. T., The interaction of the transforming growth factor-beta s with heparin heparan sulfate is isoform-specific. *Journal of Biological Chemistry* **1997,** 272, (29), 18000-18006.
45. Ruppert, R.; Hoffmann, E.; Sebald, W., Human bone morphogenetic protein 2 contains a heparin-binding site which modifies its biological activity. *European Journal of Biochemistry* **1996,** 237, (1), 295-302.
46. Aruffo, A.; Stamenkovic, I.; Melnick, M.; Underhill, C. B.; Seed, B., CD44 is the principal cell-surface receptor for hyaluronate. *Cell* **1990,** 61, (7), 1303-1313.

47. Maccarana, M.; Casu, B.; Lindahl, U., Minimal Sequence in Heparin Heparan-Sulfate Required for Binding of Basic Fibroblast Growth-Factor. *Journal of Biological Chemistry* **1993,** 268, (32), 23898-23905.
48. Berry, D.; Kwan, C. P.; Shriver, Z.; Venkataraman, G.; Sasisekharan, R., Distinct heparan sulfate glycosaminoglycans are responsible for mediating fibroblast growth factor-2 biological activity through different fibroblast growth factor receptors. *Faseb Journal* **2001,** 15, (6), -.
49. Bourin, M. C.; Lindahl, U., Glycosaminoglycans and the Regulation of Blood-Coagulation. *Biochemical Journal* **1993,** 289, 313-330.
50. Choay, J.; Petitou, M.; Lormeau, J. C.; Sinay, P.; Casu, B.; Gatti, G., Structure-Activity Relationship in Heparin - a Synthetic Pentasaccharide with High-Affinity for Anti-Thrombin-Iii and Eliciting High Anti-Factor-Xa Activity. *Biochemical and Biophysical Research Communications* **1983,** 116, (2), 492-499.
51. Petitou, M.; Herault, L. P.; Bernat, A.; Driguez, P. A.; Duchaussoy, P.; Lormeau, J. C.; Herbert, J. M., Synthesis of thrombin-inhibiting heparin mimetics without side effects. *Nature* **1999,** 398, (6726), 417-422.
52. Schatz, C.; Viton, C.; Delair, T.; Pichot, C.; Domard, A., Typical physicochemical behaviors of chitosan in aqueous solution. *Biomacromolecules* **2003,** 4, (3), 641-648.
53. Hirano, S.; Tsuchida, H.; Nagao, N., N-Acetylation in Chitosan and the Rate of Its Enzymic-Hydrolysis. *Biomaterials* **1989,** 10, (8), 574-576.
54. Rabea, E. I.; Badawy, M. E. T.; Stevens, C. V.; Smagghe, G.; Steurbaut, W., Chitosan as antimicrobial agent: Applications and mode of action. *Biomacromolecules* **2003,** 4, (6), 1457-1465.
55. Lavertu, M.; Methot, S.; Tran-Khanh, N.; Buschmann, M. D., High efficiency gene transfer using chitosan/DNA nanoparticles with specific combinations of molecular weight and degree of deacetylation. *Biomaterials* **2006,** 27, (27), 4815-4824.
56. Dodane, V.; Vilivalam, V. D., Pharmaceutical applications of chitosan. *Pharmaceutical Science & Technology Today* **1998,** 1, (6), 246-253.
57. Magnani, A.; Barbucci, R.; Montanaro, L.; Arciola, C. R.; Lamponi, S., In vitro study of blood-contacting properties and effect on bacterial adhesion of a polymeric surface with immobilized heparin and sulphated hyaluronic acid. *Journal of Biomaterials Science-Polymer Edition* **2000,** 11, (8), 801-815.
58. Ito, Y.; Imanishi, Y.; Sisido, M., In vitro platelet-adhesion and in vivo antithrombohenicity of heparinized polyetherurethaneureas. *Biomaterials* **1988,** 9, (3), 235-240.
59. Park, K. D.; Kim, W. G.; Jacobs, H.; Okano, T.; Kim, S. W., Blood compatibility of SPUU-PEO-Heparin graft-copolymers. *Journal of Biomedical Materials Research* **1992,** 26, (6), 739-756.
60. Kito, H.; Matsuda, T., Biocompatible coatings for luminal and outer surfaces of small-caliber artificial grafts. *Journal of Biomedical Materials Research* **1996,** 30, (3), 321-330.
61. Goa, K. L.; Benfield, P., Hyaluronic-acid - A review of its pharmacology and use as a surgical aid in ophthalmology, and its therapeutic potential in joint disease and wound-healing. *Drugs* **1994,** 47, (3), 536-566.

62. Barbucci, R.; Magnani, A.; Rappuoli, R.; Lamponi, S.; Consumi, M. In *Immobilisation of sulphated hyaluronan for improved biocompatibility*, 2000; 2000; pp 119-125.
63. Levesque, S. G.; Shoichet, M. S., Synthesis of cell-adhesive dextran hydrogels and macroporous scaffolds. *Biomaterials* **2006,** 27, (30), 5277-5285.
64. Moller, S.; Weisser, J.; Bischoff, S.; Schnabelrauch, M. In *Dextran and hyaluronan methacrylate based hydrogels as matrices for soft tissue reconstruction*, 2007; 2007; pp 496-504.
65. Mehvar, R., Dextrans for targeted and sustained delivery of therapeutic and imaging agents. *Journal of Controlled Release* **2000,** 69, (1), 1-25.
66. Sarmento, B.; Ribeiro, A.; Veiga, F.; Sampaio, P.; Neufeld, R.; Ferreira, D., Alginate/Chitosan nanoparticles are effective for oral insulin delivery. *Pharmaceutical Research* **2007,** 24, (12), 2198-2206.
67. Coviello, T.; Matricardi, P.; Marianecci, C.; Alhaique, F., Polysaccharide hydrogels for modified release formulations. *Journal of Controlled Release* **2007,** 119, (1), 5-24.
68. Gu, F.; Amsden, B.; Neufeld, R., Sustained delivery of vascular endothelial growth factor with alginate beads. *Journal of Controlled Release* **2004,** 96, (3), 463-472.
69. King, A.; Sandler, S.; Andersson, A., The effect of host factors and capsule composition on the cellular overgrowth on implanted alginate capsules. *Journal of Biomedical Materials Research* **2001,** 57, (3), 374-383.
70. Hwang, Y. S.; Cho, J.; Tay, F.; Heng, J. Y. Y.; Ho, R.; Kazarian, S. G.; Williams, D. R.; Boccaccini, A. R.; Polak, J. M.; Mantalaris, A., The use of murine embryonic stem cells, alginate encapsulation, and rotary microgravity bioreactor in bone tissue engineering. *Biomaterials* **2009,** 30, (4), 499-507.
71. Nagahama, H.; Nwe, N.; Jayakumar, R.; Koiwa, S.; Furuike, T.; Tamura, H., Novel biodegradable chitin membranes for tissue engineering applications. *Carbohydrate Polymers* **2008,** 73, (2), 295-302.
72. Maeda, Y.; Jayakumar, R.; Nagahama, H.; Furuike, T.; Tamura, H., Synthesis, characterization and bioactivity studies of novel beta-chitin scaffolds for tissue-engineering applications. *International Journal of Biological Macromolecules* **2008,** 42, (5), 463-467.
73. Nagahama, H.; Kashiki, T.; Nwe, N.; Jayakumar, R.; Furuike, T.; Tamura, H., Preparation of biodegradable chitin/gelatin membranes with GlcNAc for tissue engineering applications. *Carbohydrate Polymers* **2008,** 73, (3), 456-463.
74. Asensio, J. L.; Canada, F. J.; Siebert, H. C.; Laynez, J.; Poveda, A.; Nieto, P. M.; Soedjanaamadja, U. M.; Gabius, H. J.; Jimenez-Barbero, J., Structural basis for chitin recognition by defense proteins: GlcNAc residues are bound in a multivalent fashion by extended binding sites in hevein domains. *Chemistry & Biology* **2000,** 7, (7), 529-543.
75. Noh, H. K.; Lee, S. W.; Kim, J. M.; Oh, J. E.; Kim, K. H.; Chung, C. P.; Choi, S. C.; Park, W. H.; Min, B. M., Electrospinning of chitin nanofibers: Degradation behavior and cellular response to normal human keratinocytes and fibroblasts. *Biomaterials* **2006,** 27, (21), 3934-3944.

76. Li, J. L.; Pan, J. L.; Zhang, L. G.; Guo, X. J.; Yu, Y. T., Culture of primary rat hepatocytes within porous chitosan scaffolds. *Journal of Biomedical Materials Research Part A* **2003,** 67A, (3), 938-943.
77. Thierry, B.; Merhi, Y.; Silver, J.; Tabrizian, M., Biodegradable membrane-covered stent from chitosan-based polymers. *Journal of Biomedical Materials Research Part A* **2005,** 75A, (3), 556-566.
78. Zhang, L.; Ao, Q.; Wang, A. J.; Lu, G. Y.; Kong, L. J.; Gong, Y. D.; Zhao, N. M.; Zhang, X. F., A sandwich tubular scaffold derived from chitosan for blood vessel tissue engineering. *Journal of Biomedical Materials Research Part A* **2006,** 77A, (2), 277-284.
79. Seo, S. J.; Kim, I. Y.; Choi, Y. J.; Akaike, T.; Cho, C. S., Enhanced liver functions of hepatocytes cocultured with NIH 3T3 in the alginate/galactosylated chitosan scaffold. *Biomaterials* **2006,** 27, (8), 1487-1495.
80. Zhu, J. H.; Wang, X. W.; Ng, S.; Quek, C. H.; Ho, H. T.; Lao, X. J.; Yu, H., Encapsulating live cells with water-soluble chitosan in physiological conditions. *Journal of Biotechnology* **2005,** 117, (4), 355-365.
81. Ma, L.; Gao, C. Y.; Mao, Z. W.; Zhou, J.; Shen, J. C.; Hu, X. Q.; Han, C. M., Collagen/chitosan porous scaffolds with improved biostability for skin tissue engineering. *Biomaterials* **2003,** 24, (26), 4833-4841.
82. Bumgardner, J. D.; Wiser, R.; Gerard, P. D.; Bergin, P.; Chestnutt, B.; Marini, M.; Ramsey, V.; Elder, S. H.; Gilbert, J. A., Chitosan: potential use as a bioactive coating for orthopaedic and craniofacial/dental implants. *Journal of Biomaterials Science-Polymer Edition* **2003,** 14, (5), 423-438.
83. Mukherjee, D. P.; Tunkle, A. S.; Roberts, R. A.; Clavenna, A.; Rogers, S.; Smith, D., An animal evaluation of a paste of chitosan glutamate and hydroxyapatite as a synthetic bone graft material. *Journal of Biomedical Materials Research Part B-Applied Biomaterials* **2003,** 67B, (1), 603-609.
84. Muzzarelli, R. A. A.; Biagini, G.; Bellardini, M.; Simonelli, L.; Castaldini, C.; Fratto, G., Osteoconduction Exerted by Methylpyrrolidinone Chitosan Used in Dental Surgery. *Biomaterials* **1993,** 14, (1), 39-43.
85. Muzzarelli, R. A. A.; Zucchini, C.; Ilari, P.; Pugnaloni, A.; Belmonte, M. M.; Biagini, G.; Castaldini, C., Osteoconductive Properties of Methylpyrrolidinone Chitosan in an Animal-Model. *Biomaterials* **1993,** 14, (12), 925-929.
86. Sechriest, V. F.; Miao, Y. J.; Niyibizi, C.; Westerhausen-Larson, A.; Matthew, H. W.; Evans, C. H.; Fu, F. H.; Suh, J. K., GAG-augmented polysaccharide hydrogel: A novel biocompatible and biodegradable material to support chondrogenesis. *Journal of Biomedical Materials Research* **1999,** 49, (4), 534-541.
87. Masuko, T.; Iwasaki, N.; Yamane, S.; Funakoshi, T.; Majima, T.; Minami, A.; Ohsuga, N.; Ohta, T.; Nishimura, S. I., Chitosan-RGDSGGC conjugate as a scaffold material for musculoskeletal tissue engineering. *Biomaterials* **2005,** 26, (26), 5339-5347.
88. Liu, X. F.; Guan, Y. L.; Yang, D. Z.; Li, Z.; De Yao, K., Antibacterial action of chitosan and carboxymethylated chitosan. *Journal of Applied Polymer Science* **2001,** 79, (7), 1324-1335.

89. Durango, A. M.; Soares, N. F. F.; Benevides, S.; Teixeira, J.; Carvalho, M.; Wobeto, C.; Andrade, N. J., Development and evaluation of an edible antimicrobial film based on yam starch and chitosan. *Packaging Technology and Science* **2006,** 19, (1), 55-59.
90. Lee, C. H.; An, D. S.; Park, H. F.; Lee, D. S., Wide-spectrum antimicrobial packaging materials incorporating nisin and chitosan in the coating. *Packaging Technology and Science* **2003,** 16, (3), 99-106.
91. Fujita, M.; Kinoshita, M.; Ishihara, M.; Kanatani, Y.; Morimoto, Y.; Simizu, M.; Ishizuka, T.; Saito, Y.; Yura, H.; Matsui, T.; Takase, B.; Hattori, H.; Kikuchi, M.; Maehara, T., Inhibition of vascular prosthetic graft infection using a photocrosslinkable chitosan hydrogel. *Journal of Surgical Research* **2004,** 121, (1), 135-140.
92. Peng, C. K.; Yu, S. H.; Mi, F. L.; Shyu, S. S., Polysaccharide-based artificial extracellular matrix: Preparation and characterization of three-dimensional, macroporous chitosan and chondroitin sulfate composite scaffolds. *Journal of Applied Polymer Science* **2006,** 99, (5), 2091-2100.
93. Senel, S.; McClure, S. J., Potential applications of chitosan in veterinary medicine. *Advanced Drug Delivery Reviews* **2004,** 56, (10), 1467-1480.
94. Ishihara, M.; Nakanishi, K.; Ono, K.; Sato, M.; Kikuchi, M.; Saito, Y.; Yura, H.; Matsui, T.; Hattori, H.; Uenoyama, M.; Kurita, A., Photocrosslinkable chitosan as a dressing for wound occlusion and accelerator in healing process. *Biomaterials* **2002,** 23, (3), 833-840.
95. Ueno, H.; Nakamura, F.; Murakami, M.; Okumura, M.; Kadosawa, T.; Fujinaga, T., Evaluation effects of chitosan for the extracellular matrix production by fibroblasts and the growth factors production by macrophages. *Biomaterials* **2001,** 22, (15), 2125-2130.
96. Usami, Y.; Okamoto, Y.; Takayama, T.; Shigemasa, Y.; Minami, S., Chitin and chitosan stimulate canine polymorphonuclear cells to release leukotriene B-4 and prostaglandin E-2. *Journal of Biomedical Materials Research* **1998,** 42, (4), 517-522.
97. Mori, T.; Okumura, M.; Matsuura, M.; Ueno, K.; Tokura, S.; Okamoto, Y.; Minami, S.; Fujinaga, T., Effects of chitin and its derivatives on the proliferation and cytokine production of fibroblasts in vitro. *Biomaterials* **1997,** 18, (13), 947-951.
98. Muzzarelli, R. A. A., Chitins and chitosans for the repair of wounded skin, nerve, cartilage and bone. *Carbohydrate Polymers* **2009,** 76, (2), 167-182.
99. Lin, X. H.; Perrimon, N. In *Role of heparan sulfate proteoglycans in cell-cell signaling in Drosophila*, 2000; 2000; pp 303-307.
100. Iozzo, R. V., Matrix proteoglycans: From molecular design to cellular function. *Annual Review of Biochemistry* **1998,** 67, 609-652.
101. Roughley, P. J.; Melching, L. I.; Heathfield, T. F.; Pearce, R. H.; Mort, J. S., The structure and degradation of aggrecan in human intervertebral disc. *European Spine Journal* **2006,** 15, S326-S332.
102. Perrimon, N.; Bernfield, M., Specificities of heparan sulphate proteoglycans in developmental processes. *Nature* **2000,** 404, (6779), 725-728.

103. Bernfield, M.; Gotte, M.; Park, P. W.; Reizes, O.; Fitzgerald, M. L.; Lincecum, J.; Zako, M., Functions of cell surface heparan sulfate proteoglycans. *Annual Review of Biochemistry* **1999,** 68, 729-777.
104. Bathe, M.; Rutledge, G. C.; Grodzinsky, A. J.; Tidor, B., A coarse-grained molecular model for glycosaminoglycans: Application to chondroitin, chondroitin sulfate, and hyaluronic acid. *Biophysical Journal* **2005,** 88, (6), 3870-3887.
105. Luft, J. H., Fine structure of capillary and endocapillary layer as revealed by ruthenium red. *Federation Proceedings* **1966,** 25, (6P1), 1773-&.
106. Constantinescu, A. A.; Vink, H.; Spaan, J. A. E., Elevated capillary tube hematocrit reflects degradation of endothelial cell glycocalyx by oxidized LDL. *American Journal of Physiology-Heart and Circulatory Physiology* **2001,** 280, (3), H1051-H1057.
107. Nieuwdorp, M.; Meuwese, M. C.; Mooij, H. L.; Ince, C.; Broekhuizen, L. N.; Kastelein, J. J. P.; Stroes, E. S. G.; Vink, H., Measuring endothelial glycocalyx dimensions in humans: a potential novel tool to monitor vascular vulnerability. *Journal of Applied Physiology* **2008,** 104, (3), 845-852.
108. Huxley, V. H.; Williams, D. A., Role of a glycocalyx on coronary arteriole permeability to proteins: evidence from enzyme treatments. *American Journal of Physiology-Heart and Circulatory Physiology* **2000,** 278, (4), H1177-H1185.
109. Vink, H.; Duling, B. R., Identification of distinct luminal domains for macromolecules, erythrocytes, and leukocytes within mammalian capillaries. *Circulation Research* **1996,** 79, (3), 581-589.
110. Henry, C. B. S.; Duling, B. R., Permeation of the luminal capillary glycocalyx is determined by hyaluronan. *American Journal of Physiology-Heart and Circulatory Physiology* **1999,** 277, (2), H508-H514.
111. Bucior, I.; Burger, M. M., Carbohydrate-carbohydrate interactions in cell recognition. *Current Opinion in Structural Biology* **2004,** 14, (5), 631-637.
112. Iozzo, R. V.; Murdoch, A. D., Proteoglycans of the extracellular environment: Clues from the gene and protein side offer novel perspectives in molecular diversity and function. *Faseb Journal* **1996,** 10, (5), 598-614.
113. Dudhia, J., Aggrecan, aging and assembly in articular cartilage. *Cellular and Molecular Life Sciences* **2005,** 62, (19-20), 2241-2256.
114. Dean, D.; Han, L.; Grodzinsky, A. J.; Ortiz, C., Compressive nanomechanics of opposing aggrecan macromolecules. *Journal of Biomechanics* **2006,** 39, (14), 2555-2565.
115. Ng, L.; Grodzinsky, A. J.; Patwari, P.; Sandy, J.; Plaas, A.; Ortiz, C., Individual cartilage aggrecan macromolecules and their constituent glycosaminoglycans visualized via atomic force microscopy. *Journal of Structural Biology* **2003,** 143, (3), 242-257.
116. Papagiannopoulos, A.; Waigh, T. A.; Hardingham, T.; Heinrich, M., Solution structure and dynamics of cartilage aggrecan. *Biomacromolecules* **2006,** 7, (7), 2162-2172.
117. Horkay, F.; Basser, P. J.; Hecht, A. M.; Geissler, E., Gel-like behavior in aggrecan assemblies. *Journal of Chemical Physics* **2008,** 128, (13).
118. Horkay, F.; Basser, P. J.; Hecht, A. M.; Geissler, E., Gel-like behavior in aggrecan assemblies. *Journal of Chemical Physics* **2008,** 128, (13), -.

119. Seog, J.; Dean, D.; Rolauffs, B.; Wu, T.; Genzer, J.; Plaas, A. H. K.; Grodzinsky, A. J.; Ortiz, C., Nanomechanics of opposing glycosaminoglycan macromolecules. *Journal of Biomechanics* **2005,** 38, (9), 1789-1797.
120. Fujii, T.; Sun, Y. L.; An, K. N.; Luo, Z. P., Mechanical properties of single hyaluronan molecules. *Journal of Biomechanics* **2002,** 35, (4), 527-531.
121. Nap, R. J.; Szleifer, I., Structure and Interactions of Aggrecans: Statistical Thermodynamic Approach. *Biophysical Journal* **2008,** 95, (10), 4570-4583.
122. Lee, S. H.; Shin, H., Matrices and scaffolds for delivery of bioactive molecules in bone and cartilage tissue engineering. *Advanced Drug Delivery Reviews* **2007,** 59, (4-5), 339-359.
123. Li, L. P.; Herzog, W.; Korhonen, R. K.; Jurvelin, J. S., The role of viscoelasticity of collagen fibers in articular cartilage: axial tension versus compression. *Medical Engineering & Physics* **2005,** 27, (1), 51-57.
124. Pratta, M. A.; Yao, W. Q.; Decicco, C.; Tortorella, M. D.; Liu, R. Q.; Copeland, R. A.; Magolda, R.; Newton, R. C.; Trzaskos, J. M.; Arner, E. C., Aggrecan protects cartilage collagen from proteolytic cleavage. *Journal of Biological Chemistry* **2003,** 278, (46), 45539-45545.
125. Dahl, S. L. M.; Rhim, C.; Song, Y. C.; Niklason, L. E., Mechanical properties and compositions of tissue engineered and native arteries. *Annals of Biomedical Engineering* **2007,** 35, (3), 348-355.
126. Kenagy, R. D.; Plaas, A. H.; Wight, T. N., Versican degradation and vascular disease. *Trends in Cardiovascular Medicine* **2006,** 16, (6), 209-215.
127. Danielson, K. G.; Baribault, H.; Holmes, D. F.; Graham, H.; Kadler, K. E.; Iozzo, R. V., Targeted disruption of decorin leads to abnormal collagen fibril morphology and skin fragility. *Journal of Cell Biology* **1997,** 136, (3), 729-743.
128. Scott, J. E. In *Extracellular-Matrix, Supramolecular Organization and Shape*, 1995; 1995; pp 259-269.
129. Revell, D. J.; Knight, J. R.; Blyth, D. J.; Haines, A. H.; Russell, D. A., Self-assembled carbohydrate monolayers: Formation and surface selective molecular recognition. *Langmuir* **1998,** 14, (16), 4517-4524.
130. Hederos, M.; Konradsson, P.; Liedberg, B., Synthesis and self-assembly of galactose-terminated alkanethiols and their ability to resist proteins. *Langmuir* **2005,** 21, (7), 2971-2980.
131. Ostuni, E.; Chapman, R. G.; Holmlin, R. E.; Takayama, S.; Whitesides, G. M., A Survey of Structure-Property Relationships of Surfaces that Resist the Adsorption of Protein. *Langmuir* **2001,** 17, (18), 5605-5620.
132. Luk, Y. Y.; Kato, M.; Mrksich, M., Self-assembled monolayers of alkanethiolates presenting mannitol groups are inert to protein adsorption and cell attachment. *Langmuir* **2000,** 16, (24), 9604-9608.
133. Zhi, Z. L.; Powell, A. K.; Turnbull, J. E., Fabrication of carbohydrate microarrays on gold surfaces: Direct attachment of nonderivatized oligosaccharides to hydrazide-modified self-assembled monolayers. *Analytical Chemistry* **2006,** 78, (14), 4786-4793.
134. Raynor, J. E.; Petrie, T. A.; Fears, K. P.; Latour, R. A.; Garcia, A. J.; Collard, D. M., Saccharide Polymer Brushes To Control Protein and Cell Adhesion to Titanium. *Biomacromolecules* **2009,** 10, (4), 748-755.

135. Cao, X.; Pettit, M. E.; Conlan, S. L.; Wagner, W.; Ho, A. D.; Clare, A. S.; Callow, J. A.; Callow, M. E.; Grunze, M.; Rosenhahn, A., Resistance of Polysaccharide Coatings to Proteins, Hematopoietic Cells, and Marine Organisms. *Biomacromolecules* **2009,** 10, (4), 907-915.
136. Decher, G., Fuzzy nanoassemblies: Toward layered polymeric multicomposites. *Science* **1997,** 277, (5330), 1232-1237.
137. Decher, G., Polyelectrolyte multilayers, an overview. In *Multilayer Thin Films Sequential Essembly of Nanocomposite Materials*, Decher, G.; Schlenoff, J. B., Eds. Wiley-VCH Verlag GmbH & Co.: Weinheim, **2003**; pp 1-46.
138. Decher, G.; Hong, J. D., Buildup of ultrathin multilayer films by a self-assembly process .2. Consecutive adsoption of anionic and cationic bipolar amphiphilies and polyelectrolytes on charged surfaces. *Berichte Der Bunsen-Gesellschaft-Physical Chemistry Chemical Physics* **1991,** 95, (11), 1430-1434.
139. Decher, G.; Hong, J. D.; Schmitt, J., Buildup of Ultrathin Multilayer Films by a Self-Assembly Process .3. Consecutively Alternating Adsorption of Anionic and Cationic Polyelectrolytes on Charged Surfaces. *Thin Solid Films* **1992**, 831-835.
140. Decher, G.; Lehr, B.; Lowack, K.; Lvov, Y.; Schmitt, J. New nanocomposite films for biosensors - layer-by-layer adsorbed films of polyelectrolytes, proteins of DNA. *Biosensors and bioelectronics* **1994**, 9, (9-10), 677-684.
141. Bertrand, P.; Jonas, A.; Laschewsky, A.; Legras, R., Ultrathin polymer coatings by complexation of polyelectrolytes at interfaces: suitable materials, structure and properties. *Macromolecular Rapid Communications* **2000,** 21, (7), 319-348.
142. Hammond, P. T., Recent explorations in electrostatic multilayer thin film assembly. *Current Opinion in Colloid & Interface Science* **1999,** 4, (6), 430-442.
143. Caruso, F.; Niikura, K.; Furlong, D. N.; Okahata, Y., Assembly of alternating polyelectrolyte and protein multilayer films for immunosensing .2. *Langmuir* **1997,** 13, (13), 3427-3433.
144. Schneider, S.; Feilen, P. J.; Slotty, V.; Kampfner, D.; Preuss, S.; Berger, S.; Beyer, J.; Pommersheim, R., Multilayer capsules: a promising microencapsulation system for transplantation of pancreatic islets. *Biomaterials* **2001,** 22, (14), 1961-1970.
145. Crouzier, T.; Ren, K.; Nicolas, C.; Roy, C.; Picart, C., Layer-By-Layer Films as a Biomimetic Reservoir for rhBMP-2 Delivery: Controlled Differentiation of Myoblasts to Osteoblasts. *Small* **2009,** 5, (5), 598-608.
146. Itoh, Y.; Matsusaki, M.; Kida, T.; Akashi, M., Locally controlled release of basic fibroblast growth factor from multilayered capsules. *Biomacromolecules* **2008,** 9, (8), 2202-2206.
147. Dubas, S. T.; Schlenoff, J. B., Factors controlling the growth of polyelectrolyte multilayers. *Macromolecules* **1999,** 32, (24), 8153-8160.
148. Kato, N.; Schuetz, P.; Fery, A.; Caruso, F., Thin Multilayer Films of Weak Polyelectrolytes on Colloid Particles. *Macromolecules* **2002,** 35, 9780-9787.
149. Choi, J.; Rubner, M. F., Influence of the degree of ionization on weak polyelectrolyte multilayer assembly. *Macromolecules* **2005,** 38, (1), 116-124.
150. Steitz, R.; Jaeger, W.; von Klitzing, R., Influence of charge density and ionic strength on the multilayer formation of strong polyelectrolytes. *Langmuir* **2001,** 17, (15), 4471-4474.

151. Boddohi, S.; Killingsworth, C. E.; Kipper, M. J., Polyelectrolyte multilayer assembly as a function of pH and ionic strength using the polysaccharides chitosan and heparin. *Biomacromolecules* **2008,** 9, 2021-2028.
152. Hoogeveen, N. G.; Stuart, M. A. C.; Fleer, G. J.; Bohmer, M. R., Formation and stability of multilayers of polyelectrolytes. *Langmuir* **1996,** 12, (15), 3675-3681.
153. Hiller, J.; Rubner, M. F., Reversible molecular memory and pH-switchable swelling transitions in polyelectrolyte multilayers. *Macromolecules* **2003,** 36, (11), 4078-4083.
154. Shiratori, S. S.; Rubner, M. F., pH-dependent thickness behavior of sequentially adsorbed layers of weak polyelectrolytes. *Macromolecules* **2000,** 33, (11), 4213-4219.
155. Schoeler, B.; Kumaraswamy, G.; Caruso, F., Investigation of the influence of polyelectrolyte charge density on the growth of multilayer thin films prepared by the layer-by-layer technique. *Macromolecules* **2002,** 35, (3), 889-897.
156. Sui, Z. J.; Salloum, D.; Schlenoff, J. B., Effect of molecular weight on the construction of polyelectrolyte multilayers: Stripping versus sticking. *Langmuir* **2003,** 19, (6), 2491-2495.
157. Stockton, W. B.; Rubner, M. F., Molecular-level processing of conjugated polymers .4. Layer-by-layer manipulation of polyaniline via hydrogen-bonding interactions. *Macromolecules* **1997,** 30, (9), 2717-2725.
158. Plummer, S. T.; Wang, Q.; Bohn, P. W.; Stockton, R.; Schwartz, M. A., Electrochemically derived gradients of the extracellular matrix protein fibronectin on gold. *Langmuir* **2003,** 19, (18), 7528-7536.
159. Shimazaki, Y.; Mitsuishi, M.; Ito, S.; Yamamoto, M., Preparation of the layer-by-layer deposited ultrathin film based on the charge-transfer interaction. *Langmuir* **1997,** 13, (6), 1385-1387.
160. Li, D.; Jiang, Y. D.; Wu, Z. M.; Chen, X. D.; Li, Y. R., Fabrication of self-assembled polyaniline films by doping-induced deposition. *Thin Solid Films* **2000,** 360, (1-2), 24-27.
161. Hatzor, A.; Moav, T.; Cohen, H.; Matlis, S.; Libman, J.; Vaskevich, A.; Shanzer, A.; Rubinstein, I., Coordination-controlled self-assembled multilayers on gold. *Journal of the American Chemical Society* **1998,** 120, (51), 13469-13477.
162. Schonhoff, M., Self-assembled polyelectrolyte multilayers. *Current Opinion in Colloid & Interface Science* **2003,** 8, (1), 86-95.
163. Yoo, D.; Shiratori, S. S.; Rubner, M. F., Controlling bilayer composition and surface wettability of sequentially adsorbed multilayers of weak polyelectrolytes. *Macromolecules* **1998,** 31, (13), 4309-4318.
164. Fu, J. H.; Ji, J.; Yuan, W. Y.; Shen, J. C., Construction of anti-adhesive and antibacterial multilayer films via layer-by-layer assembly of heparin and chitosan. *Biomaterials* **2005,** 26, (33), 6684-6692.
165. Kujawa, P.; Moraille, P.; Sanchez, J.; Badia, A.; Winnik, F. M., Effect of molecular weight on the exponential growth and morphology of hyaluronan/chitosan multilayers: A surface plasmon resonance spectroscopy and atomic force microscopy investigation. *Journal of the American Chemical Society* **2005,** 127, (25), 9224-9234.

166. Thierry, B.; Winnik, F. M.; Merhi, Y.; Silver, J.; Tabrizian, M., Bioactive coatings of endovascular stents based on polyelectrolyte multilayers. *Biomacromolecules* **2003,** 4, (6), 1564-1571.
167. Richert, L.; Lavalle, P.; Payan, E.; Shu, X. Z.; Prestwich, G. D.; Stoltz, J. F.; Schaaf, P.; Voegel, J. C.; Picart, C., Layer by layer buildup of polysaccharide films: Physical chemistry and cellular adhesion aspects. *Langmuir* **2004,** 20, (2), 448-458.
168. Elbert, D. L.; Herbert, C. B.; Hubbell, J. A., Thin polymer layers formed by polyelectrolyte multilayer techniques on biological surfaces. *Langmuir* **1999,** 15, (16), 5355-5362.
169. Richert, L.; Lavalle, P.; Vautier, D.; Senger, B.; Stoltz, J. F.; Schaaf, P.; Voegel, J. C.; Picart, C., Cell interactions with polyelectrolyte multilayer films. *Biomacromolecules* **2002,** 3, (6), 1170-1178.
170. Serizawa, T.; Yamaguchi, M.; Akashi, M., Alternating bioactivity of polymeric layer-by-layer assemblies: Anticoagulation vs procoagulation of human blood. *Biomacromolecules* **2002,** 3, (4), 724-731.
171. Yang, M. C.; Lin, W. C., Protein adsorption and platelet adhesion of polysulfone membrane immobilized with chitosan and heparin conjugate. *Polymers for Advanced Technologies* **2003,** 14, (2), 103-113.
172. Meng, S.; Liu, Z.; Shen, L.; Guo, Z.; Chou, L. L.; Zhong, W.; Du, Q.; Ge, J., The effect of a layer-by-layer chitosan-heparin coating on the endothelialization and coagulation properties of a coronary stent system. *Biomaterials* **2009,** 30, (12), 2276-2283.
173. Kreke, M. R.; Badami, A. S.; Brady, J. B.; Akers, R. M.; Goldstein, A. S., Modulation of protein adsorption and cell adhesion by poly(allylamine hydrochloride) heparin films. *Biomaterials* **2005,** 26, (16), 2975-2981.
174. Morgan, S. E.; Jones, P.; Lamont, A. S.; Heidenreich, A.; McCormick, C. L., Layer-by-layer assembly of pH-responsive, compositionally controlled (co)polyelectrolytes synthesized via RAFT. *Langmuir* **2007,** 23, (1), 230-240.
175. Schneider, A.; Vodouhe, C.; Richert, L.; Francius, G.; Le Guen, E.; Schaaf, P.; Voegel, J. C.; Frisch, B.; Picart, C., Multifunctional polyelectrolyte multilayer films: Combining mechanical resistance, biodegradability, and bioactivity. *Biomacromolecules* **2007,** 8, (1), 139-145.
176. Picart, C.; Elkaim, R.; Richert, L.; Audoin, T.; Arntz, Y.; Cardoso, M. D.; Schaaf, P.; Voegel, J. C.; Frisch, B., Primary cell adhesion on RGD-functionalized and covalently crosslinked thin polyelectrolyte multilayer films. *Advanced Functional Materials* **2005,** 15, (1), 83-94.
177. Schneider, A.; Francius, G.; Obeid, R.; Schwinte, P.; Hemmerle, J.; Frisch, B.; Schaaf, P.; Voegel, J. C.; Senger, B.; Picart, C., Polyelectrolyte multilayers with a tunable Young's modulus: Influence of film stiffness on cell adhesion. *Langmuir* **2006,** 22, (3), 1193-1200.
178. Kolarik, L.; Furlong, D. N.; Joy, H.; Struijk, C.; Rowe, R., Building assemblies from high molecular weight polyelectrolytes. *Langmuir* **1999,** 15, (23), 8265-8275.
179. Boddohi, S.; Almodovar, J.; Zhang, H.; Johnson, P. A.; Kipper, M. J., Layer-by-layer assembly of polysaccharide-based nanostructured surfaces containing

polyelectrolyte complex nanoparticles. *Colloids and Surfaces B-Biointerfaces* **2009 (Submitted)**.

180. Lin, Q.-K.; Ren, K.-F.; Ji, J., Hyaluronic acid and chitosan-DNA complex multilayered thin film as surface-mediated nonviral gene delivery system. *Colloids and Surfaces B: Biointerfaces* **2009,** 74, (1), 298-303.
181. Ma, L.; Zhou, J.; Gao, C. Y.; Shen, J. C., Incorporation of basic fibroblast growth factor by a layer-by-layer assembly technique to produce bioactive substrates. *Journal of Biomedical Materials Research Part B-Applied Biomaterials* **2007,** 83B, (1), 285-292.
182. Matsusaki, M.; Sakaguchi, H.; Serizawa, T.; Akashi, M., Controlled release of vascular endothelial growth factor from alginate hydrogels nano-coated with polyelectrolyte multilayer films. *Journal of Biomaterials Science -- Polymer Edition* **2007,** 18, (6), 775-783.
183. Thunemann, A. F.; Muller, M.; Dautzenberg, H.; Joanny, J. F. O.; Lowne, H., Polyelectrolyte complexes. *Polyelectrolytes with Defined Molecular Architecture Ii* **2004,** 166, 113-171.
184. Philipp, B.; Dautzenberg, H.; Linow, K. J.; Kotz, J.; Dawydoff, W., Poly-Electrolyte Complexes - Recent Developments and Open Problems. *Progress in Polymer Science* **1989,** 14, (1), 91-172.
185. Tsuchida, E.; Osada, Y.; Ohno, H., Formation of intepolymer complexes. *Journal of Macromolecular Science-Physics* **1980,** B17, (4), 683-714.
186. Tsuchida, E.; Abe, K., Interactions between macromolecules in solution and intermacromolecular complexes. *Advances in Polymer Science* **1982,** 45, 1-119.
187. Tsuchida, E.; Osada, Y.; Sanada, K., Interaction of poly(styrene sulfonate) with polycations carrying charges in the chain backbone. *Journal of Polymer Science: Polymer Chemistry Edition* **1972,** 10, 3397-3404.
188. Kabanov, V.; Zezin, A., Soluble interpolymeric complexes as a new class of synthetic polyelectrolytes. *Pure and Applied Chemistry* **1984,** 56, (3), 343-354.
189. Kabanov, V. A.; Zezin, A. B.; Rogacheva, V. B.; Ryzhikov, S. V., Disproportionation of nonstoichiometric poly-electrolyte complexes in water-salt solutions. *Doklady Akademii Nauk Sssr* **1982,** 267, (4), 862-865.
190. Dautzenberg, H., Polyelectrolyte complex formation in highly aggregating systems. 1. Effect of salt: Polyelectrolyte complex formation in the presence of NaCl. *Macromolecules* **1997,** 30, (25), 7810-7815.
191. Tsuchida, E., Formation of Polyelectrolyte Complexes and Their Structures. *Journal of Macromolecular Science-Pure and Applied Chemistry* **1994,** A31, (1), 1-15.
192. Dautzenberg, H.; Karibyants, N., Polyelectrolyte complex formation in highly aggregating systems. Effect of salt: response to subsequent addition of NaCl. *Macromolecular Chemistry and Physics* **1999,** 200, (1), 118-125.
193. Dautzenberg, H.; Jaeger, W., Effect of charge density on the formation and salt stability of polyelectrolyte complexes. *Macromolecular Chemistry and Physics* **2002,** 203, (14), 2095-2102.
194. Kikuchi, Y.; Noda, A., Polyelectrolyte Complexes of Heparin with Chitosan. *Journal of Applied Polymer Science* **1976,** 20, (9), 2561-2563.

195. Kikuchi, Y., Polyelectrolyte complexes of heparin with chitosan. *Nippon Kagaku Kaishi* **1973**, (12), 2436-2438.
196. Kikuchi, Y., Polyelectrolyte Complex of Heparin with Chitosan. *Makromolekulare Chemie-Macromolecular Chemistry and Physics* **1974,** 175, (7), 2209-2211.
197. Schatz, C.; Domard, A.; Viton, C.; Pichot, C.; Delair, T., Versatile and efficient formation of colloids of biopolymer-based polyelectrolyte complexes. *Biomacromolecules* **2004,** 5, (5), 1882-1892.
198. Schatz, C.; Lucas, J. M.; Viton, C.; Domard, A.; Pichot, C.; Delair, T., Formation and properties of positively charged colloids based on polyelectrolyte complexes of biopolymers. *Langmuir* **2004,** 20, (18), 7766-7778.
199. Drogoz, A.; David, L.; Rochas, C.; Domard, A.; Delair, T., Polyelectrolyte complexes from polysaccharides: Formation and stoichiometry monitoring. *Langmuir* **2007,** 23, (22), 10950-10958.
200. Chen, W. B.; Wang, L. F.; Chen, J. S.; Fan, S. Y., Characterization of polyelectrolyte complexes between chondroitin sulfate and chitosan in the solid state. *Journal of Biomedical Materials Research Part A* **2005,** 75A, (1), 128-137.
201. Denuziere, A.; Ferrier, D.; Domard, A., Chitosan-chondroitin sulfate and chitosan-hyaluronate polyelectrolyte complexes. Physico-chemical aspects. *Carbohydrate Polymers* **1996,** 29, (4), 317-323.
202. Denuziere, A.; Ferrier, D.; Damour, O.; Domard, A., Chitosan-chondroitin sulfate and chitosan-hyaluronate polyelectrolyte complexes: biological properties. *Biomaterials* **1998,** 19, (14), 1275-1285.
203. Kweon, D. K.; Lim, S. T., Preparation and characteristics of a water-soluble chitosan-heparin complex. *Journal of Applied Polymer Science* **2003,** 87, (11), 1784-1789.
204. Boddohi, S.; Moore, N.; Johnson, P. A.; Kipper, M. J., Polysaccharide-based polyelectrolyte complex nanoparticles from chitosan, heparin, and hyaluronan. *Biomacromolecules* **2009,** 10, 1402-1409.
205. Davidenko, N.; Blanco, M. D.; Peniche, C.; Becheran, L.; Guerrero, S.; Teijon, J. M., Effects of Different Parameters on the Characteristics of Chitosan-Poly(acrylic acid) Nanoparticles Obtained by the Method of Coacervation. *Journal of Applied Polymer Science* **2009,** 111, (5), 2362-2371.
206. Chen, Q.; Hu, Y.; Chen, Y.; Jiang, X. Q.; Yang, Y. H., Microstructure formation and property of chitosan-poly (acrylic acid) nanoparticles prepared by macromolecular complex. *Macromolecular Bioscience* **2005,** 5, (10), 993-1000.
207. Singh, R.; Lillard, J. W., Nanoparticle-based targeted drug delivery. *Experimental and Molecular Pathology* **2009,** 86, (3), 215-223.
208. Moghimi, S. M.; Hunter, A. C.; Murray, J. C., Long-circulating and target-specific nanoparticles: Theory to practice. *Pharmacological Reviews* **2001,** 53, (2), 283-318.
209. Calvo, P.; RemunanLopez, C.; VilaJato, J. L.; Alonso, M. J., Chitosan and chitosan ethylene oxide propylene oxide block copolymer nanoparticles as novel carriers for proteins and vaccines. *Pharmaceutical Research* **1997,** 14, (10), 1431-1436.

210. Calvo, P.; RemunanLopez, C.; VilaJato, J. L.; Alonso, M. J., Novel hydrophilic chitosan-polyethylene oxide nanoparticles as protein carriers. *Journal of Applied Polymer Science* **1997,** 63, (1), 125-132.
211. van der Lubben, I. M.; Verhoef, J. C.; Borchard, G.; Junginger, H. E., Chitosan and its derivatives in mucosal drug and vaccine delivery. *European Journal of Pharmaceutical Sciences* **2001,** 14, (3), 201-207.
212. Motwani, S. K.; Chopra, S.; Talegaonkar, S.; Kohl, K.; Ahmad, F. J.; Khar, R. K., Chitosan-sodium alginate nanoparticles as submicroscopic reservoirs for ocular delivery: Formulation, optimisation and in vitro characterisation. *European Journal of Pharmaceutics and Biopharmaceutics* **2008,** 68, (3), 513-525.
213. de la Fuente, M.; Seijo, B.; Alonso, M. J., Novel hyaluronan-based nanocarriers for transmucosal delivery of macromolecules. *Macromolecular Bioscience* **2008,** 8, (5), 441-450.
214. Teijeiro-Osorio, D.; Remunan-Lopez, C.; Alonso, M. J., New Generation of Hybrid Poly/Oligosaccharide Nanoparticles as Carriers for the Nasal Delivery of Macromolecules. *Biomacromolecules* **2009,** 10, (2), 243-249.
215. Hartig, S. M.; Greene, R. R.; Carlesso, G.; Higginbotham, J. N.; Khan, W. N.; Prokop, A.; Davidson, J. M., Kinetic analysis of nanoparticulate polyelectrolyte complex interactions with endothelial cells. *Biomaterials* **2007,** 28, (26), 3843-3855.
216. Jean, M.; Smaoui, F.; Lavertu, M.; Methot, S.; Bouhdoud, L.; Buschmann, M. D.; Merzouki, A., Chitosan-plasmid nanoparticle formulations for IM and SC delivery of recombinant FGF-2 and PDGF-BB or generation of antibodies. *Gene Therapy* **2009,** 16, (9), 1097-1110.
217. Liu, W. G.; Sun, S. J.; Cao, Z. Q.; Xin, Z.; Yao, K. D.; Lu, W. W.; Luk, K. D. K., An investigation on the physicochemical properties of chitosan/DNA polyelectrolyte complexes. *Biomaterials* **2005,** 26, (15), 2705-2711.
218. Prego, C.; Garcia, M.; Torres, D.; Alonso, M. J. In *Transmucosal macromolecular drug delivery*, 2005; 2005; pp 151-162.
219. Zhang, Y. Z.; Su, B.; Ramakrishna, S.; Lim, C. T., Chitosan nanofibers from an easily electrospinnable UHMWPEO-doped chitosan solution system. *Biomacromolecules* **2008,** 9, (1), 136-141.
220. Vondran, J. L.; Sun, W.; Schauer, C. L., Crosslinked, electrospun chitosan-poly(ethylene oxide) nanofiber mats. *Journal of Applied Polymer Science* **2008,** 109, (2), 968-975.
221. Sajeev, U. S.; Anand, K. A.; Menon, D.; Nair, S., Control of nanostructures in PVA, PVA/chitosan blends and PCL through electrospinning. *Bulletin of Materials Science* **2008,** 31, (3), 343-351.
222. Yoshimoto, H.; Shin, Y. M.; Terai, H.; Vacanti, J. P., A biodegradable nanofiber scaffold by electrospinning and its potential for bone tissue engineering. *Biomaterials* **2003,** 24, (12), 2077-2082.
223. Xu, C. Y.; Inai, R.; Kotaki, M.; Ramakrishna, S., Aligned biodegradable nanotibrous structure: a potential scaffold for blood vessel engineering. *Biomaterials* **2004,** 25, (5), 877-886.

224. Li, W. J.; Tuli, R.; Okafor, C.; Derfoul, A.; Danielson, K. G.; Hall, D. J.; Tuan, R. S., A three-dimensional nanofibrous scaffold for cartilage tissue engineering using human mesenchymal stem cells. *Biomaterials* **2005,** 26, (6), 599-609.
225. Ohkawa, K.; Cha, D. I.; Kim, H.; Nishida, A.; Yamamoto, H., Electrospinning of chitosan. *Macromolecular Rapid Communications* **2004,** 25, (18), 1600-1605.
226. Torres-Giner, S.; Ocio, M. J.; Lagaron, J. M., Development of active antimicrobial fiber based chitosan polysaccharide nanostructures using electrospinning. *Engineering in Life Sciences* **2008,** 8, (3), 303-314.
227. Duan, B.; Dong, C. H.; Yuan, X. Y.; Yao, K. D., Electrospinning of chitosan solutions in acetic acid with poly(ethylene oxide). *Journal of Biomaterials Science-Polymer Edition* **2004,** 15, (6), 797-811.
228. Bhattarai, N.; Edmondson, D.; Veiseh, O.; Matsen, F. A.; Zhang, M. Q., Electrospun chitosan-based nanofibers and their cellular compatibility. *Biomaterials* **2005,** 26, (31), 6176-6184.
229. Viswanathan, G.; Murugesan, S.; Pushparaj, V.; Nalamasu, O.; Ajayan, P. M.; Linhardt, R. J., Preparation of biopolymer fibers by electrospinning from room temperature ionic liquids. *Biomacromolecules* **2006,** 7, (2), 415-418.
230. Subramanian, A.; Vu, D.; Larsen, G. F.; Lin, H. Y., Preparation and evaluation of the electrospun chitosan/PEO fibers for potential applications in cartilage tissue engineering. *Journal of Biomaterials Science-Polymer Edition* **2005,** 16, (7), 861-873.
231. Muller, K.; Quinn, J. F.; Johnston, A. P. R.; Becker, M.; Greiner, A.; Caruso, F., Polyelectrolyte functionalization of electrospun fibers. *Chemistry of Materials* **2006,** 18, (9), 2397-2403.
232. Reihs, T.; Müller, M.; Lunkwitz, K., Preparation and adsorption of refined polyelectrolyte complex nanoparticles. *Journal of Colloid and Interface Science* **2004,** 271, (1), 69-79.
233. Sennerfors, T.; Bogdanovic, G.; Tiberg, F., Formation, chemical composition, and structure of polyelectrolyte-nanoparticle multilayer films. *Langmuir* **2002,** 18, (16), 6410-6415.
234. Bogdanovic, G.; Sennerfors, T.; Zhmud, B.; Tiberg, F., Formation and structure of polyelectrolyte and nanoparticle multilayers: Effect of particle characteristics. *Journal of Colloid and Interface Science* **2002,** 255, (1), 44-51.
235. Grigoriev, D.; Gorin, D.; Sukhorukov, G. B.; Yashchenok, A.; Maltseva, E.; Mohwald, H., Polyelectrolyte/magnetite nanoparticle multilayers: Preparation and structure characterization. *Langmuir* **2007,** 23, (24), 12388-12396.
236. Li, Q.; Quinn, J. F.; Wang, Y. J.; Caruso, F., Preparation of nanoporous polyelectrolyte multilayer films via nanoparticle templating. *Chemistry of Materials* **2006,** 18, (23), 5480-5485.

Chapter 3

Polyelectrolyte Multilayer Assembly as a Function of pH and Ionic Strength Using the Polysaccharides Chitosan and Heparin

- **S. Boddohi**, C.E. Killingsworth, M.J. Kipper, "Polyelectrolyte multilayer assembly as a function of pH and ionic strength using the polysaccharides chitosan and heparin." *Biomacromolecules,* 9, 2021-2028, 2008.

3.1 Abstract

The goal of this work is to explore the effects of solution ionic strength and pH on polyelectrolyte multilayer (PEM) assembly, using biologically derived polysaccharides as the polyelectrolytes. We used the layer-by-layer (LBL) technique to assemble PEM of the polysaccharides heparin (a strong polyanion) and chitosan (a weak polycation) and characterized the sensitivity of the PEM composition and layer thickness to changes in processing parameters. Fourier-transform surface plasmon resonance (FT-SPR) and spectroscopic ellipsometry provided *in situ* and *ex situ* measurements of the PEM thickness, respectively. Vibrational spectroscopy and X-ray photoelectron spectroscopy (XPS) provided details of the chemistry (i.e. composition, electrostatic interactions) of the PEM. We found that when PEM were assembled from 0.2 M buffer, the PEM thickness could be increased from less than 2 nm per bilayer to greater than 4 nm per bilayer by changing the solution pH; higher and lower ionic strength buffer solutions resulted in narrower ranges of accessible thickness. Molar composition of the PEM was not very

sensitive to solution pH or ionic strength, but pH did affect the interactions between the sulfonates in heparin and amines in chitosan when PEM were assembled from 0.2 M buffer. Changes in the PEM thickness with pH and ionic strength can be interpreted through descriptions of the charge density and conformation of the polyelectrolyte chains in solution.

3.2 Introduction

During the past decade, the layer-by-layer (LBL) deposition of polyelectrolyte multilayers (PEM) has been demonstrated to be a simple, reproducible technique for the fabrication of structural and functional nanoscale thin films deposited on solid substrates such as gold, glass, or silicon.[1, 2] PEM are of scientific and technological interest because of the many possible variations on a single simple theme and the ability to accurately control the assembly of materials at the nanometer length scale. In the LBL deposition of PEM, oppositely charged polymers are alternately adsorbed to a charged surface. The surface charge density is inverted at each adsorption step, limiting the layer thickness and preparing the surface for the subsequent adsorption step.[3] Electrostatic interactions between the polyelectrolyte in solution and the surface are the key to the final structure of the PEM.[4] The electrostatic interactions governing the LBL assembly are affected by solution conditions such as the charge density of the polymers, solution pH,[5, 6] salt concentration,[3] and valency of small molecular weight ions. The pH-dependent electrostatics of weak polyelectrolytes have been exploited by several groups to tune PEM structure.[7-9] Dependence of multilayer thickness on pH was studied in detail by Shiratori and co-workers, using a synthetic weak polyanion/polycation pair.[8] Most of the

experimental research aimed at understanding the physical chemistry of PEM assembly has been conducted using synthetic polyelectrolytes.

Biologically derived polysaccharides, many of which are polyelectrolytes, are rapidly gaining a place of prominence as chemistries with enormous potential for new biomedical technologies.[10] Because heparin and other glycosaminoglycans are presented in materials organized at the nanometer length scale *in vivo* (as components of both the extracellular matrix and the glycocalyx of many organs and tissues), we propose that exploiting their biochemical functionality to design new biomaterials will require an ability to tune the structure and composition of these materials at the nanometer length scale.

This work uses the polysaccharides chitosan (a weak polycation) and heparin (a strong polyanion). Figure 3.1 shows the structure of chitosan and heparin. The pendent primary amines make chitosan a weak polyanion, with an intrinsic pK_a varying from 6.46 to 7.32.[11] Chitosan is insoluble in most solvents and insoluble in aqueous solutions above its pK_a, but protonation of the amine below its pK_a makes chitosan soluble in dilute aqueous solutions of organic acids such as acetic acid, formic acid, succinic acid, lactic acid and malic acid.[12, 13] The conformation and the size of chitosan chains in dilute solution depend upon the charge density and ionic strength.[14] Reducing the charge density of chitosan, either by increasing solution pH or ionic strength, results in reduction in chain dimensions corresponding to collapse of the polymer.[15] Heparin consists of sulfonated D-glucosamine units, joined in alternating sequence by $\alpha(1,4)$-glycosidic linkages, to either D-glucuronic or L-iduronic acid.[16] Heparin has the highest negative charge density of any known biological polyanion, due to the presence of carboxyl and sulfonate groups.[17] It thus is prone to ionic interaction with a variety of proteins such as

extra cellular matrix proteins, enzymes, and growth factors. The ability of heparin to bind and activate fibroblast growth factors[18, 19] and bone morphogenetic proteins[20, 21] involved in osteoblast and chondrocyte activation and differentiation suggest heparin is a promising candidate material for skeletal tissue engineering.[22]

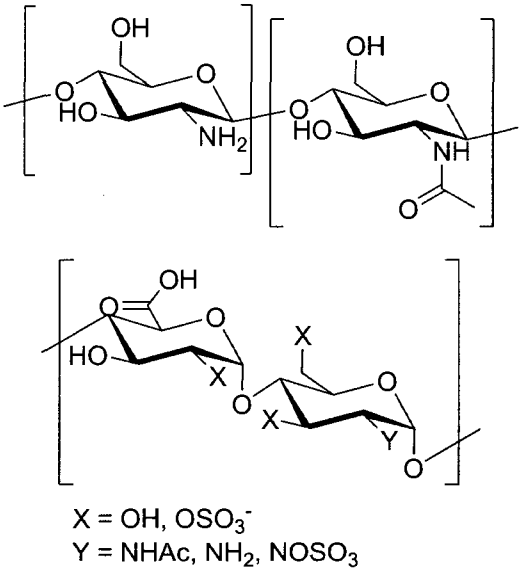

Figure 3.1. Chitosan (top) and heparin (bottom).

The electrostatic complexation of heparin and chitosan has been described both in solution,[23-25] and at surfaces.[26] Fu *et al.* characterized PEM of chitosan and heparin assembled on modified poly(ethylene terephthalate) surfaces by contact angle, atomic force microscopy, lateral force microscopy, and UV-visible spectroscopy.[26] Their focus was on the film roughness, wetability, and antimicrobial activity.[26]

In this paper we characterize the affect of processing parameters on thickness of the heparin/chitosan PEM using *in-situ* Fourier-transform surface plasmon resonance (FT-SPR) and *ex-situ* ellipsometry. We have investigated the assembly of PEM from chitosan

and heparin by their sequential electrostatic adsorption onto gold surfaces from aqueous solutions with pH and ionic strength varied over the range from 4.6 to 5.8, and 0.1 M to 0.5 M, respectively. We have investigated whether nanoscale control can be achieved over the film thickness by varying these reproducible processing conditions. Furthermore, we characterized the chemistry of these materials using X-ray photoelectron spectroscopy (XPS) and polarization modulation infra-red reflection absorption spectroscopy (PM-IRRAS). It is important to note that all of the characterization described above was performed on PEM assembled on a single platform. That is, the PEM thickness measurements from FT-SPR and ellipsometry, and the chemical analysis using PM-IRRAS and XPS were all performed on PEM assembled on gold surfaces.

3.3 Experimental

3.3.1 Materials.

Chitosan (poly (β-(1,4)-D-glucosamine-*co*-*N*-acetyl-D-glucosamine)) (4.7 % acetylated) was purchased from Biosyntech Inc. (Laval, Canada). Heparin sodium (from porcine intestinal mucosa, 12.5 % sulfur) was purchased from Celsus Laboratories (Cincinnati, OH). 11-mercaptoundecanioc acid 95% (MUA) was purchased from Sigma-Aldrich (St. Louis, MO). 18 mm by 18 mm SF10 glass chips were purchased from GWC Technologies Inc. (Madison, WI). Gold was purchased from Alfa Aesar (Ward Hill, MA). Glacial acetic acid and ethanol (200 proof 99.5+ %) were purchased from Acros Organics (Geel, Belgium). Sodium acetate was purchased from Fisher Scientific (Pittsburgh, PA). A Millipore Synthesis water purification unit was used to obtain 18.2 MΩ water, used for making all aqueous solutions (Millipore, Billerica, MA).

Chitosan and heparin were analyzed using a Viscotek gel permeation chromatograph (GPC) (Houston, TX) using a GPC Max (autosampler, solvent delivery pump, and solvent degasser) equipped with a column oven, differential refractive index detector (VE3580 RI Detector), low-angle and right-angle laser light scattering detector, and four-capillary viscometer (270 Dual Detector). Polymer solutions (1 mg/ml for chitosan and 5 mg/ml for heparin) were prepared in 0.2 M pH 4.6 acetate buffer. Chitosan solutions were stirred for 1 to 2 h at 40 °C. Both chitosan and heparin solutions were injected at 5 different injection volumes (140, 120, 100, 80, and 60 μl) in order to determine the refractive index increment (dn/dc). Samples were eluted at 1 ml min^{-1} across two analytical PL aquagel-OH MIXED 8 μm columns (Polymer Labs, Amherst, MA), kept at 38 °C. The molecular weights obtained from light scattering, and the hydrodynamic radii, R_H, and Mark-Houwink parameters (K and a) obtained from viscometry are summarized in Table 3.1. The Mark-Houwink parameters agree with those previously reported in the literature for similar solvent conditions.[15, 27] The relatively high Mark-Houwink exponent, a, for heparin indicates that it behaves as a relatively stiff coil, while chitosan behaves as a more flexible coil. The conformation of chitosan in solution is known to be a strong function of pH, ionic strength, and degree of acetylation, with experimentally reported Mark-Houwink exponents ranging from less than 0.6 to greater than 1.1.[15]

Table 3.1. Polysaccharide properties obtained by GPC.

Polymer	Mw (Da)	PDI	$Log_{10}(K \times g\ dl^{-1})$	A	R_H (nm)
Chitosan	289,000	2.05	-3.1 ± 0.1	0.77 ± 0.02	34.0 ± 0.3
Heparin	14,400	1.13	-4.57 ± 0.07	0.95 ± 0.02	3.72 ± 0.01

3.3.2 Substrate Preparation

All SF10 glass substrates were coated with a chromium adhesion layer (< 1 nm) followed by gold (45 nm). Chromium and gold coating were accomplished using a BTT-IV vacuum evaporator (Denton Vacuum, Moorestown, NJ) with a MDC-260 deposition controller (Maxtek, Inc., East Syracuse, NY). Gold-coated substrates were annealed for 2 h at 250 °C to obtain a smooth gold(1,1,1) surface.[28] The annealed gold surfaces were modified with a self assembled monolayer (SAM) of MUA, by soaking in a 1 mM ethanolic solution for at least 20 h, followed by a brief ethanol rinse, and drying with a gentle stream of dry N_2.[29, 30] The MUA SAM provides a well-characterized surface revealing carboxylic acid groups suitable for adsorption of a polycation from solution. The MUA SAM thickness of 1.7 nm was confirmed using a JA Woollam spectroscopic ellipsometer (Lincoln, NE), as described below.

3.3.3 Heparin and Chitosan Solution Preparation

Polysaccharide solutions were prepared in acetate buffer (sodium acetate and acetic acid) at four different pH values (4.6, 5.0, 5.4 and 5.8) and three different buffer ionic

strengths (0.1 M, 0.2 M, and 0.5 M). Chitosan solutions were stirred for 1 to 2 h at 40 °C. Solutions were prepared to be 0.01 M on a repeat unit basis for chitosan and on a sulfonate basis for heparin and were clarified by filtration through 0.22 μm syringe filters (PVDF, Fisher Scientific).

3.3.4 LBL Assembly and *In Situ* Fourier-Transform Surface Plasmon Resonance (FT-SPR)

FT-SPR measures the intensity of *p*-polarized light reflected from the back side of the gold film on which the PEM are assembled, as a function of wavelength. A reflectivity minimum corresponding to the wavelength of light that is in resonance with surface plasmons in the gold film is sensitive to changes in the dielectric constant of the layer in contact with the thin metal film. Thus, changes in refractive index or thickness of the PEM on the gold can be detected in real time.[31] LBL assembly of PEM was conducted in the flow cell of an SPR-100 module coupled to a Nicolet 8700 FT-IR spectrometer (Thermo-Electron, Madison, WI). A Masterflex peristaltic pump (Cole-Parmer, Vernon Hills, IL), connected to a 6-way valve (Upchurch Scientific, Oak Harbor, WA) that can be used to select among rinse, polycation, and polyanion solutions, was used to pump these solutions through the FT-SPR flow cell, at a flow rate of 1.3 ml min^{-1}. The interferometer in the FT-IR instrument was used to scan wavelength at a fixed angle of incidence. In these experiments, FT-SPR was performed using a white light/near infrared source with a CaF_2 beam splitter at the interferometer and an InGaS detector. Data were collected using the Omnic 7.3 software (Thermo Electron), at 8 cm^{-1} resolution over the range from 6000

to 12,000 cm^{-1}. 16 scans were co-added at each time point to produce an FT-SPR spectrum every 4.7 seconds.

Substrates were first exposed to a rinse solution (18.2 MΩ water acidified to pH 4.0 with acetic acid). PEM were then produced by alternately exposing the substrate to the respective solutions of polycation and polyanion for 5 min. The substrates were rinsed for 5 min between each adsorption step. Ten–layer PEM were assembled at each combination of buffer ionic strength and pH, except for 0.1 M, pH 5.8 buffer. Chitosan was insoluble in this buffer. Duplicate PEM were prepared from fresh solutions at each combination of pH and ionic strength studied. During PEM assembly, the shift in the position of the FT-SPR peak center of gravity was used to determine the layer thickness, by comparing the experimental curves to those predicted from multiphase Fresnel calculations.[31, 32] These calculations require the refractive index of each layer (SF10 glass, gold, PEM, and solution), the thickness of the gold and PEM layers, and the angle of the incident *p*-polarized light. The refractive indices of the SF10 glass, gold, and rinse solution are accurately known. Over reasonable ranges of the remaining parameters (gold thickness and incident angle), the slope of a plot of peak position vs. PEM thickness is only sensitive to the PEM refractive index. Thus, if the PEM refractive index is known, the change in thickness can be accurately determined from the change in the position of the FT-SPR peak. The PEM refractive index over the wavenumber range of interest was determined from spectroscopic ellipsometry.

3.3.5 Spectroscopic Ellipsometry

Variable angle spectroscopic ellipsometry data for the MUA SAMs and PEM films were acquired using JA Woollam VASE ellipsometer in the wavelength range 400-1200 nm (energy range 4.13-1.03 eV) at two angles of incidence 65° and 75°. Optical modeling and data analysis were done using the J.A. Woollam WVASE32 software package. The reflected light was modeled from each layer using the Cauchy equation relating the refractive index and thickness of each layer. For all PEM samples the refractive index of the PEM layer was about 1.41. This value was used to interpret the FT-SPR data.

3.3.6 Polarization Modulation Infrared Reflection Absorption Spectroscopy (PM-IRRAS)

PM-IRRAS is an infra-red spectroscopy technique that uses *p*-polarized and *s*-polarized light reflected from a surface. PM-IRRAS is useful for characterizing thin films on metallic substrates when a grazing angle of incidence is used.[33] PM-IRRAS was conducted using a Nicolet 8700 FT-IR spectrometer (Thermo-Electron) configured with a Tabletop Optics Module, equipped with a PEM-90 photoelastic modulator (Hinds Instruments, Hillsboro, OR), to provide a polarization of the incident infrared light, grazing angle sampling optics (86° for gold substrates), a liquid N_2-cooled MCT-A detector, and a demodulator (GWC Technologies) to process the *s*- and *p*-polarized spectra. Ten-layer PEM were investigated with PM-IRRAS to characterize their chemistry. PM-IRRAS spectra were collected at 8 cm^{-1} resolution with 1000 scans for each sample.

PM-IRRAS spectra contain a component that is a second-order Bessel function of the first kind (J_2), which can be accounted for by dividing by a baseline. The simplest method for determining the baseline is to use a cubic spline, with spline points selected in regions of the spectrum in which no IR absorption peaks appear.[34] To ensure consistency of this processing, raw PM-IRRAS spectra from each of the ten-layer PEM and the MUA SAM were exported to spectroscopy analysis software (Igor Pro 5.0.5.7, WaveMetrics, Inc., Portland, OR). Each spectrum was analyzed by determining the cubic spline (background) function from a predefined set of spline points and dividing by the background function. The spectrum of the MUA SAM was then subtracted from each of the PEM spectra. The PM-IRRAS spectrum of the MUA SAM is shown in Figure 3.2, along with the spline points and the curve representing the background. The processed spectrum is plotted on the secondary axis. This correction procedure results in a higher signal-to-noise ratio near the Bessel function maxima, and much more noise near the Bessel function minima. Thus, the best data are obtained in the region of interest around 1500 cm^{-1} in Figure 3.2. The MUA SAM shows characteristic absorption bands associated with the C-H vibrations (C-H ν_{as} 2900 to 3000 and C-H ν_s at 2850), carbonyl stretch of the carboxylic acid (weak peaks at 1715 and 1725), carboxylate stretch (COO^- ν_{as} from 1570 to 1650 and strong COO^- ν_s at 1425) overlapping with the methylene scissors (CH_2 δ at 1470), and carboxylic acid C-OH stretch (peak at 1170) overlapping with other methylene modes.[28, 33, 34] The relative weakness of the carboxylic acid peaks (1715 to 1725) has been reported for MUA exposed to ethanol, and indicates a high degree of ionization when compared to the relatively strong carboxylate peak.[34]

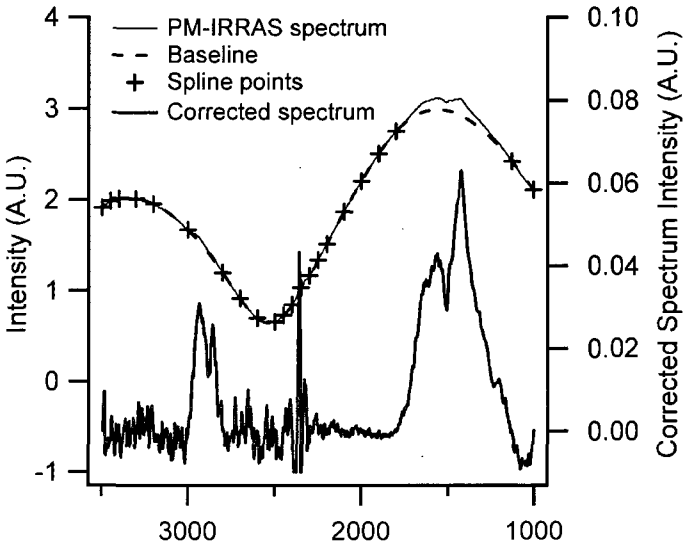

Figure 3.2. Baseline correction for MUA SAM. The left axis is for the PM-IRRAS spectrum and baseline and the right axis is for the corrected spectrum.

3.3.7 X-ray Photoelectron Spectroscopy (XPS)

XPS experiments were performed on a Physical Electronics 5800 spectrometer (Chanhassen, MN). This system has a monochromatic Al Kα X-ray source (hν = 1486.6 eV), hemispherical analyzer, and multichannel detector. A low energy (30 eV) electron gun was used for charge neutralization on the non-conducting samples. The binding energy scales for the samples were referenced to the C1s peak at 284.7 eV. High resolution spectra of the N1s and S2p envelopes were acquired at an analyzer pass energy of 23.5 eV, with 0.1 eV steps, and an X-ray spot size of 800 μm. XPS elemental compositions of samples were obtained using pass energies of 187.85 and 0.8 eV steps.[35] All XPS analyses were performed at a photoelectron takeoff angle of 45°. The composition of the PEM was computed from the atom balances on nitrogen and sulfur. These calculations are detailed in the supporting information. PEM composition is reported as the ratio of heparin to chitosan on a saccharide unit basis.

3.4 Results

3.4.1 PEM Assembly and *In Situ* FT-SPR

In situ FT-SPR data were collected during PEM assembly. The incident angle of the near-IR light (~53°) was adjusted such that the initial position of the FT-SPR peak was 9000 cm^{-1}. The peak position as a function of time during PEM assembly was determined from the COG (center of gravity method provided in the OMNIC software). Representative FT-SPR (absorbance) spectra for the PEM assembly from pH 4.6, 0.1 M buffer are shown in Figure 3.3a, and the COG as a function of time for this experiment is shown in Figure 3.3b. In Figure 3.3a, the curves shown represent the FT-SPR spectra collected during the rinse following each adsorption step. During the first five minutes of each experiment, the surface was exposed to the rinse solution. This is followed by a five-minute chitosan adsorption step. A large peak shift occurs during chitosan adsorption (from 5 min to 10 min in Figure 3.3b), caused both by a change in the refractive index of the solution, as well as chitosan adsorption on the surface. During the subsequent five-minute rinse step, the peak returns to a value closer to the value obtained during the initial rinse (from 10 min to 15 min in Figure 3.3b). This rinse was followed by a five-minute heparin adsorption step, and another five-minute rinse, to complete the first bilayer. Subsequent bilayers were assembled by iteration of this procedure. PEM assembly was continued for a total of 10 layers (5 bilayers) with a five-minute rinse following each adsorption step. The data shown in Figure 3.3 are qualitatively similar to the data from all PEM adsorption experiments conducted at other buffer conditions. In all cases, the peak shift associated with the heparin adsorption was smaller than that associated with chitosan adsorption.

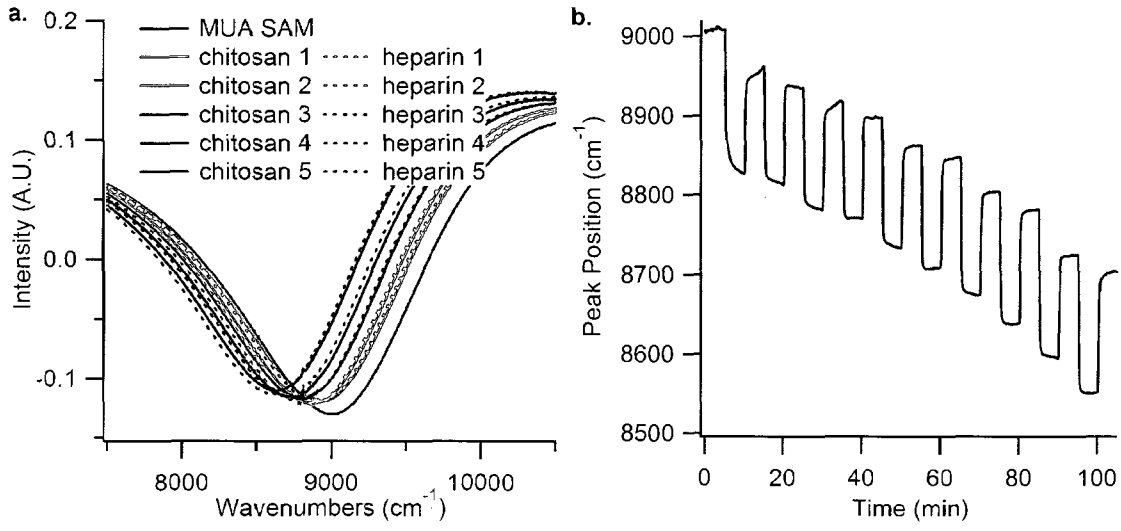

Figure 3.3. Kinetics of PEM assembly from *in situ* FT-SPR for the PEM assembled at pH 4.6 from 0.1 M buffer. FT-SPR traces for the initial rinse (MUA SAM) and each rinse following an adsorption step (a). Peak position (center of gravity) as a function of time during PEM assembly showing 5-minute rinse and adsorption intervals (b).

The refractive index of the PEM (1.41) was used to determine the PEM thickness from the COG data. A wave number shift of -28 cm^{-1} corresponds to an increase in the PEM thickness of approximately 1 nm. Figure 3.4a, b, and c show the *in situ* thickness data (mean of duplicate PEM for each condition) obtained from FT-SPR for the 0.1 M, 0.2 M, and 0.5 M buffers respectively. In each data set, layer 0 represents the MUA SAM, odd-numbered layers represent the thickness obtained during the rinse following chitosan adsorption, and even-numbered layers represent the thickness obtained following heparin adsorption steps. The mean and range of the final PEM thickness from the duplicate experiments at each condition are also shown in Table 3.2. The average incremental bilayer thickness for each of the buffer conditions is shown in Figure 3.5. The mean and standard deviations of the contributions to the bilayer thickness from the chitosan and heparin adsorption steps are also shown in Figure 3.5.

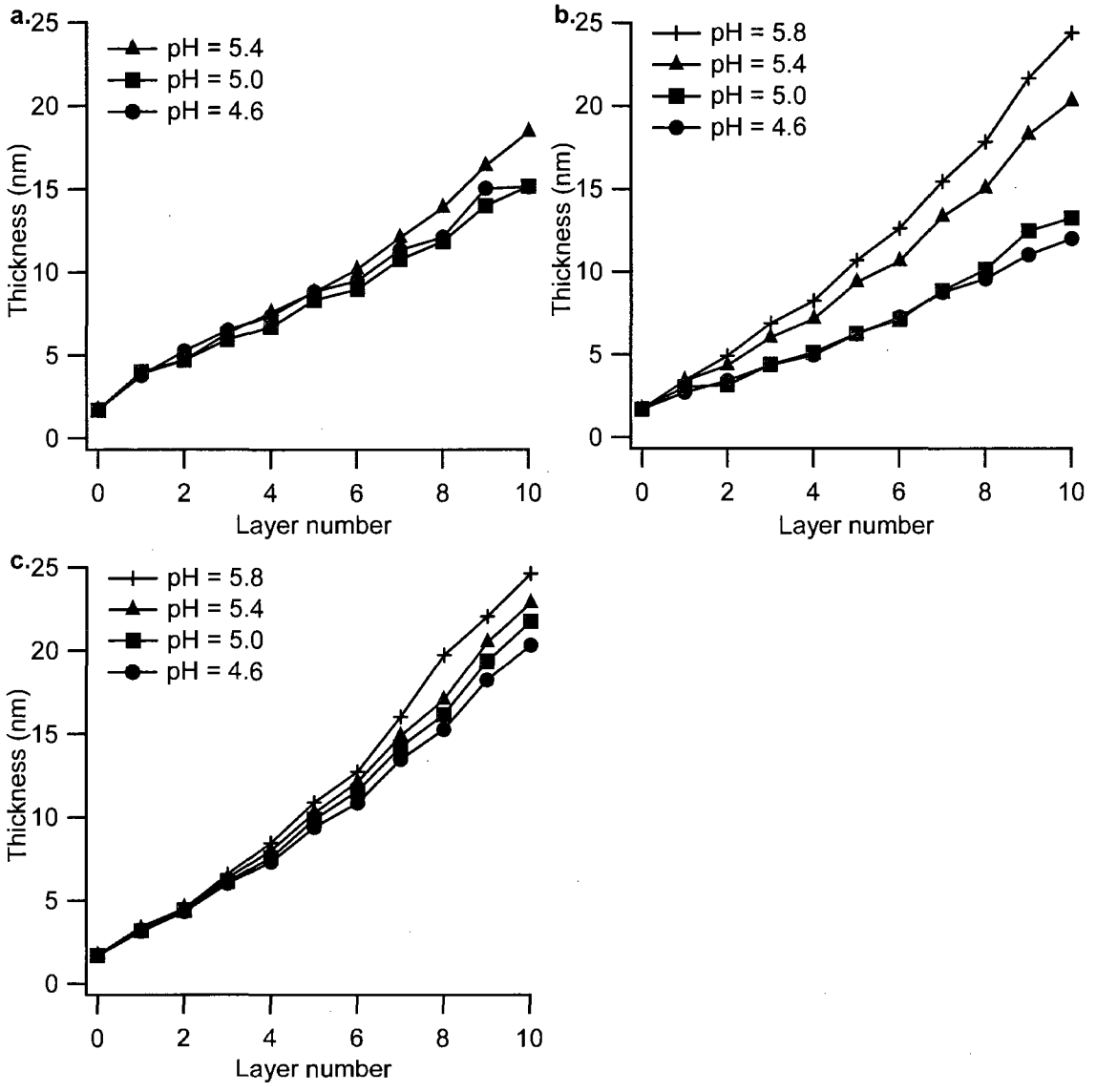

Figure 3.4. PEM thickness obtained from *in situ* FT-SPR data as a function of layer number and pH for 0.1 M buffer (a), 0.2 M buffer (b), and 0.5 M buffer (c). In all three plots, layer zero represents the MUA SAM thickness (1.7 nm). Odd-numbered layers are chitosan and even-numbered layers are heparin. Data for each condition are the averages of two replicate experiments. Uncertainties on the mean layer thickness and final PEM thickness for each condition are reported in Figure 3.5 and Table 3.2, respectively.

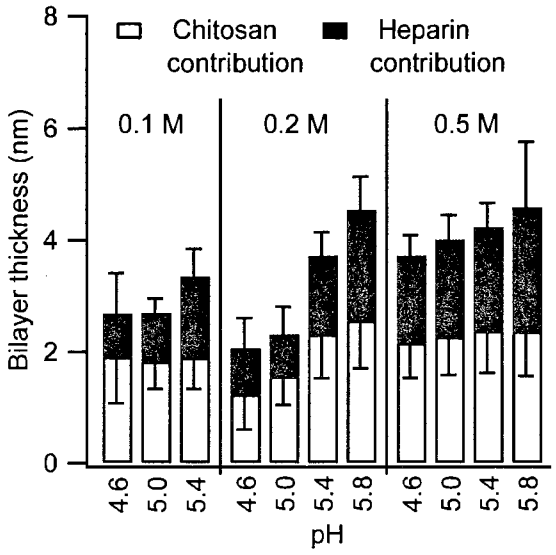

Figure 3.5. Average incremental bilayer thickness of PEM measured by *in situ* FT-SPR for PEM assembled at different buffer conditions. Error bars on top represent the standard deviations of the heparin contributions and error bars on the bottom represent the standard deviations of the chitosan contributions, from duplicate experiments for each condition, with five heparin and five chitosan layer thickness measurements per PEM.

At each condition, the thickness increase associated with the chitosan adsorption steps is always larger than the thickness increase associated with the heparin adsorption steps. The chitosan used in this study was much higher molecular weight than the heparin (Table 3.1). Furthermore, GPC analysis indicates that the strong polyanion heparin adopts a more extended conformation in solution (Mark-Houwink exponent > 0.9). This could allow the heparin to adsorb in an extended conformation, leading to thinner layers. In contrast, the charge density of the weak polycation, chitosan, is expected to be affected by changing pH. Decreasing its charge density (by increasing pH) or increasing ionic strength causes chitosan to collapse in solution.[15] (Chitosan becomes completely insoluble as the pH of the solution approaches the pK_a.) Thus, we observe in Figure 3.5 that the average thickness of the adsorbed chitosan layer increases at increased pH. The heparin layer thickness also increases with increasing pH. This is likely due to increased

mass of chitosan on the surface requiring additional heparin to accomplish complete charge reversal. In Figures 3.4 and 3.5 and Table 3.2, it is clear that the 0.2 M buffer conditions demonstrate a relatively broad range of accessible PEM thickness as pH is modulated. The increase in thickness with increased pH is consistent with the observations of Shiratori *et al.* that PEM thickness can increase as charge density on weak polyelectrolytes is decreased.[8] Some of the observed changes in PEM thickness may also be due to differences in the charge density of the underlying MUA SAM as a function of pH, during the adsorption of the first chitosan layer. The pK_a of the MUA SAM ranges between 4.7 and 6.4, depending upon the surface coverage.[36]

Our observed increase in the film thickness with increasing ionic strength is similar to the effects observed in previous studies.[37-39] Poptoshev *et al.* attributed increased PEM thickness at increased ionic strength to screening of electrostatic charges among the polyelectrolyte molecules.[38] In another study, Sui *et al.* proposed that at high buffer molarity, PEM thickness can also be decreased by "stripping" when one or both of the polyelectrolytes are relatively low molecular weight (e.g. the heparin in our system).[39] In this proposed process, during adsorption of the higher molecular weight component, soluble complexes of the polyanion and polycation form and the lower molecular weight polymer is carried into solution.[39] They observed significantly reduced PEM thickness when PEM were formed from a long polycation and a short polyanion at ionic strengths higher than 0.6 M.[39] We do not observe this stripping phenomenon in our experiments. Because we only investigated ionic strengths < 0.6 M, the charge screening effect dominates.

The FT-SPR thickness data in Table 3.2 also demonstrate that for the 0.1 M buffer conditions and for pH 4.6 0.2 M buffer, control of the PEM thickness by solution pH is not precise. In these cases, the uncertainty is $\geq$ 10 % of the measured value. The 0.5 M buffer conditions are much less sensitive to changes in pH than the 0.2 M buffer conditions, but the PEM thickness is repeatable (uncertainty between 0.1 % and 6 %). We hypothesize that for 0.1 M buffers, the decreased buffer capacity results in less control over the PEM thickness, because the polyelectrolytes can influence the local pH (e.g. near the PEM surface). For the 0.5 M buffers, the much higher concentration of sodium and acetate ions in solution may result in significant screening of the electrostatic charges.[38] This electrostatic screening may reduce the sensitivity of the layer thickness to the chitosan charge density by reducing electrostatic repulsion and improving the chitosan solubility. This also improves the repeatability of the PEM formation.

Table 3.2. PEM thicknesses from both FT-SPR and ellipsometry. Thicknesses represent the mean and range of measurements from duplicate experiments.

		Thickness (nm)	
Molarity	pH	FT-SPR	ellipsometry
0.1	4.6	15.1 ± 2.6	8.2 ± 1.0
0.1	5.0	15.2 ± 1.8	11.2 ± 0.3
0.1	5.4	18.4 ± 1.8	16.9 ± 1.8
0.2	4.6	12.0 ± 5.0	5.8 ± 1.9
0.2	5.0	13.3 ± 0.2	11.6 ± 0.6
0.2	5.4	20.3 ± 1.5	12.7 ± 1.6
0.2	5.8	24.4 ± 2.1	19.0 ± 1.0
0.5	4.6	20.3 ± 0.2	14.4 ± 3.0
0.5	5.0	21.8 ± 0.7	15.7 ± 1.8
0.5	5.4	22.9 ± 1.1	16.0 ± 1.8
0.5	5.8	24.6 ± 1.6	18.1 ± 0.5

3.4.2 Ellipsometry

PEM assembled under each buffer condition were removed from the flow cell, rinsed with ethanol, and analyzed *ex situ* by ellipsometry to determine the thickness and refractive index. The best fits to the ellipsometry data were obtained when the PEM and MUA SAM were modeled as a single layer. Table 3.2 compares the thickness data (mean and range of duplicate PEM at each condition) obtained from *in situ* FT-SPR and *ex situ* ellipsometry. All thicknesses obtained from ellipsometry are thinner than those obtained from *in situ* FT-SPR. The difference in thickness is attributed to some drying and collapse of the PEM, as the ellipsometry measurements are obtained in air after an ethanol rinse.

All ellipsometry thickness measurements confirm the trends with pH and ionic strength observed in the FT-SPR data. Increasing pH increases PEM thickness over the pH range studied, and the 0.2 M buffer condition provides the broadest range of PEM thickness.

3.4.3 PM-IRRAS

The chemistry of each 10-layer PEM was characterized with PM-IRRAS. Figure 3.6a, b, and c show the corrected PM-IRRAS spectra for PEM (with the MUA SAM spectrum subtracted) assembled under the 0.1, 0.2, and 0.5 M buffer conditions, respectively. All PEM have a strong amide I peak (C=O ν_{as} at 1660) from acetylated saccharides in chitosan and heparin, with possible contributions from the carboxylate groups in heparin, expected at 1680.[25] The carboxylic acid peak (1730) is strengthened at the expense of the carboxylate peaks (1425 and 1570 to 1650) that were observed for the MUA SAM. The strong peak at 1260 is attributed to the asymmetric sulfonate stretch in heparin.[40, 41] A small peak at 1170 is also present. The peaks at 1170 and 1100 could have contributions from C-OH stretch and C-N stretch or complex sugar modes.[42] The PM-IRRAS spectra for 0.1 M and 0.2 M at pH 4.6 and 5.0 exhibit weaker absorption bands than the spectra for the pH 5.4 and 5.8. All of the spectra for 0.5 M buffer exhibit relatively strong absorption bands. This correlates well to the thickness data (Table 3.2), indicating that PEM assembled at lower pH from 0.1 and 0.2 M buffer have less total polymer adsorbed.

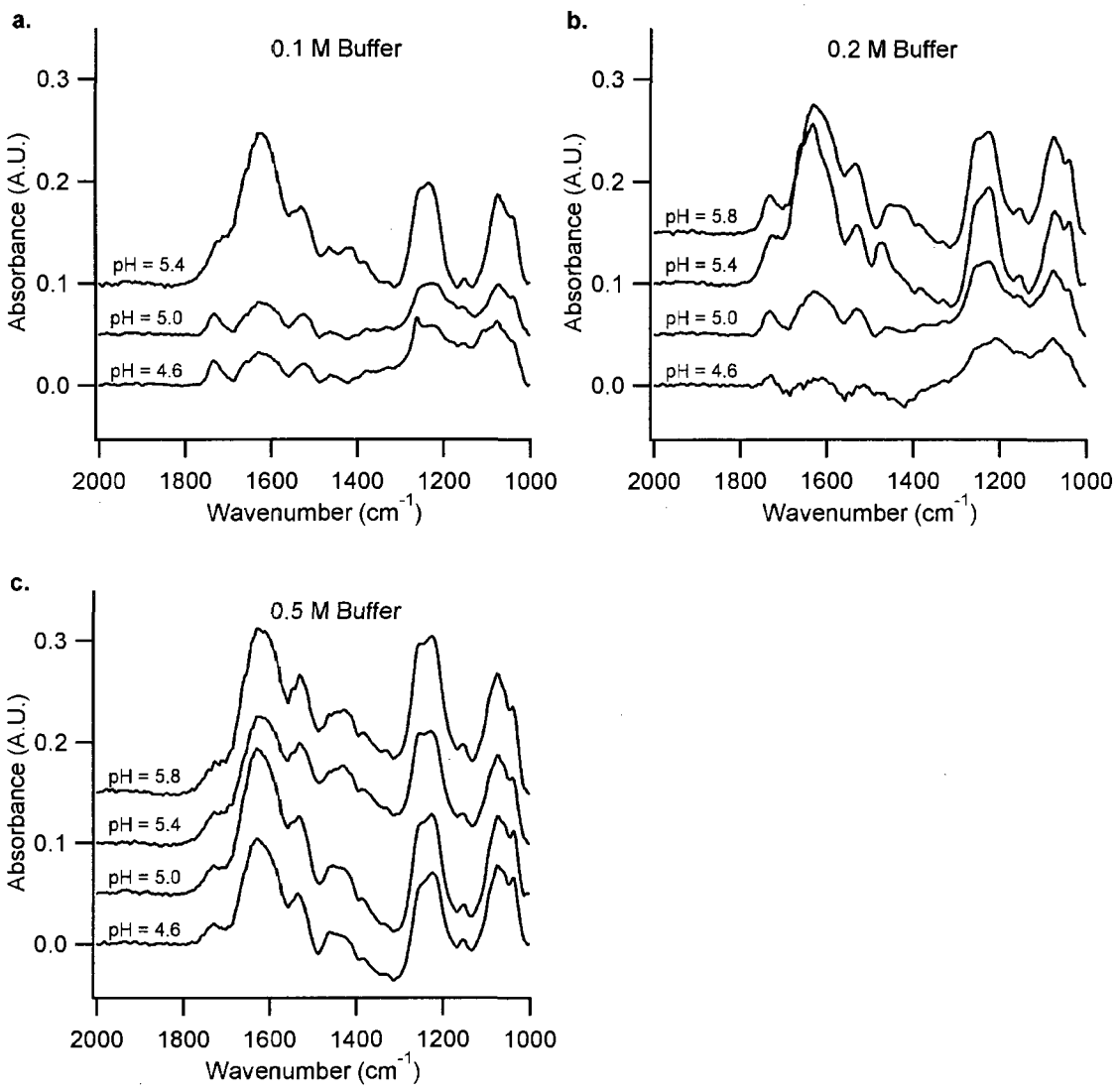

Figure 3.6. PM-IRRAS spectra for PEM assembled from 0.1 M (a), 0.2 M (b), and 0.5 M (c) buffer. All spectra have the MUA spectrum shown in Figure 3.2 subtracted from them. Spectra are sequentially offset to separate them on the vertical axes.

3.4.4 X-ray Photoelectron Spectroscopy (XPS)

PEM composition was also assayed using X-ray photoelectron spectroscopy. The molar compositions of the PEM on a saccharide unit basis were computed from the S/N atom ratios, as described in the supporting information. These data are summarized in Table 3.3. Figure 3.7 shows the nitrogen N1s envelope and the sulfur S2p envelope for

the PEM assembled from 0.2 M (a) and 0.5 M (b) buffers at all four pH values studied. Each of these envelopes contained two primary peaks, the ratios of which are also reported in Table 3.3.

Table 3.3. Composition of PEM from XPS.

		Molar composition from XPS [a]		Peak area ratio	
Molarity	pH	S/N	Hep/Chi	N1s 402/399.6	S2p 164.8/169
0.1	4.6	0.68	0.74	1.1	0.33
0.1	5.0	0.68	0.74	1.1	0.25
0.1	5.4	0.73	0.82	1.2	0.23
0.2	4.6	0.87	1.05	1.3	0.27
0.2	5.0	0.84	1.00	1.7	0.12
0.2	5.4	0.90	1.11	1.9	0.07
0.2	5.8	0.92	1.15	2.0	0.06
0.5	4.6	0.91	1.14	1.7	0.05
0.5	5.0	0.86	1.04	2.2	0.05
0.5	5.4	0.93	1.19	2.3	0.04
0.5	5.8	0.94	1.19	2.0	0.03

[a]The S/N ratio includes only the sulfur peak centered at 169 eV, to eliminate the sulfur from the MUA SAM (peak centered at 164.8). The heparin to chitosan ratio (Hep/Chi) is reported on a saccharide unit basis.

In Figure 3.7, the S2p envelope shows a contribution from the sulfonate in heparin (169 eV) and a smaller peak representing the gold thiolate in the MUA SAM (164.8 eV). For the PEM assembled from 0.2 M buffer, the intensity of the sulfonate peak increases

and the intensity of the gold thiolate peak decreases as the pH is increased. For the PEM assembled from 0.5 M buffer, the relative change in the peak areas of the sulfonate and thiolate follow the same trend, but are less sensitive to pH. This confirms the large increase in PEM thickness as pH is increased for the 0.2 M buffer, and the relatively small change in thickness observed for the 0.5 M buffer.

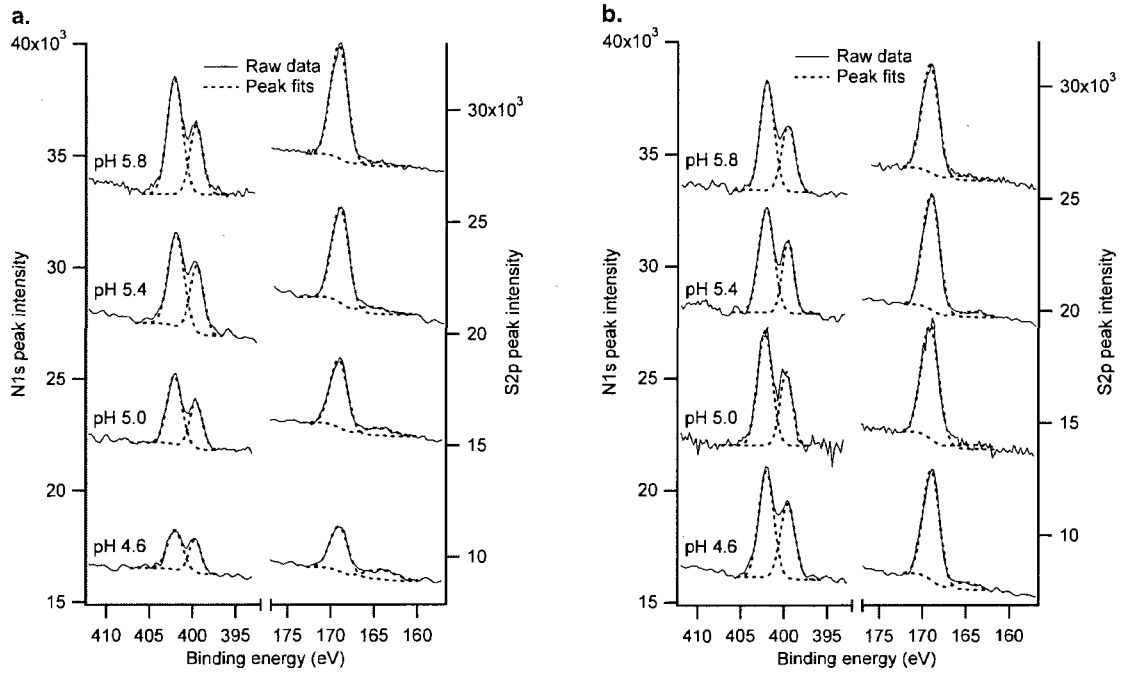

Figure 3.7. N1s (392-412 eV) and S2p (157-177 eV) envelopes from XPS spectra of PEM assembled from 0.2 M (a) and 0.5 M (b) buffers. Spectra are sequentially offset to separate on the vertical axes.

In the N1s envelope, two peaks can be observed. The peak at 402 eV is associated with protonated amine. The peak at 399.6 contains contributions from three different species: deprotonated amine, amide, and protonated amine interacting with sulfonate, possibly through hydrogen bonds.[43, 44] For the PEM assembled from 0.2 M buffer, the

fraction of nitrogens in the protonated amine increases with increasing pH. This cannot be explained through consideration of the pH alone. However, this trend can be understood in light of the pH dependence of the chitosan layer thickness. Recall that higher pH resulted in thicker PEM, with more chitosan being adsorbed during each adsorption step (cf. Figures 3.4b, 3.5, and 3.6b). We propose that for the thicker chitosan layers assembled at higher pH, a smaller fraction of the primary amines are available for interaction with the sulfonates in heparin (due to steric constraints and increased hydrophobicity of chitosan at higher pH). These non-interacting amines can be protonated during the pH 4.0 rinse step and contribute to the peak at 402 eV, while the amines that interact with sulfonates in heparin contribute to the peak at 399.6 eV. Morales-Cruz *et al.* have observed a similar N1s peak position at lower binding energy when protonated primary amines interact with sulfonates in polyelectrolyte multilayers and attribute this to possible H-bond.[43] The two peaks in the N1s envelope for the PEM assembled from 0.5 M buffer exhibit a similar trend, however, the relative change in peak area ratios is much less pronounced. This again confirms that PEM assembly from 0.2 M buffer is much more sensitive to pH than PEM assembly from 0.5 M buffer.

3.5 Conclusions

In this paper the assembly of PEM from biomedically relevant polysaccharides as a function of pH and ionic strength of the polyelectrolyte solutions was examined using *in situ* FT-SPR, ellipsometry, vibrational spectroscopy, and XPS. This combination of the chemical information from XPS and PM-IRRAS and the physical information from ellipsometry and FT-SPR provides a more complete understanding of the PEM assembly.

We have demonstrated that the LBL technique can be used to tune the nanoscale structure of heparin/chitosan surface coatings by modulating simple processing conditions. The thickness of the PEM increased with increasing pH over the range from 4.6 to 5.8. Buffer ionic strength also affected the accessible thickness range. An intermediate buffer ionic strength (0.2 M) provided the broadest range of accessible PEM thickness, which ranged from less than 2 nm per bilayer at pH 4.6 to greater than 4 nm per bilayer at pH 5.8. Higher (0.5 M) buffer ionic strength resulted in less pH sensitivity. At lower (0.1 M) buffer ionic strength, control over PEM thickness by modulating solution pH is not as precise as at higher buffer ionic strengths. These general trends in effects of pH and ionic strength on layer thickness were observed in both *in situ* and *ex situ* measurements. Chemical analysis by XPS and vibrational spectroscopy also confirmed that increasing pH increases the molar amount of polyelectrolyte adsorbed over the pH range studied. From XPS analysis, it appears that thicker PEM assembled at higher pH have a smaller fraction of the primary amines from chitosan interacting with sulfonates in heparin, possibly due to steric constraints or increased hydrophobicity of the chitosan. Surprisingly the PEM composition (ratio of heparin to chitosan) was not very sensitive to changes in adsorption conditions, even though the PEM thickness and chitosan charge density vary significantly over the range investigated. It is also interesting to note that the incremental thickness associated with the chitosan adsorption steps is always greater than the incremental thickness associated with heparin (Figure 3.5), even though the ratio of heparin to chitosan is equal to or slightly greater than unity for all of the PEM formed from 0.2 and 0.5 molar buffer conditions (Table 3.3). Additional experiments detailing the structure of the PEM may be required to understand the relationship between the

molar composition and the incremental PEM thickness associated with each adsorption step.

This work contributes to understanding the physical chemistry and polyelectrolyte behavior of an important class of biological macromolecules. In their biological context, many polysaccharides are organized at the nanometer length scale. Thus, they provide both nanostructural and biochemical cues to cells. As polysaccharides are becoming increasingly important in biomaterials research, the ability to control the structure and composition of polysaccharide-based surface coatings at the nanometer length scale will provide further means to tune their biological functionality. Our ongoing research efforts in this area will build upon the work presented here, to develop additional nanostructured polysaccharide-based materials.

3.6 Supporting Information (Appendix 1)

Details of the methods used to compute the PEM composition from the XPS atom ratios are in the supporting information. This information is available free of charge via the Internet at http: //pubs.acs.org.

3.7 References

1. Bertrand, P.; Jonas, A.; Laschewsky, A.; Legras, R., Ultrathin polymer coatings by complexation of polyelectrolytes at interfaces: suitable materials, structure and properties. *Macromolecular Rapid Communications* **2000,** 21, (7), 319-348.
2. Hammond, P. T., Recent explorations in electrostatic multilayer thin film assembly. *Current Opinion in Colloid & Interface Science* **1999,** 4, (6), 430-442.
3. Dubas, S. T.; Schlenoff, J. B., Factors controlling the growth of polyelectrolyte multilayers. *Macromolecules* **1999,** 32, (24), 8153-8160.
4. Decher, G., Polyelectrolyte multilayers, an overview. In *Multilayer Thin Films Sequential Essembly of Nanocomposite Materials*, Decher, G.; Schlenoff, J. B., Eds. Wiley-VCH Verlag GmbH & Co.: Weinheim, 2003; pp 1-46.
5. Hiller, J.; Rubner, M. F., Reversible molecular memory and pH-switchable swelling transitions in polyelectrolyte multilayers. *Macromolecules* **2003,** 36, (11), 4078-4083.
6. Choi, J.; Rubner, M. F., Influence of the degree of ionization on weak polyelectrolyte multilayer assembly. *Macromolecules* **2005,** 38, (1), 116-124.
7. Morgan, S. E.; Jones, P.; Lamont, A. S.; Heidenreich, A.; McCormick, C. L., Layer-by-layer assembly of pH-responsive, compositionally controlled (co)polyelectrolytes synthesized via RAFT. *Langmuir* **2007,** 23, (1), 230-240.
8. Shiratori, S. S.; Rubner, M. F., pH-dependent thickness behavior of sequentially adsorbed layers of weak polyelectrolytes. *Macromolecules* **2000,** 33, (11), 4213-4219.
9. Kato, N.; Schuetz, P.; Fery, A.; Caruso, F., Thin Multilayer Films of Weak Polyelectrolytes on Colloid Particles. *Macromolecules* **2002,** 35, 9780-9787.
10. Dove, A., The bittersweet promise of glycobiology. *Nature Biotechnology* **2001,** 19, (10), 913-917.
11. Sorlier, P.; Denuziere, A.; Viton, C.; Domard, A., Relation between the degree of acetylation and the electrostatic properties of chitin and chitosan. *Biomacromolecules* **2001,** 2, (3), 765-772.
12. Ding, W.; Lian, Q.; Samuels, R. J.; Polk, M. B., Synthesis and characterization of a novel derivative of chitosan. *Polymer* **2003,** 44, (3), 547-556.
13. Ramos, V. M.; Rodriguez, N. M.; Rodriguez, M. S.; Heras, A.; Agullo, E., Modified chitosan carrying phosphonic and alkyl groups. *Carbohydrate Polymers* **2003,** 51, (4), 425-429.
14. Schatz, C.; Viton, C.; Delair, T.; Pichot, C.; Domard, A., Typical physicochemical behaviors of chitosan in aqueous solution. *Biomacromolecules* **2003,** 4, (3), 641-648.
15. Kasaai, M. R., Calculation of Mark-Houwink-Sakurada (MHS) equation viscometric constants for chitosan in any solvent-temperature system using experimental reported viscometric constants data. *Carbohydrate Polymers* **2007,** 68, (3), 477-488.
16. Lindahl, U.; Kusche, M.; Lidholt, K.; Oscarsson, L. G., Biosynthesis of Heparin and Heparan-Sulfate. *Ann. N.Y. Acad. Sci.* **1989,** 556, 36-50.
17. Salmivirta, M.; Lidholt, K.; Lindahl, U., Heparan sulfate: A piece of information. *FASEB J.* **1996,** 10, (11), 1270-1279.

18. Guimond, S.; Maccarana, M.; Olwin, B. B.; Lindahl, U.; Rapraeger, A. C., Activating and inhibitory heparin sequences for FGF-2 (basic FGF) - distinct requirements for FGF-1, FGF-2, and FGF-4. *Journal of Biological Chemistry* **1993,** 268, (32), 23906-23914.
19. Maccarana, M.; Casu, B.; Lindahl, U., Minimal Sequence in Heparin Heparan-Sulfate Required for Binding of Basic Fibroblast Growth-Factor. *J. Biol. Chem.* **1993,** 268, (32), 23898-23905.
20. Ruppert, R.; Hoffmann, E.; Sebald, W., Human bone morphogenetic protein 2 contains a heparin-binding site which modifies its biological activity. *European Journal of Biochemistry* **1996,** 237, (1), 295-302.
21. Takada, T.; Katagiri, T.; Ifuku, M.; Morimura, N.; Kobayashi, M.; Hasegawa, K.; Ogamo, A.; Kamijo, R., Sulfated polysaccharides enhance the biological activities of bone morphogenetic proteins. *Journal of Biological Chemistry* **2003,** 278, (44), 43229-43235.
22. Blanquaert, F.; Saffar, J. L.; Colombier, M. L.; Carpentier, G.; Barritault, D.; Caruelle, J. P., Heparan-like molecules induce the repair of skull defects. *Bone* **1995,** 17, (6), 499-506.
23. Kikuchi, Y., Polyelectrolyte Complex of Heparin with Chitosan. *Makromol. Chem. Macromol. Chem. Phys.* **1974,** 175, (7), 2209-2211.
24. Kikuchi, Y.; Noda, A., Polyelectrolyte complexes of heparin with chitosan. *Journal of Applied Polymer Science* **1976,** 20, (9), 2561-2563.
25. Kweon, D. K.; Lim, S. T., Preparation and characteristics of a water-soluble chitosan-heparin complex. *Journal of Applied Polymer Science* **2003,** 87, (11), 1784-1789.
26. Fu, J. H.; Ji, J.; Yuan, W. Y.; Shen, J. C., Construction of anti-adhesive and antibacterial multilayer films via layer-by-layer assembly of heparin and chitosan. *Biomaterials* **2005,** 26, (33), 6684-6692.
27. Bertini, S.; Bisio, A.; Torri, G.; Bensi, D.; Terbojevich, M., Molecular weight determination of heparin and dermatan sulfate by size exclusion chromatography with a triple detector array. *Biomacromolecules* **2005,** 6, (1), 168-173.
28. Jordan, C. E.; Frey, B. L.; Kornguth, S.; Corn, R. M., Characterization of poly-L-Lysine adsorption onto alkanethiol-modified gold surfaces with polarization-modulation Fourier-transform infrared-spectroscopy and surface-plasmon resonance measurements. *Langmuir* **1994,** 10, (10), 3642-3648.
29. Bain, C. D.; Evall, J.; Whitesides, G. M., Formation of monolayers by the coadsorption of thiols on gold - variation in the head group, tail group, and solvent. *Journal of the American Chemical Society* **1989,** 111, (18), 7155-7164.
30. Bain, C. D.; Troughton, E. B.; Tao, Y. T.; Evall, J.; Whitesides, G. M.; Nuzzo, R. G., Formation of monolayer films by the spontaneous assembly of organic thiols from solution onto gold. *Journal of the American Chemical Society* **1989,** 111, (1), 321-335.
31. Frutos, A. G.; Weibel, S. C.; Corn, R. M., Near-infrared surface plasmon resonance measurements of ultrathin films. 2. Fourier transform SPR spectroscopy. *Analytical Chemistry* **1999,** 71, (18), 3935-3940.

32. Jordan, C. E.; Corn, R. M., Surface plasmon resonance imaging measurements of electrostatic biopolymer adsorption onto chemically modified gold surfaces. *Analytical Chemistry* **1997,** 69, (7), 1449-1456.
33. Frey, B. L.; Corn, R. M., Covalent attachment and derivatization of poly(L-lysine) monolayers on gold surfaces as characterized by polarization-modulation FT-IR spectroscopy. *Anal. Chem.* **1996,** 68, (18), 3187-3193.
34. Methivier, C.; Beccard, B.; Pradier, C. M., *In situ* analysis of a mercaptoundecanoic acid layer on gold in liquid phase, by PM-IRAS. Evidence for chemical changes with the solvent. *Langmuir* **2003,** 19, (21), 8807-8812.
35. McCurdy, P. R.; Sturgess, L. J.; Kohli, S.; Fisher, E. R., Investigation of the PECVD TiO2-Si(100) interface. *Applied Surface Science* **2004,** 233, (1-4), 69-79.
36. Sugihara, K.; Teranishi, T.; Shimazu, K.; Uosaki, K., Structure dependence of the surface pKa of mercaptoundecanoic acid SAM on gold. *Electrochemistry* **1999,** 67, (12), 1172-1174.
37. Miller, M. D.; Bruening, M. L., Correlation of the swelling and permeability of polyelectrolyte multilayer films. *Chemistry of Materials* **2005,** 17, (21), 5375-5381.
38. Poptoshev, E.; Schoeler, B.; Caruso, F., Influence of solvent quality on the growth of polyelectrolyte multilayers. *Langmuir* **2004,** 20, (3), 829-834.
39. Sui, Z. J.; Salloum, D.; Schlenoff, J. B., Effect of molecular weight on the construction of polyelectrolyte multilayers: Stripping versus sticking. *Langmuir* **2003,** 19, (6), 2491-2495.
40. Serizawa, T.; Yamaguchi, M.; Akashi, M., Alternating bioactivity of polymeric layer-by-layer assemblies: Anticoagulation vs procoagulation of human blood. *Biomacromolecules* **2002,** 3, (4), 724-731.
41. Amarasekara, A. S.; Opoku, G.; Qiu, X. D.; Doctor, V., Effect of oversulfation on the chemical and biological properties of chondroitin-6-sulfate. *Carbohydrate Polymers* **2007,** 68, (1), 116-121.
42. Barth, A.; Zscherp, C., What vibrations tell us about proteins. *Quarterly Reviews of Biophysics* **2002,** 35, (4), 369-430.
43. Morales-Cruz, A. L.; Fachini, E. R.; Miranda, F. A.; Cabrera, C. R., Surface analysis monitoring of polyelectrolyte deposition on Ba0.5Sr0.5TiO3 thin films. *Applied Surface Science* **2007,** 253, (22), 8846-8857.
44. Strother, T.; Hamers, R. J.; Smith, L. M., Covalent attachment of oligodeoxyribonucleotides to amine-modified Si (001) surfaces. *Nucleic Acids Research* **2000,** 28, (18), 3535-3541.

Chapter 4

Experimental Investigation of the Solution Behavior and Polyelectrolyte Multilayer Formation of Polysaccharides

Some of the results from the work in this chapter are published in following:

- **S. Boddohi**, N. Moore, P.A. Johnson, M.J. Kipper, "Size and composition of polysaccharide-based polyelectrolyte complex nanoparticles at different charge molar ratios." *Biomacromolecules,* 10, 1402-1409, 2009
- **S. Boddohi**, C.E. Killingsworth, M.J. Kipper, "Polyelectrolyte multilayer assembly as a function of pH and ionic strength using the polysaccharides chitosan and heparin." *Biomacromolecules,* 9, 2021-2028, 2008.

4.1 Introduction

Many polysaccharides have properties which make them valuable as biomedical materials. In biological systems, many polysaccharides are organized at the nanometer length scale.[1, 2] Their nanoscale organization in biological systems, suggests that control over the structure and composition of these materials at the nanometer length scale will enable tuning of their biological functionality. Many biologically derived polysaccharides are also polyelectrolytes. We have studied the self assembly and electrostatic complex formation of the polysaccharides chitosan, heparin, and hyaluronan.[3-5] This electrostatic complex formation might be controlled by tuning the charge density and solution conformation of the polysaccharide-based polyelectrolytes. This can be done by changing the pH and ionic strength of the polymer solutions. In this chapter, we characterize how

the solution conformation and polyelectrolyte multilayer (PEM) assembly are affected by solution conditions.

In this work, 4.7 % acetylated chitosan with molecular weight of 290,000 Da was used. Chitosan has a pKa of 6.4 in pH over the range of 4.6 to 5.8. Chitosan is mainly produced from partial *N*-deacetylation of chitin.[6] Deacetylation of chitosan makes it more soluble in aqueous solution. Chitosan is soluble in aqueous organic acids such as acetic acid.[7] Heparin is a glycosaminoglycan (GAGs) that has the highest negative charge density of any known biological polyanion due to the presence of both carboxyl and sulfate groups.[8] Heparin used in this work was derived biologically from porcine intestinal mucosa (12.5 % sulfur). Hyaluronan is a natural macromolecule composed of D-glucuronic acid and *N*-acetyl-D-glucosamine linked together via alternating β-1,4 and β-1,3 glycosidic bonds. Hyaluronan as a weak polyanion has a pKa of 2.9.

The conformation of chitosan macromolecules and their physical properties in solution have been investigated both experimentally and theoretically.[9, 10] These studies showed that the dimensions of chitosan molecules increase when solution pH is decreased. This increase in the dimensions of chitosan is accompanied by an increase in the differential refractive index of the solution. In a theoretical study, the physical properties of chitosan in solution, including the diffusion coefficient, hydrodynamic radius, and radius of gyration have been obtained as functions of the solution ionic strength.[9]

Hyaluronan has also been characterized using several analytical techniques. Hokputsa *et al.* worked on hyaluronan samples of differing molar mass in order to investigate the difference in hydrodynamic parameters.[11] In this work, degradation of hyaluronan using a

depolymerization method to obtain different molecular weight fractions revealed information concerning intrinsic viscosities, Mark-Houwink parameters (K and a), and other physical properties.[11] Lapcik *et al.* worked on the structure and properties of Hyaluronan in solution for biomedical applications, obtaining information about hyaluronan hydrodynamic behavior, molecular weight, and intrinsic viscosity, and also examined the interaction between hyaluronan and other biologically relevant macromolecules.[12] Other studies have investigated the influence of pH and ionic strength on size, viscosity, and polymer chain conformation of hyaluronan.[13, 14] More recently it has been shown that the Mark-Houwink exponent (a) is dependent on the ionic strength and pH of the hyaluronan solution.[15-17]

The conformation of heparin has been studied by several groups with experimental and theoretical methods.[18-20] Povlov *et al.* investigated the conformation of different molecular weights of heparin with hydrodynamic and scattering methods to obtain diffusion coefficients, intrinsic viscosities, and hydrodynamic properties. Scattering methods have also been used to estimate the radius of gyration and Kuhn length for each molecule. Ortega *et al.* worked on worm-like macromolecules like heparin and could verify the consistency of the hydrodynamic properties in both experimental and theoretical methods.[19]

Finally, Layer by layer (LBL) assembly of chitosan-hyaluronan (chi-ha) polyelectrolyte multilayers (PEMs) was performed and thicknesses as a function of layer number was obtained at different solution pH and ionic strength values. Ellipsometry measurements were performed on a single condition to obtain refractive index of the PEMs in dry condition. Ellipsometry data also verified results from previous chapter on

PEM thicknesses. Thicknesses were obtained at different pH and ionic strength to determine how these solution properties affect assembly of the PEMs. The overall goal of this work was to obtain conformational properties for each polymer and determine how the solution conformation influences the assembly of PEMs.

4.2 Methods of Characterization

4.2.1 Gel Permeation Chromatography (GPC)

GPC is a chromatographic method that separates molecules based on hydrodynamic radius or volume. In this work a GPC system (Viscotek, Houston, TX) using a GPC Max (autosampler, solvent delivery pump, and solvent degasser) equipped with a column oven, differential refractive index detector (VE3580 RI Detector), low-angle and right-angle laser light scattering detector, and four-capillary viscometer (270 Dual Detector) was employed. Samples were eluted at 1 ml min^{-1} across two analytical PL aquagel-OH MIXED 8 μm columns (Polymer Labs, Amherst, MA), kept at 38 °C.

The refractive index increment of the samples (dn/dc) was calculated based on the RI signal obtained from RI detector in a Fix concentration of different injection volumes. The slope of the area beneath the RI signal during sample elution as a function of injection volume provides an accurate value for dn/dc. After measuring dn/dc, the molecular weight distribution of the polyelectrolyte can be obtained by low angle light scattering (LALLS) and average molecular weight can be measured using the Zimm equation (4.1). The importance of the LALLS direct measurement becomes most apparent when the analysis involves large molecules such as hyaluronan. These molecules have a very high angular dependence on the scattered light intensity that can cause significant

error when employing other light scattering methods such as multi-angle light scattering. This can be easily seen by plotting the scattering function versus the molecular weight of the macromolecules, where it can be observed that at the 7° angle, the particle scattering function, $P_{\theta,}$ stays constant and independent of molecular weight. The fundamental equation for the scattering of light from polymer solutions is the Zimm equation (4.1).

$$\frac{KC}{R_\theta} = \frac{1}{M_w P_\theta} + 2A_2 C \quad , \tag{4.1}$$

R_θ is the Rayleigh factor (function of scattered light intensity), M_w is the molecular weight of the polymer sample, C is the sample concentration, A_2 is the second virial coefficient of the solution that corrects for the interaction of polymer molecules with each other and can be calculated from the concentration dependence of the light scattering signal. P_θ is the measure of the angular dissymmetry of the scattered light and it is related to the size and the angle at which the scattering is determined. K is a composite of optical and fundamental constants.

The viscometer was used to obtain information about the size of the macromolecules by measuring the solution intrinsic viscosity. The intrinsic viscosity is obtained from Equation 4.2, by measuring the solution specific viscosity and concentration.

$$[\eta] = \frac{\eta_{sp}}{c}\Big|_{c\to 0} \tag{4.2}$$

The parameters of the Mark-Houwink equation were also determined. The exponent, *a*, in the equation (equation 4.3) provides a measure of the conformation of the polymer chains.[21]

$$[\eta] = KM_w^{\ a} \tag{4.3}$$

K is a constant and *a* represents the stiffness of the polymer chain. The hydrodynamic radius (R_H) of the polymer in solution is obtained from the Stokes-Einstein relationship, (equation 4.4).

$$[\eta] \times M_w = \frac{\frac{10}{3} \times \pi \times R_h^{\ 3}}{N_A} \tag{4.4}$$

N_A is Avogadro's number.

4.2.2 Fourier-Transform Surface Plasmon Resonance (FT-SPR)

LBL assembly of PEMs was conducted in the flow cell of an SPR-100 module coupled to a Nicolet 8700 Fourier-transform infrared (FT-IR) spectrometer (Thermo-Electron, Madison, WI). All hardware and software settings were similar to the LBL assembly and *in situ* FT-SPR section in Chapter 3. Sample preparation and conditions were similar to the ones explained in Chapter 3, expect here hyaluronan is used as a weak polyanion instead of heparin. Ten–layer PEMs were assembled at each combination of buffer ionic strength and pH, except for 0.1 M, pH 5.8 buffer. Chitosan was insoluble in this buffer. The method used to obtain PEM thickness from FT-SPR data is also similar to

the method described in Chapter 3, except the PEM refractive index over the wavenumber range of interest was determined from spectroscopic ellipsometry and it is 1.37.

4.2.3 Spectroscopic Ellipsometry

Variable angle spectroscopic ellipsometry data for a PEM film were acquired using JA Woollam VASE ellipsometer in the wavelength range 400-1200 nm (energy range 4.13-1.03 eV) at two angles of incidence 65° and 75°. Optical modeling and data analysis were done using the J.A. Woollam WVASE32 software package. The reflected light was modeled from each layer using the Cauchy equation which relates the refractive index to the wavelength.

4.3 Results

4.3.1 GPC

As previously discussed, the polyelectrolyte behavior in solution can be studied by GPC coupled to laser light scattering[9] and viscometry.[22] The combination of these three analytical techniques can provide detailed information about polymer conformation, size, and molecular weight distribution. Experiments were performed using acetate buffer mobile phases with pH values ranging from 4.6 to 5.8 and ionic strengths of 0.1, 0.2, and 0.5 mol L^{-1}. Polymer solutions were also made at the same conditions. Polymer solutions (0.9 mg/mL for chitosan, 4.75 mg mL^{-1} for heparin, and 1 mg mL^{-1} for hyaluronan) were injected in different injection volumes (140, 120, 100, 80, and 60 µl) into the GPC. The different volumes allow dn/dc, the change in refractive index for a given concentration, to

be calculated using a differential refractometer. Figure 4.1 shows typical data collected by the GPC system for heparin pH 5, 0.2 M buffer condition.

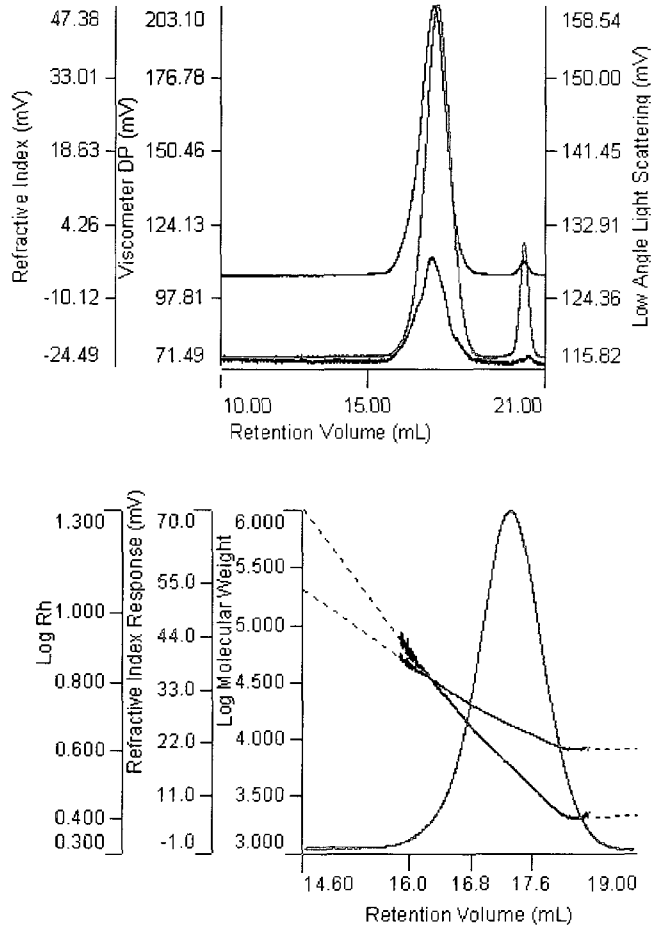

Figure 4.1. Responses of the refractive index, viscometer, and light scattering detectors as a function of retention time (top). Distribution of molecular weight, refractive index response, and hydrodynamic radius versus retention volume (bottom). Results are for the heparin at pH 5, 0.2 M acetate buffer.

Figure 4.2 shows the general concept of the weak polycation conformation behavior in solution with respect to changing the pH and ionic strength. Increasing the pH causes a decrease in the degree of ionization. The resulting reduction in electrostatic repulsion and

solubility causing the polymer chain to collapse. Similarly, increasing ionic strength provides an increase of counter ions, which can screen electrostatic repulsions or decrease the charge density on the polymer chain, causing the polymer chain to collapse.

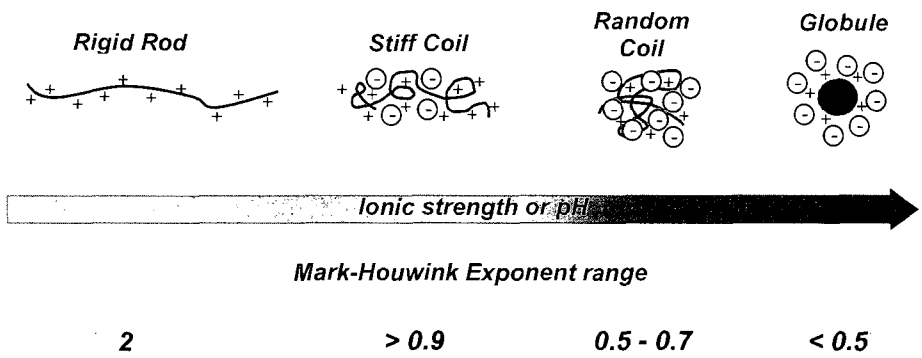

Figure 4.2. Scheme of polycation chain conformation in solution with respect to changing pH and ionic strength of the buffer solution.

Figures 4.3, 4.4, and 4.5 show the R_H and a of the three polyelectrolytes determined from GPC. Figure 4.3 shows R_H and a for chitosan, where the data show no significant trends for pH changes from pH 4.6 to pH 5.8; however, there is a weak trend corresponding to a change in ionic strength due to the buffer capacity at each buffer concentration. At 0.1 M buffer, because of the low capacity of the acetate buffer, the chitosan chain is not collapsing, thus the R_H is relatively higher than other ionic strength conditions. At 0.2 M buffer, there is a balance between buffer capacity and charge density of the chain, where there are more counter ions than 0.1 M condition and those could neutralize some of the charges on the polymer chain. At 0.5 M buffer, there is some charge screening of counter ions due to the stronger buffer capacity. This phenomenon can cause the collapse of the chitosan chain by reducing the electrostatic repulsion, thus a

reduction of R_H was expected with increasing ionic strength, resulting for polymer chain to have relatively more flexible coil shape. These phenomena can also affect a as well.

Heparin molecules at all three buffer concentrations exhibit relative reduction of a with increasing buffer capacity. R_H is not significantly different in all cases, which could be due to interacting of some counter ion associating with heparin in solution. In 0.5 M buffer condition, heparin chains will collapse relative to the two other buffer conditions. Heparin exhibits to have a stiff coil shape.

The relatively low charge density of the polyanion hyaluronan results in a different behavior for this polyanion than was observed for the heparin. At the lowest pH (pH = 4.6), which is the closest pH to the pKa of hyaluronan, the pH of the solution was 4.2 after adding the hyaluronan. This reduction of the pH is due to the low capacity of the 0.1 M buffer. The charge density had an important affect on a, which indicated a decrease in the flexibility of the hyaluronan chain by increasing ionic strength of the solution. Ionic strength also affected a as well, specifically at higher pH, but due to another reason. At pH 5.4, higher than the pKa of hyaluronan, charge screening of the buffer influenced a. There is some collapsing of hyaluronan chains by increasing the ionic strength. The R_H didn't change significantly and there is no obvious trend for this behavior. hyaluronan exhibits a random coil shape in all conditions.

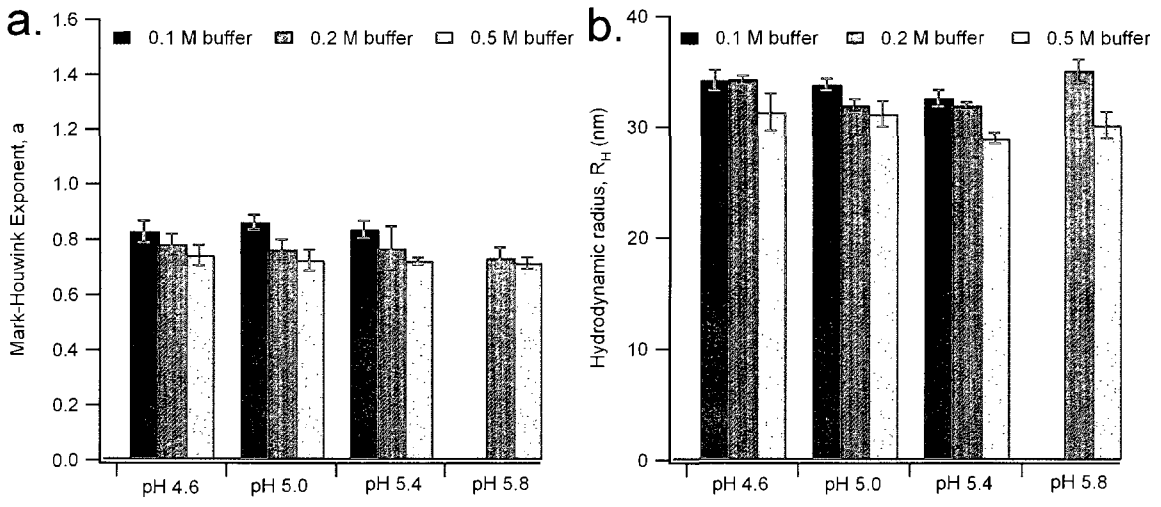

Figure 4.3. Mark-Houwink exponent (a) and hydrodynamic radius (b) of chitosan. Error bars show the value for a and R_H obtained from 5 different injection volumes (140, 120, 100, 80, and 60 µl).

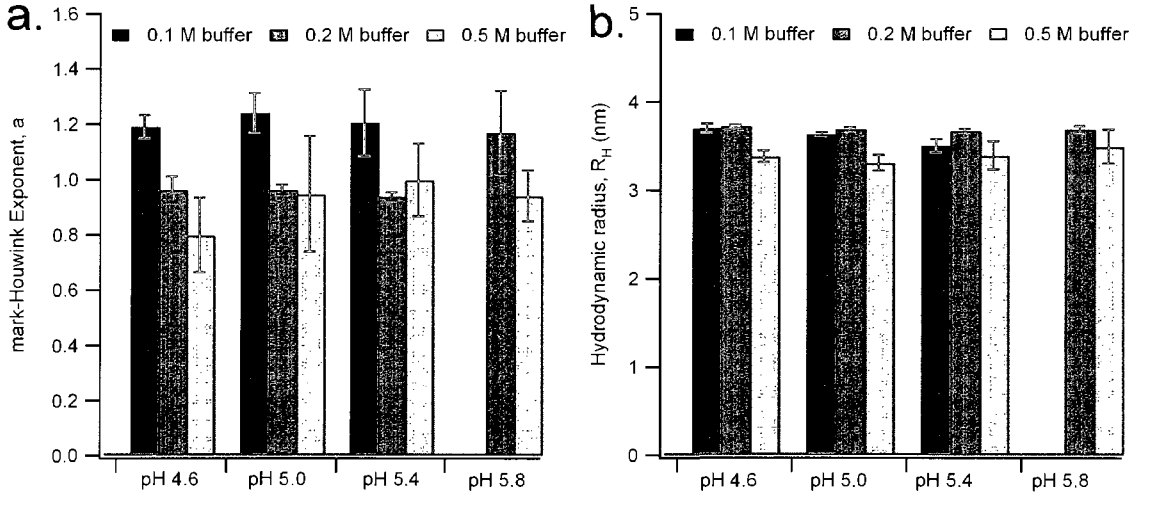

Figure 4.4. Mark-Houwink exponent (a) and hydrodynamic radius (b) of heparin. Error bars show the value for the a and R_H obtained from 5 different injection volumes (140, 120, 100, 80, and 60 µl).

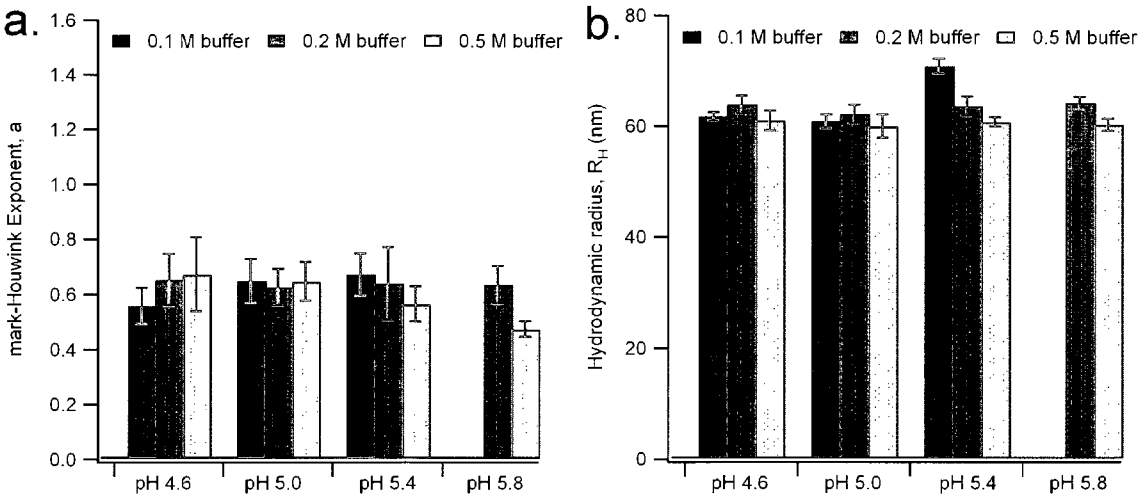

Figure 4.5. Mark-Houwink exponent (a) Hydrodynamic radius (b) of hyaluronan Error bars show the value for the a and R_H obtained from 5 different injection volumes (140, 120, 100, 80, and 60 μl).

Although there are some apparent trends observed in the data in Figures 4.3, 4.4, and 4.5, none of these trends are statistically significant. Thus, neither the a nor R_H of the polymers are dependent upon the solution pH and ionic strength under the conditions studied. Table 4.1 compares the range of a and R_H obtained in this work and previous work published by other groups.

Table 4.1. Range of a and R_H for chitosan, heparin, and hyaluronan in this work and some other published works.

		Hydrodynamic radius (R_H) (nm)		Mark-Houwink Exponent (a)	
Polymer	Solvent [a]	This work	Ref. [b]	This work	Ref. [b]
Chitosan	Acetate buffer	29 – 35	25 – 42[9]	–	–
	HCl / NaCl	–	–	0.71 – 0.88	0.52 – 0.71[23]
Heparin	$NaNO_3$	3.3 – 3.7	3.57 – 3.69[20]	0.8 – 1.24	0.82 – 0.94[20]
HA	Phosphate buffer	59 – 70	65 – 70[17]	–	–
	NaCl	–	–	0.47 – 0.67	0.6 – 0.78[24]

[a] Range of ionic strengths used by other groups are 0.01 – 0.3 M

[b] The molecular weight of chitosan was 194000 ± 5000 Da and 78000 – 914000 Da in references 9 and 23 respectively. The molecular weight of heparin in reference 20 was 16400 – 18500 kDa. The molecular weight of hyaluronan was 1.9 × 10^6 kDa in reference 17. Reference 24 reported that for hyaluronan $M_w < 1 \times 10^6$, a is 0.78 and for $M_w > 1 \times 10^6$, a is 0.6.

4.3.2 Thickness Obtained by FT-SPR for Chi-ha Multilayers

In the previous chapter, assembly of PEM using FT-SPR was used to characterize the chitosan-heparin (chi-hep) system at different PEM assembly conditions. In this chapter PEMs formation for the chi-ha pair was investigated at the same conditions. Figure 4.6 shows the thicknesses obtained by *in situ* FT-SPR as a function of layer number. Figure 4.6a shows the thickness for 0.1 M buffer at pH 4.6, 5.0, and 5.4 as a function of layer number. Results indicate that PEM thicknesses were influenced by the solution pH. At 0.2 and 0.1 M buffer conditions, there is a strong increase in the layer thickness with increasing solution pH where as in 0.5 M buffer, this trend is not significant. As the ionic strength is reduced, this effect is stronger. In 0.5 M buffer condition, screening of polyelectrolyte charges is governing the thicknesses without the effect of pH on each condition. Therefore thicknesses are close to each other in the pH ranging from 4.6 to 5.8.

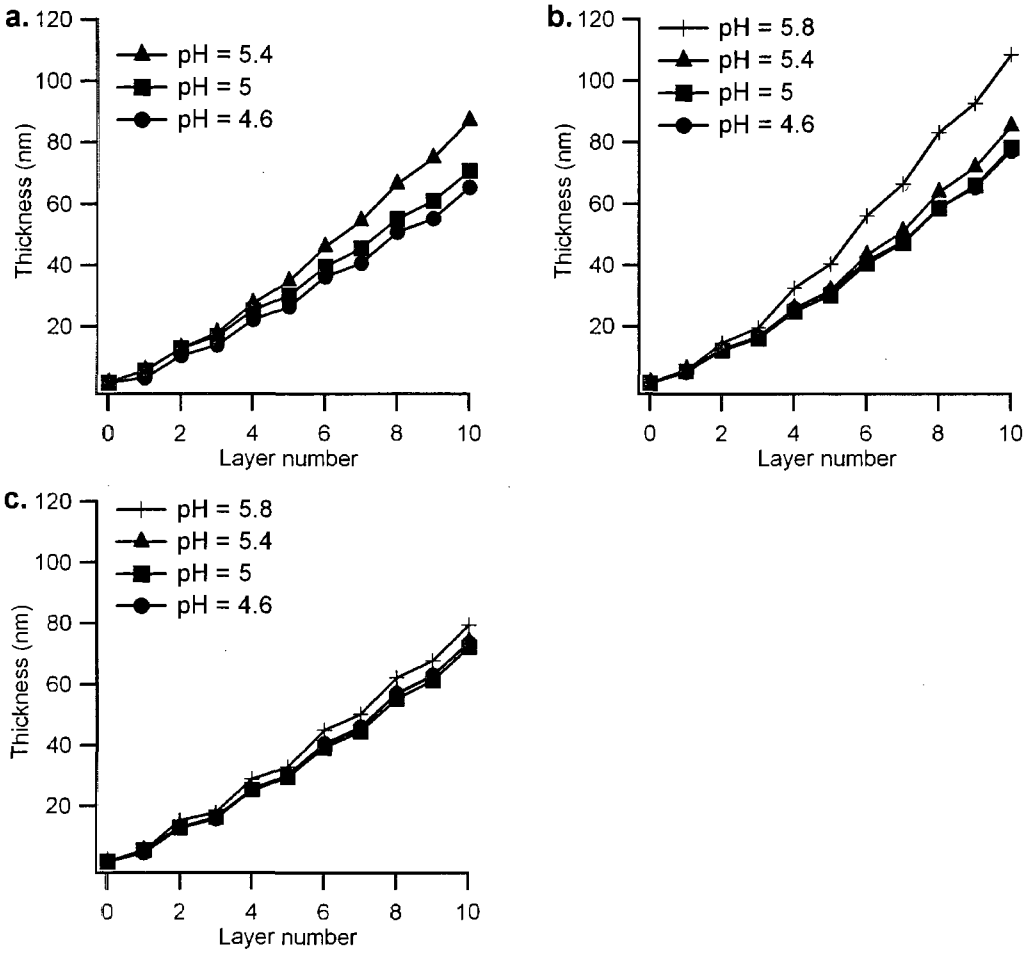

Figure 4.6 PEM thickness obtained from *in situ* FT-SPR data as a function of layer number and pH for 0.1 M buffer (a), 0.2 M buffer (b), and 0.5 M buffer (c). In all three plots, layer zero represents the MUA SAM thickness (1.7 nm). Odd-numbered layers are chitosan and even-numbered layers are hyaluronan. Refractive index used to calculate the thicknesses is 1.37 from spectroscopy ellipsometry.

Electrostatic interaction, charge density, and charge screening can all influence the behavior of the polyelectrolytes both in solution and at surfaces. A comparison of the FT-SPR data and GPC data indicates that several physical properties influence the PEM layer thickness over the range of conditions studied here. Polymer chain conformation in solution is not a strong function of pH; however PEM thickness is a function of pH for the 0.1 and 0.2 M buffer conditions. The conformation of chitosan in solution becomes

more compact at higher ionic strengths, and at this condition the PEM thickness has little pH dependence. The results above indicate that the changes in PEM thickness observed with changes in solution properties are not caused by changes in the conformation of the polymer chains in solution.

4.3.3 Ellipsometry

Chi-ha PEMs at pH 5, 0.2 M buffer condition was rinsed with ethanol, and analyzed *ex situ* by ellipsometry to determine the thickness and refractive index at dry condition. In Chapter 3, a similar set of experiments is reported obtained for the chi-hep thickness measurement using ellipsometry and data indicated that thicknesses measured from ellipsometry are thinner than that obtained by *in situ* FT-SPR, due to the drying and collapse of the sample, as the ellipsometry measurements are obtained in air. In order to confirm our measurement for another system of PEMs, *ex situ* ellipsometry was done on a chi-ha PEMs formed from pH 5, 0.2 M buffer, and the measured thickness was 36 nm. The corresponding refractive index of the dry PEMs measured from ellipsometry was 1.47. Ellipsometry was also conducted on a wet film, and the refractive index was determined to be 1.37.[5] This refractive index was used to calculate the chi-ha PEM from the FT-SPR data.[5, 25] The thickness obtained from FT-SPR, which is measured *in-situ* was 78 nm for the same condition. Results clearly indicates that refractive index of wet and dry sample are significantly different for chi-ha PEMs. Figure 4.7 shows ψ as a function of wavelength for chi-ha PEMs at two different angles. Experimental results successfully overlaps with model fit which is obtained by Cauchy equation.[3]

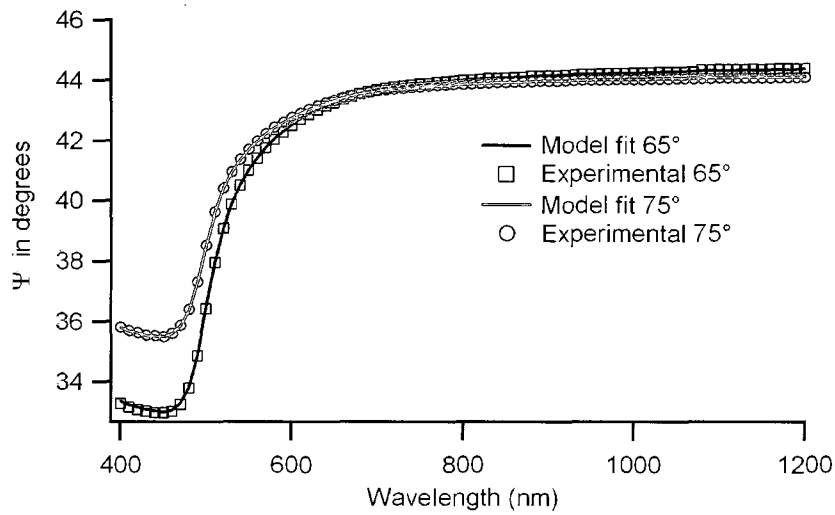

Figure 4.7 Experimental and model fit measurements for ψ (degree) as a function of wavenumber in two different angles, 65° and 75°, from spectroscopic ellipsometry for chi-ha PEMs assembled from pH 5, 0.2 M buffer.

4.4 Conclusions

The goal of the work presented in this chapter was to determine how the pH and ionic strength of buffer solutions influences the conformation of dissolved polyelectrolytes, and to determine whether this solution behavior could be related to the film thickness obtained from PEMs assembly. In general, we found that all three polysaccharides adopt more compact conformations in solution as the ionic strength of the solution is increased, except for hyaluronan at the lowest pH. This is probably due to screening of electrostatic repulsion at high ionic strength, and increased electrostatic repulsion at low ionic strength. However, these differences were not statistically significant. We also found for both chi-HA and chi-hep (c.f. Chapter 3) PEMs that the PEM thickness has little pH dependence at the highest buffer ionic strength. As the electrostatic screening is reduced, by reducing the ionic strength, the pH has a greater affect on the PEM thickness, but pH

has little influence over the polymer conformation in solution. Thus, it can be concluded from this work that at reduced solution ionic strength, pH has a stronger influence over the complexation at surfaces, independent of the solution conformation, while at high ionic strength, the electrostatic screening tends to reduce the influence of electrostatic interactions in both individual polymer chains in solution and between oppositely charged polymer chains at surfaces.

4.5 References

1. Lee, M. K.; Lander, A. D., Analysis of affinity and structural selectivity in the binding of proteins to glycosaminoglycans - development of a sensitive electrophoretic approach. *Proceedings of the National Academy of Sciences of the United States of America* **1991,** 88, (7), 2768-2772.
2. Kuschert, G. S. V.; Coulin, F.; Power, C. A.; Proudfoot, A. E. I.; Hubbard, R. E.; Hoogewerf, A. J.; Wells, T. N. C., Glycosaminoglycans interact selectively with chemokines and modulate receptor binding and cellular responses. *Biochemistry* **1999,** 38, (39), 12959-12968.
3. Boddohi, S.; Killingsworth, C. E.; Kipper, M. J., Polyelectrolyte multilayer assembly as a function of pH and ionic strength using the polysaccharides chitosan and heparin. *Biomacromolecules* **2008,** 9, (7), 2021-2028.
4. Boddohi, S.; Moore, N.; Johnson, P. A.; Kipper, M. J., Polysaccharide-Based Polyelectrolyte Complex Nanoparticles from Chitosan, Heparin, and Hyaluronan. *Biomacromolecules* **2009,** 10, 1402-1409.
5. Boddohi, S., Yonemura, S., and Kipper, M.J., Polysaccharides with tailored nanostructures for biomedical applications. *Polymer Preprints* **2009,** 50, (1), 331-332.
6. Baxter, A.; Dillon, M.; Taylor, K. D. A.; Roberts, G. A. F., Improved method for IR determination of the degree of N-Acetylation of chitosan. *International Journal of Biological Macromolecules* **1992,** 14, (3), 166-169.
7. Schatz, C.; Viton, C.; Delair, T.; Pichot, C.; Domard, A., Typical physicochemical behaviors of chitosan in aqueous solution. *Biomacromolecules* **2003,** 4, (3), 641-648.
8. Salmivirta, M.; Lidholt, K.; Lindahl, U., Heparin sulfate: A piece of information. *Faseb Journal* **1996,** 10, (11), 1270-1279.
9. Buhler, E.; Rinaudo, M., Structural and dynamical properties of semirigid polyelectrolyte solutions: A light-scattering study. *Macromolecules* **2000,** 33, (6), 2098-2106.
10. Pa, J. H.; Yu, T. L., Light scattering study of chitosan in acetic acid aqueous solutions. *Macromolecular Chemistry and Physics* **2001,** 202, (7), 985-991.
11. Hokputsa, S.; Jumel, K.; Alexander, C.; Harding, S. E., Hydrodynamic characterisation of chemically degraded hyaluronic acid. *Carbohydrate Polymers* **2003,** 52, (2), 111-117.
12. Lapcik, L.; De Smedt, S.; Demeester, J.; Chabrecek, P., Hyaluronan: Preparation, structure, properties, and applications. *Chemical Reviews* **1998,** 98, (8), 2663-2684.
13. Balazs, E. A.; Laurent, T. C., Viscosity function of hyaluronic acid polyelectrolyte. *Journal of Polymer Science* **1951,** 6, (5), 665-667.
14. Cleland, R. L., Ionic polysaccharides .2. comparison of polyelectrolyte behavior of hyaluronate with that of carboxymethyl cellulose. *Biopolymers* **1968,** 6, (11), 1519-&.
15. Fouissac, E.; Milas, M.; Rinaudo, M., Shear-rate, concentration, molecular-weight, and temprature viscosity dependences of hyaluronate, a wormlike polyelectrolyte. *Macromolecules* **1993,** 26, (25), 6945-6951.

16. Fouissac, E.; Milas, M.; Rinaudo, M.; Borsali, R., Influence of the ionic-stregnth on the dimensions of sodium hyaluronate. *Macromolecules* **1992,** 25, (21), 5613-5617.
17. Maleki, A.; Lafitte, G.; Kjoniksen, A. L.; Thuresson, K.; Nystrom, B., Effect of pH on the association behavior in aqueous solutions of pig gastric mucin. *Carbohydrate Research* **2008,** 343, (2), 328-340.
18. Pavlov, G.; Finet, S.; Tatarenko, K.; Korneeva, E.; Ebel, C. In *Conformation of heparin studied with macromolecular hydrodynamic methods and X-ray scattering*, 2003; 2003; pp 437-449.
19. Ortega, A.; de la Torre, J. G., Equivalent radii and ratios of radii from solution properties as indicators of macromolecular conformation, shape, and flexibility. *Biomacromolecules* **2007,** 8, (8), 2464-2475.
20. Bertini, S.; Bisio, A.; Torri, G.; Bensi, D.; Terbojevich, M., Molecular weight determination of heparin and dermatan sulfate by size exclusion chromatography with a triple detector array. *Biomacromolecules* **2005,** 6, (1), 168-173.
21. Zhang, H.; Neau, S. H., In vitro degradation of chitosan by a commercial enzyme preparation: effect of molecular weight and degree of deacetylation. *Biomaterials* **2001,** 22, (12), 1653-1658.
22. Anthonsen, M. W.; Varum, K. M.; Smidsrod, O., Solution properties of chitosans-conformation and chain stiffness of chitosans with different degrees of N-acetylation. *Carbohydrate Polymers* **1993,** 22, (3), 193-201.
23. Tsaih, M. L.; Chen, R. H., Molecular weight determination of 83% degree of decetylation chitosan with non-gaussian and wide range distribution by high-performance size exclusion chromatography and capillary viscometry. *Journal of Applied Polymer Science* **1999,** 71, (11), 1905-1913.
24. Bothner, H.; Waaler, T.; Wik, O., Limiting viscosity number and weight average molecular-weight of hyaluronate samples produced by heat degradation. *International Journal of Biological Macromolecules* **1988,** 10, (5), 287-291.
25. Miller, M. D.; Bruening, M. L., Correlation of the swelling and permeability of polyelectrolyte multilayer films. *Chemistry of Materials* **2005,** 17, (21), 5375-5381.

Chapter 5

Polysaccharide-based Polyelectrolyte Complex Nanoparticles from Chitosan, Heparin, and Hyaluronan

- **S. Boddohi**, N. Moore, P.A. Johnson, M.J. Kipper, "Size and composition of polysaccharide-based polyelectrolyte complex nanoparticles at different charge molar ratios." *Biomacromolecules,* 10, 1402-1409, 2009

5.1 Abstract

The formation of polyelectrolyte complex nanoparticles (PCN) was investigated at different charge mixing ratios for the chitosan-heparin (chi-hep) and chitosan-hyaluronan (chi-ha) polycation-polyanion pairs. The range of 0.08–19.2 for charge mixing ratio (+/-) was examined. The one-shot addition of polycation and polyanion solutions used for the formation of the PCN permitted formation of both cationic and anionic particles from both polysaccharide pairs. The influence of the charge mixing ratio on the size and zeta potential of the particles was investigated. The morphology and stability of the particles when adsorbed to surfaces was studied by scanning electron microscopy (SEM). For most conditions studied, colloidally stable, non-stoichiometric PCN were formed in solution. However, PCN formation was inhibited by flocculation at charge mixing ratios near 1. When adsorbed to surfaces, and dried, some formulations resulted in discrete nanoparticles, while others partially or completely aggregated or coalesced, leading to different surface morphologies.

5.2 Introduction

Several techniques have been reported for the formation of nanoparticles from soft materials. These include both nanoparticle-surfactant, and polymer-polymer complex formation.[1-4] Oppositely charged polyelectrolytes are known to form stable intermolecular complexes.[2, 5] The formation of soluble complexes between oppositely charged polyelectrolytes was studied early on by Tsuchida.[6] Subsequently, the formation of soluble PCN from polymers containing both weak and strong ionic groups was demonstrated and studied extensively.[7] Many experimental parameters can influence the size of polyelectrolyte complex nanoparticles (PCN), including charge mixing ratio, polyelectrolyte size and charge density, the presence of low molecular weight ions, and concentration of polyelectrolytes.[3, 8-11] The ability of a polycation-polyanion pair to form stable PCN may also be influenced by the local polymer chain stiffness, depending upon the relative molecular weights and the charge mixing ratio, as discussed by Schatz *et al.* for the chitosan-dextran sulfate system.[9] The complexation between proteins and synthetic polyelectrolytes has been studied.[12] In one such study, the aggregation of these complexes was shown to depend only on the mixing ratios of the polymer and protein, and not on their concentrations.[12]

Recent investigations into the practical uses of PCN in biomedical applications has driven the desire to produce PCN from biomedically relevant polyelectrolytes.[13, 14] Evidence suggests that the nanoscale organization of surface features and surface chemistries can influence biological responses to materials.[15-19] Thus, we are interested in developing techniques to tune the nanostructure of polysaccharide-based surfaces.[20] Polyelectrolyte complex nanoparticles (PCN) represent a potentially useful means for

introducing nanoscale features into biomaterials' surfaces. In this work the formation of PCN containing the polysaccharide chitosan, a weak polycation, and two different anionic polysaccharides was studied. The structures of these three polysaccharides are shown in Figure 5.1.

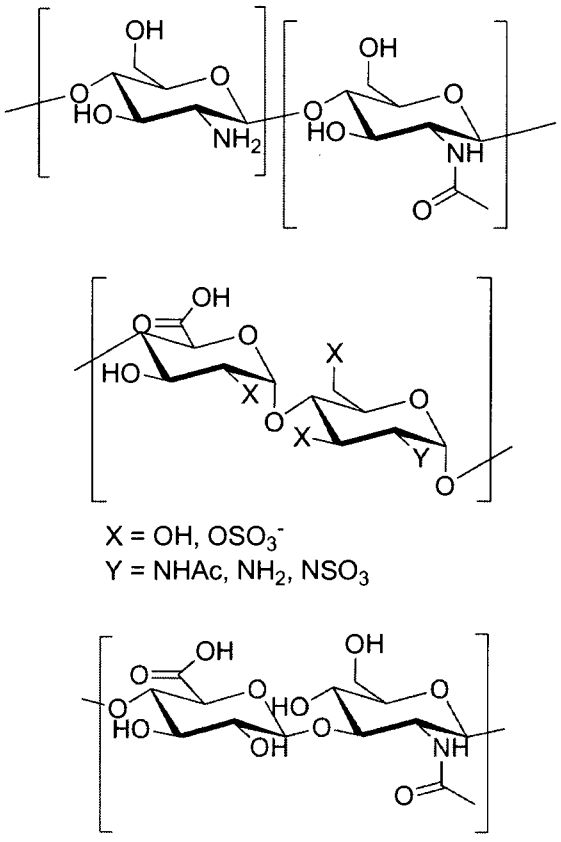

Figure 5.1. Chitosan (top), heparin (center), and hyaluronan (bottom).

All three of these polysaccharides are of particular interest to the tissue engineering community. The ability to form nanostructures with controlled size and composition from these polysaccharides is an important step to engineering the nanostructure of polysaccharide-based materials and surfaces for tissue engineering applications. Chitosan has demonstrated antimicrobial activity and has been shown to promote wound healing.[21-

[23] The conformation and the size of chitosan chains in dilute solution depend upon the charge density and ionic strength.[24] Chitosan is insoluble in most solvents and insoluble in aqueous solutions above its pK_a, but protonation of the amine below its pK_a makes chitosan soluble in dilute aqueous solutions of organic acids such as acetic acid.[25] Heparin behaves as a strong polyanion and hyaluronan behaves as a weak polyanion. Heparin has the highest negative charge density of any known biological polyanion, due to the presence of carboxyl and sulfate groups.[26] It has high sequence variability, with multiple possible sulfation sites and some D-glucuronic acid residues replaced with L-iduronic acid.[27] Heparin contains sequences which bind a variety of proteins including enzymes, and growth factors.[28] In particular, heparin binds, stabilizes, and potentiates the activity of fibroblast growth factors, and members of the transforming growth factor beta superfamily.[28-33] Hyaluronan is a non-sulfated glycosaminoglycan and is an important component of the extracellular matrix of joint tissues.[34]

The two goals of this work are to demonstrate the formation of both anionic and cationic polysaccharide-based PCN and characterize their morphology and aggregation when adsorbed to surfaces. We use the chitosan-heparin (chi-hep) and chitosan-hyaluronan (chi-ha) polyelectrolyte pairs. These polyelectrolyte pairs are both "asymmetric" in the sense that the molecular weights of the two constituent polyelectrolytes are very different. The chi-hep pair represents a relatively high-molecular weight weak polycation paired with a relatively low-molecular weight strong polyanion. The chi-ha pair represents a relatively high-molecular weight weak polyanion paired with a lower molecular weight weak polycation. Thus, successful formation of both anionic and cationic PCN from these two systems represents a broad range of accessible

polysaccharide-based PCN formulations. The effect of charge mixing ratio on the size, zeta potential, and stability of PCN particles is also evaluated.

5.3 Experimental

5.3.1 Materials

Purified chitosan (poly(β-(1,4)-D-glucosamine-*co*-*N*-acetyl-D-glucosamine; 4.7% acetylated) was purchased from Biosyntech Inc. (Laval, Canada). Heparin sodium (from porcine intestinal mucosa, 12.5% sulfur) was purchased from Celsus Laboratories (Cincinnati, OH). Hyaluronic acid sodium salt was purchased from Sigma-Aldrich (St. Louis, MO). Glacial acetic acid and ethanol (200 proof 99.5+ %) were purchased from Acros Organics (Geel, Belgium). Sodium acetate was purchased from Fisher Scientific (Pittsburgh, PA). A Millipore Synthesis water purification unit was used to obtain 18.2 MΩ water, used for making all aqueous solutions (Millipore, Billerica, MA).

Chitosan, heparin, and hyaluronan were analyzed using a Viscotek gel permeation chromatograph (GPC; Houston, TX) using a GPC Max (auto sampler, solvent delivery pump, and solvent degasser) equipped with a column oven, differential refractive index detector (VE3580 RI Detector), low-angle and right-angle laser light scattering detector, and four capillary viscometer (270 Dual Detector). For GPC analysis, polymer solutions (0.9 mg/mL for chitosan, 4.75 mg mL^{-1} for heparin, and 1 mg mL^{-1} for hyaluronan) were prepared using a 0.1 M, pH 5.0 acetate buffer. Chitosan solutions were stirred for 1 to 2 hours at 40 °C. The refractive index increments (dn/dc) of chitosan, heparin, and hyaluronan were determined by differential refractive index measurements from five different injection volumes (60, 80, 100, 120, and 140 μL). Elution took place at 1 mL

min^{-1} across two analytical PL Aquagel-OH MIXED 8 μm columns (Polymer Laboratories, Amherst, MA) at 38 °C. The weight-average molecular weights and polydispersity indices obtained from light scattering, and the hydrodynamic radii obtained from viscometry are summarized in Table 5.1. Also reported in Table 1 are the parameters of the Mark-Houwink equation for the molecular weight dependence of the intrinsic viscosity, $[\eta] = KM_W^a$, obtained from viscometry.

Table 5.1. Polysaccharide properties obtained by GPC.

Polymer	M_w (Da)	PDI	$Log_{10}(K \times g\ dl^{-1})$	a	R_H (nm)
Chitosan	302,000	1.52	-3.7 ± 0.2	0.86 ± 0.04	34.0 ± 0.5
Heparin	14,700	1.14	-4.6 ± 0.1	0.96 ± 0.02	3.68 ± 0.02
Hyaluronan	743,000	1.16	-2.5 ± 0.5	0.64 ± 0.07	61 ± 1

The Mark-Houwink exponent, a, can be used to characterize the conformation of the polymer chains in solution. Smaller values indicate a more compact or globule conformation while larger values indicate increased chain stiffness. The Mark-Houwink exponent, a, for hyaluronan indicates that it exhibits random-coil behavior. The relatively high value of a obtained for heparin indicates that it exhibits stiff coil behavior, while the a value for chitosan indicates that it exhibits a more flexible coil behavior. The conformation of chitosan in solution has been found to be a strong function of ionic strength, degree of acetylation, and pH, with reported experimental Mark-Houwink exponents ranging from less than 0.6 to greater than 1.1.[35]

5.3.2 PCN Preparation

Pure polymer solutions (0.9 mg mL^{-1} for chitosan, 0.95 mg mL^{-1} for heparin, and 1 mg mL^{-1} for hyaluronan) were prepared in 0.1 M, pH 5.0 acetate buffer. At pH 5.0 chitosan has sufficient protonated amines to form complexes with sulfate groups of heparin and carboxylate groups in hyaluronan and heparin. These solutions were filtered using 0.22 μm syringe filters (PVDF, Fisher Scientific). All mixed polymer solutions were prepared with 20 mL of total solution. The charge density of each polymer was computed assuming pK_a = 6.4 for the amine groups in chitosan, and pK_a = 2.9 for the carboxylic acid groups in hyaluronan, and assuming that each heparin disaccharide contains 3 sulfate groups. For example, for chitosan, the charge density (positively charged groups per gram of chitosan) was computed by accounting for the fraction of monomer units that would carry a positive charge at pH 5.0 given a pK_a of 6.4 for the primary amine, accounting for the fraction of monomer units that are de-acetylated. PCN were prepared at room temperature by one-shot addition[9] using chitosan as the starting solution for cationic particles and heparin or hyaluronan as the starting solution for anionic particles. The appropriate volume of the oppositely charged polymer solution was then added to the starting solution to obtain the desired charge mixing ratio. Charge mixing ratio was calculated based on the charge density of each polymer in solution. It has been shown that one-shot addition can help to inhibit some flocculation of PCN when the charge mixing ratio is close to 1, and that the size of the resulting PCN is less sensitive to the order of mixing than for the dropwise titration method used in some previous work.[9] A constant magnetic stirring of 800 rpm for 3 hours was maintained during the complex formation. After 3 hours of stirring, all solutions were allowed to

settle overnight to remove aggregated particles. After settling, the solutions containing dissolved PCN were decanted. Decanted solutions were centrifuged at 4500×g for 15 minutes to separate the particles from un-complexed polymer, using an Eppendorf 5804 centrifuge, (Eppendorf, Westbury, NY). After centrifuging, the upper part of the solution was disposed of, leaving behind only the particles. These particles were then resuspended in 10 mL of the pH 5.0 0.1 M acetate buffer. Ten different charge mixing ratios were attempted for chi-hep PCN and six different charge mixing ratios were attempted for chi-ha particles. The range of charge mixing ratios investigated was from 0.08 to 19.17 (+/-).

5.3.3 Yield of Particles

After the resuspension of PCN, 2 mL of that solution were used for estimating the particle yield at each condition. Solutions were centrifuged at 4500×g for 15 minutes. The majority of the supernatant was then removed, without removing the particles. Approximately 50 to 100 μL of buffer remained mixed with the particles so that the particles could easily be transferred for drying. The collected particles were dried in aluminum dishes of known mass in a drying oven to constant mass at 80 °C. The mass of the dried particles was then determined by difference, and the particle yield was estimated as the mass of dry PCN obtained per mass of polymer in the starting solutions.

5.3.4 Dynamic Light Scattering (DLS)

A DynaPro Titan (Wyatt Technologies, Santa Barbara, CA) instrument was used to perform DLS, using an 830-nm laser. All measurements were performed at a fixed angle of 90° at 25 °C. Five measurements of 50 s each were performed for each 10-μL sample

of suspended PCN. DLS correlation functions were analyzed by two separate methods that are commonly used to interpret light scattering of polymer solutions and colloids. First, the regularization algorithm in the Dynamics software package (Wyatt, Version 6.10.1.2) was used to determine relaxation rates, Γ_i, corresponding to the diffusion of nanoparticles (and, potentially, other modes of relaxation in the samples). The regularization algorithm is a regression method for obtaining a distribution of relaxation rates that fit the field autocorrelation function to a superposition of multiple relaxations according to:

$$g^{(1)}(\tau) = \sum_i w_i \exp(-\Gamma_i \tau) \tag{5.1}$$

The relative intensity weight of the i^{th} relaxation rate, Γ_i, is w_i. ($\Sigma_i w_i = 1$.) Second, field autocorrelation functions were also fit to a function containing a "fast" single exponential followed by a "slow" stretched exponential (Williams-Watts equation) of the form:

$$g^{(1)}(\tau) = A\exp(\Gamma_f \tau) + (1-A)\exp\left[-(\Gamma_s \tau)^{\beta}\right] \tag{5.2}$$

In equation 5.2, Γ_f and Γ_s represent the characteristic fast and slow relaxation rates, respectively, and the parameter β is a measure of the breadth of the distribution of relaxation rates for the stretched exponential component. This method has been found to be a good description of DLS for amphiphillic polymers in aqueous solutions in general, and for polysaccharides in particular, which are capable of interparticle interactions that result in a coupling of the individual particle dynamics to the surroundings. [36-41] In both methods hydrodynamic radii were obtained using the Stokes-Einstein relationship.

Equation 5.1 (the regularization method) provides a distribution of relaxation rates corresponding to a distribution of particles sizes, while equation 5.2 (the stretched exponential) assumes a single characteristic relaxation rate corresponding to the diffusion of the particle population sampled. Thus use of equation 5.2 requires far fewer parameters, and allows for the existence of non-diffusive modes of relaxation. Equation 5.1 is capable of characterizing multimodal distributions, but because its solution is ill-posed, it may result in minor peaks in the relaxation rate distribution that arise from experimental uncertainty and rounding errors in the numerical fitting algorithm. The details of these analyses are provided in the Supporting Information.

5.3.5 Zeta Potential

The zeta potential of the chi-hep and chi-ha nanoparticles in acetate buffer solution (pH 5.0, 0.1 M at 25 °C) was measured using a ZetaPALS instrument (Brookhaven Instruments Corp., Holtsville, NY). Each sample was measured 5 times and the values reported are the mean zeta potential for each sample ± the standard error of the mean. The zeta potentials of each sample were also measured by a Zetasizer nano series (Malvern Instruments, Westborough, MA). Three measurements for each sample were taken. The data from the Malvern instrument confirmed the results from the Brookhaven instrument, and are therefore not reported.

5.3.6 Scanning Electron Microscopy (SEM)

The shape and size of PCN adsorbed to surfaces was investigated by SEM using a JEOL JSM-6500F field emission scanning electron microscope (Jeol, Peabody, MA). To

prepare the SEM samples, a droplet of nanoparticles was deposited on carbon stickers on aluminum stubs, dried in a desiccator, and coated with 10 nm of gold using an argon atmosphere evaporator. Images at four different magnifications (330×, 1000×, 3300×, and 33000×) were collected for each sample. Some of the negatively charged PCN interacted very strongly with the adhesive on the carbon stickers, causing the PCN to sink into the adhesive. Negatively charged PCN were therefore also deposited either directly on the aluminum stubs or on gold-coated aluminum stubs.

5.4 Results

5.4.1 Yield of Particles

Estimates (± 5 %) of the experimental yields of the chi-hep and chi-ha PCN at different charge mixing ratios are shown in Table 5.2 and Table 5.3, respectively. In general, conditions that yielded measurable quantities of PCN had yields less than 40 %. This raises the possibility that the composition of the particles might not be well-correlated to the composition of the mixed solutions, as significant fractions of polymer may have formed aggregates, or (particularly the polymer in excess) may have remained in solution once the polymer in default was depleted. For both the chi-hep and chi-ha systems, the conditions with charge mixing ratios nearest to 1 did not form soluble PCN (0.78 and 1.42 for the chi-hep and chi-ha systems, respectively). Also, for the chi-ha system the condition with the largest excess of chitosan did not form soluble PCN.

Table 5.2. Yield, hydrodynamic radii from the regularization method ($R_{H(reg)}$) and the stretched exponential method ($R_{H(se)}$), and zeta potential for chi-hep PCN at each charge mixing ratio.

Charge mixing ratio (+/-)	Yield (mass %)	$R_{H(reg)}$ (nm)[a]	$R_{H(se)}$ (nm)[b]	Zeta potential (mV)
17.55	30	227 ± 4	232 ± 2	21.7 ± 0.8
10.53	30	271 ± 9	244 ± 3	29.5 ± 1.7
4.68	25	260 ± 10	260 ± 4	31.2 ± 0.6
2.73	18	304 ± 6	306 ± 4	29.7 ± 0.9
1.75	23	318 ± 6	329 ± 7	25.1 ± 0.9
0.78	0	-	-	-
0.50	38	298 ± 8	261 ± 8	-25.4 ± 2.3
0.29	25	217 ± 3	199 ± 3	-20.8 ± 0.6
0.13	23	175 ± 1	184 ± 4	-18.7 ± 3.3
0.08	28	170 ± 3	174 + 2	-22.8 ± 0.7

[a]Mean ± 95 % confidence interval, for R_H determined by fitting the primary peak in the distribution of relaxation rates obtained from equation 5.1 to a log-normal distribution.

[b]R_H ± 95 % confidence interval, obtained from the fast relaxation rate, Γ_f, from equation 5.2.

Table 5.3. Yield, hydrodynamic radii from the regularization method ($R_{H(reg)}$) and the stretched exponential method ($R_{H(se)}$), and zeta potential for chi-hep PCN at each charge mixing ratio.

Charge mixing ratio (+/-)	Yield (mass %)	$R_{H(reg)}$[a] (nm)	$R_{H(se)}$[b] (nm)	Zeta potential (mV)
19.2	0	-	-	26.7 ± 2.3
8.52	18	277 ± 2	292 ± 4	26.7 ± 1.5
3.19	13	225 ± 2	235 ± 1	24.6 ± 1.0
1.4	0	-	-	-
0.53	23	197 ± 2	193 ± 5	-22.1 ± 0.9
0.23	23	184 ± 4	200 ± 12	-21.4 ± 1.3

[a]Mean ± 95 % confidence interval, for R_H determined by fitting the primary peak in the distribution of relaxation rates obtained from equation 5.1 to a log-normal distribution.

[b]R_H ± 95 % confidence interval, obtained from the fast relaxation rate, Γ_f, from equation 5.2.

5.4.2 Dynamic Light Scattering of PCN

Figure 5.2 shows the field autocorrelation functions, $g^{(1)}(\tau)$, for representative examples of positively and negatively-charged chi-hep and chi-ha PCN. The data shown in Figure 5.2 are the means of the five replicate measurements for each sample. Fits to equations 5.1 and 5.2 are also shown. Beyond 10^4 μs, as the intensity autocorrelation function nears 1 for all samples, the measurement uncertainty is amplified. This could have a significant effect on the estimation of parameters in equation 5.2.[42] Therefore, the parameters for equation 5.2 were obtained from fits over the range from 1 to 10^4 μs. For equation 5.1, the behavior at very long relaxation times has little influence over the estimates of the relaxations at shorter times. Thus, the data for the five replicate

measurements of each formulation were individually fit to equation 5.1 over the entire range of the data. For each replicate, the distribution of relaxation rates, w_i, obtained from equation 5.1 contained a primary peak (generally accounting for > 90% of the total distribution) that was attributed to the diffusion of the PCN. Peaks in the relaxation rate distribution that represented faster or slower rates generally accounted for less than 10 % of the distribution of relaxation rates for all samples. These secondary peaks were often present, but did not appear at the same relaxation rates in all five replicate measurements for any of the formulations. They likely arise from a combination of small amounts of contaminants in the PCN samples (e.g. uncomplexed polymer, or PCN aggregates) and from uncertainty in fitting the data to the superposition of exponential decays. In all cases, the primary relaxations occur in the region from 10^3 to 10^4 μs. Both methods fit the data with residuals less than ± 0.01 over the range from 1 to 10^4 μs. (Residuals are shown below each plot in Figure 5.2.) The inset in Figure 5.2a shows the field autocorrelation function plotted versus τ^{β}, showing the linear behavior of the logarithm of $g^{(1)}(\tau)$ in equation 5.2.

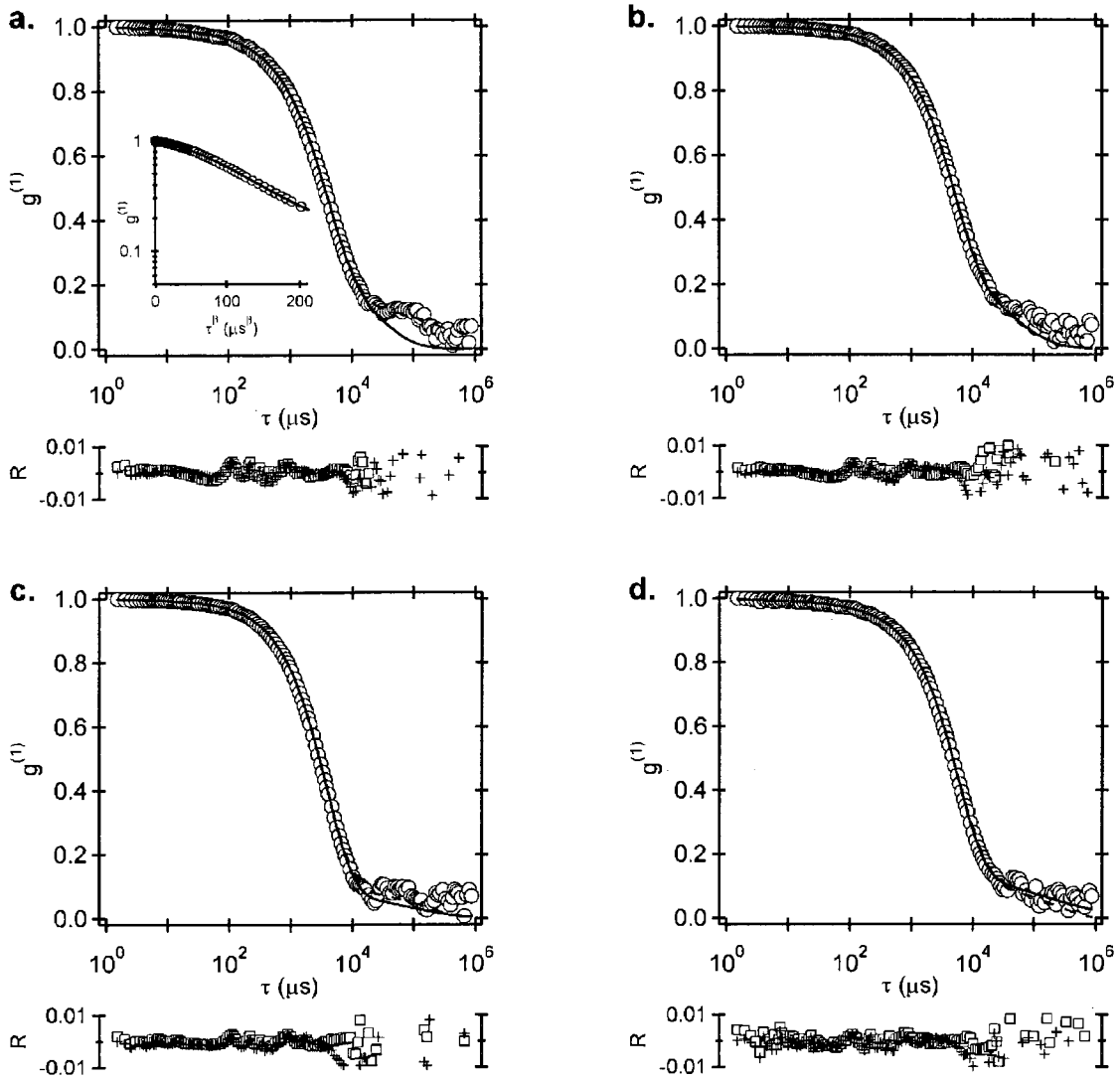

Figure 5.2. Electric field autocorrelations for chi-hep PCN formed at charge mixing ratios of 0.29 and 4.68 (a. and b., respectively) and for chi-ha PCN formed at charge mixing ratios of 0.53 and 8.52 (c. and d., respectively). In all four plots, O represents experimental data, the solid curve is the fit to equation 5.2 (fit parameters obtained over the region from 1 to 10^4 μs), and the broken curve is the fit to equation 5.1 (over the entire range of the data). The residuals (R = data – fit) are shown for equation 5.2 (□) and equation 5.1 (+) on the secondary axis below each plot. The inset in Figure 5.2a shows the range of linear behavior of the logarithm of $g^{(1)}(\tau)$ versus τ^{β} predicted by equation 5.2.

The distributions of relaxation rates obtained from the regularization method were used to compute a distribution of PCN hydrodynamic radii for each sample. These

distributions of hydrodynamic radii for chi-hep and chi-ha PCN are shown in parts a and b of Figure 5.3 and Figure 5.4, respectively. These particle size distributions are well-represented by log-normal distributions. Figure 5.5 shows the distributions of relaxation rates, w_i, plotted versus $1/\Gamma_i$, from which the particle size distributions in Figures 5.3 and 5.4 were determined. Using equation 5.1, the distributions of relaxation rates cannot be very finely resolved, *i.e.* the primary peak contains only 5 to 15 data points. Fitting these data to a log-normal distribution therefore enables estimates of the mean particle size and the confidence intervals for each distribution. Part c of Figures 5.3 and 5.4 shows the geometric mean ± the standard deviation of the distribution of particle sizes for a log-normal distribution that best fits the particle size distributions shown in parts a and b of the corresponding figures, as a function of charge mixing ratio. Tables 5.2 and 5.3 also show the mean hydrodynamic radii ($R_{H(\text{reg})}$) of particles obtained at each condition. The uncertainties on $R_{H(\text{reg})}$ shown in Tables 5.2 and 5.3 represent the 95 % confidence interval on determination of the mean from the five replicate measurements made at each charge mixing ratio. Also shown in Tables 5.2 and 5.3 are the hydrodynamic radii (± 95 % confidence interval) corresponding to the fast relaxation times obtained from fitting the data to equation 5.2 ($R_{H(\text{se})}$).

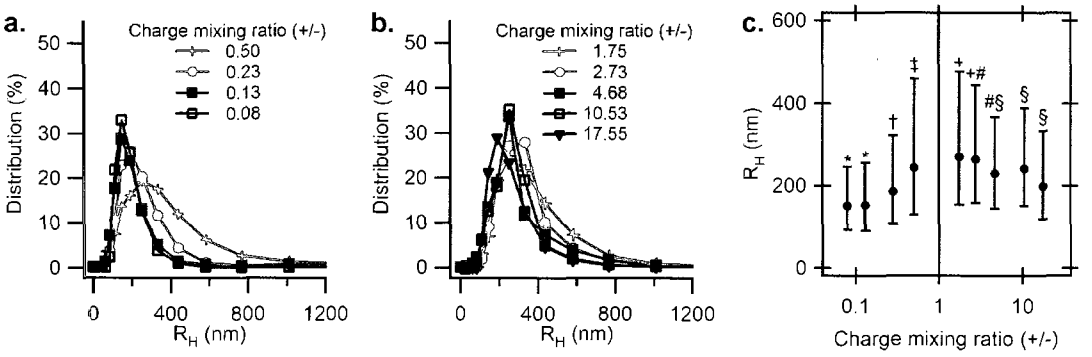

Figure 5.3. Size distributions of negatively charged (a.) and positively charged (b.) chi-hep PCN at different charge mixing ratios, determined from the regularization method (equation 5.1). Approximate log-normal size distributions represented as the geometric mean ± standard deviation of the distribution (c.) for each of the distributions shown in a. and b. as a function of charge mixing ratio. In c., the data marked with symbols are statistically different ($p < 0.05$) from data of not marked with the same symbol. (Comparisons were only made among particles with like charge, i.e. charge mixing ratio either greater than or less than 1.) Statistical differences were determined by comparing the means determined from log-normal fits to the five replicate measurements made on each sample, using a two-tailed t-test ($p < 0.05$). 95 % confidence intervals on each mean are reported in Table 5.2.

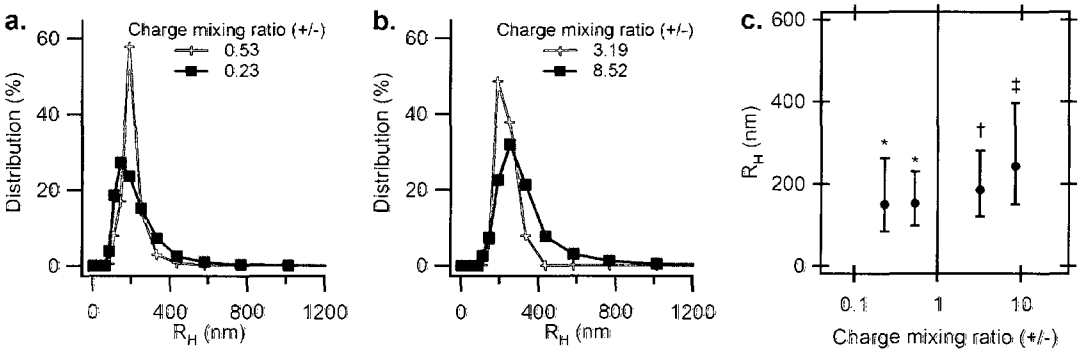

Figure 5.4. Size distributions of negatively charged (a.) and positively charged (b.) chi-ha PCN at different charge mixing ratios, determined from the regularization method (equation 5.1). Approximate log-normal size distributions represented as the geometric mean ± standard deviation of the distribution (c.) for each of the distributions shown in a. and b. as a function of charge mixing ratio. In c., the data marked with symbols are statistically different ($p < 0.05$) from data of not marked with the same symbol. (Comparisons were only made among particles with like charge, i.e. charge mixing ratio either greater than or less than 1.) Statistical differences were determined by comparing the means determined from log-normal fits to the five replicate measurements made on each sample, using a two-tailed t-test ($p < 0.05$). 95 % confidence intervals on each mean are reported in Table 5.3.

For chi-hep particles (Figure 5.3, Table 5.2), the mean size increases significantly as the charge mixing ratio approaches 1 for both anionic and cationic particles. The breadth of the size distribution also increases (Figure 5.3). PCN formation close to a charge mixing ratio of 1 (+/- = 0.78) was not possible, presumably because the colloidal stability is reduced as the net particle charge is reduced. As the charge mixing ratio gets farther from 1, the particle size is reduced. We attribute this reduction in particle size to an increase in the magnitude of the net charge on the resulting particles and a corresponding increase in the colloidal stability of smaller particles.

For the chi-ha PCN, particles formed at a charge mixing ratio closer to 1 appear to have narrower size distributions (Figure 5.4). Note that no statistical difference was determined between the size distributions for the two negatively charged chi-ha PCN formulations. This is because the parametric test used to determine statistical difference compares only the means of the particle size distributions. These two formulations have similar means, but appear to have different distribution widths.

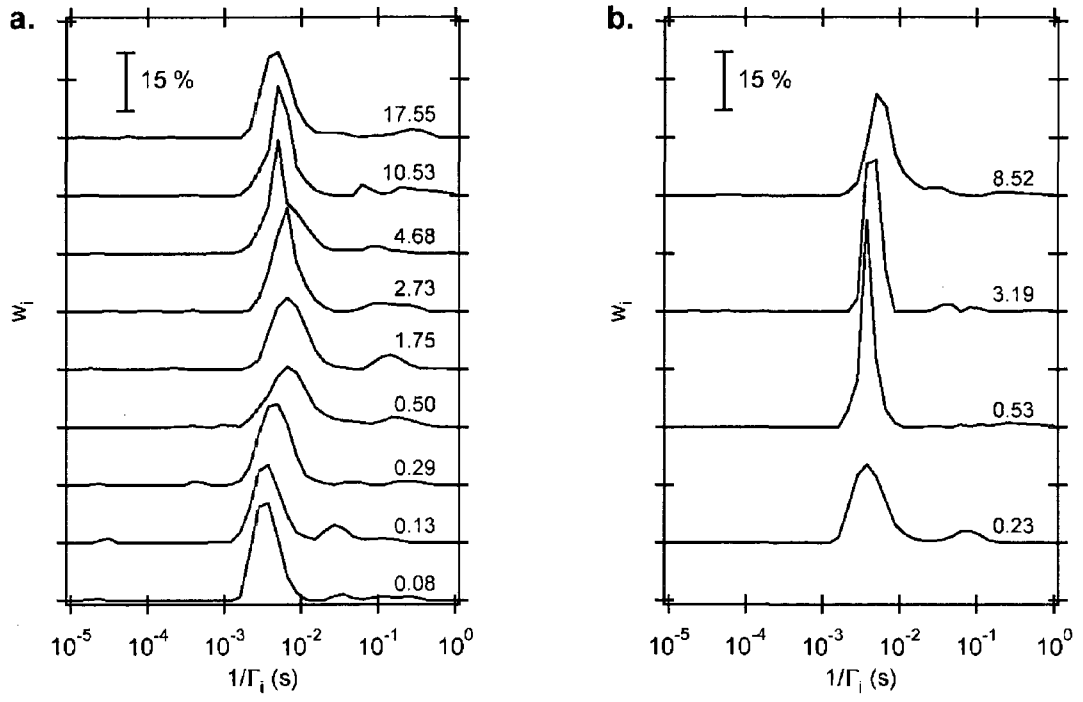

Figure 5.5. Intensity % versus decay time for chi-hep PCN (a.) and chi-ha PCN (b). Each trace is labeled with the charge mixing ratio.

Figure 5.5 shows the distributions of relaxation times ($1/\Gamma_i$), obtained by fitting of the intensity autocorrelation functions to equation 5.1. The primary peak in all of the distributions corresponds to the translational diffusion of the PCN. Notice that for the chi-hep PCN (Figure 5.5a) the primary peak represents a slower relaxation rate, corresponding to larger particles when the charge mixing ratio is closer to 1. Also, for the chi-ha PCN, the primary peak is noticeably narrower for the charge mixing ratios closer to 1, as indicated by the distributions of hydrodynamic radii in Figure 5.4. In addition to the primary peak corresponding to PCN diffusion, all distributions have secondary peaks at longer relaxation times. These secondary peaks were not consistently represented among the five replicates of each sample. They could represent large aggregates of PCN. Alternatively, they could represent the constrained relaxations associated with

coordinated diffusion of PCN, or they could arise due to uncertainty in accurately fitting the relatively noisy data at long relaxation times to a superposition of multiple relaxations.

The fast relaxation rates obtained from the fits to the stretched exponential (Γ_f) indicate the same trend in hydrodynamic radii, $R_{H(se)}$, as the mean hydrodynamic radii of the log-normal fit to the distribution of radii obtained from the regularization method, $R_{H(reg)}$. (See Tables 5.2 and 5.3.) The other fit parameters obtained from the stretched exponential function are reported in Tables SI.1 (appendix 2) and SI.2 (appendix 2) in the Supporting Information. In summary, for the chi-hep PCN the values of the stretching exponent do not indicate particularly weak coupling, however the ratio of the relative contributions of the fast to the slow relaxations indicates that any coupling between particles and their surroundings that would retard their relaxation rates is relatively weak. The only exception is for the chi-hep PCN with charge mixing ratio of 0.50, which is the case closest to the point where the particle dispersion becomes unstable. This condition also has the broadest distribution of apparent PCN radii, according to the regularization method. Thus, the significant contribution of the stretched exponential in this case could arise from the relatively broad distribution of PCN sizes. It is apparent that this condition is likely approaching the flocculation point and the sample likely contains some small aggregates. These observations indicate that the conditions studied here (< 1.0 mg mL^{-1}) are likely in the dilute regime where the PCN size can be accurately determined by the regularization method. The chi-ha samples all exhibited even less contribution of the stretched exponential component, again indicating that there is very little coupling of the particle dynamics in these samples.

5.4.3 Zeta Potential Measurement

The zeta potential measurements confirm that both anionic and cationic PCN can be formed from both the chi-ha and chi-hep polysaccharide pairs. The magnitude of the zeta potential for most formulations is less than 30 mV, suggesting that the PCN may be prone to aggregation. Ultimately, we are interested in using these PCN to introduce nanoscale topographical features and nanoscale regions of varying surface chemistry to polysaccharide-based surfaces. To achieve control over such features at the nanoscale, it is important to know how these PCN may aggregate when adsorbed to surfaces. The adsorption behavior was investigated by SEM. SEM images also provide some confirmation of the PCN sizes measured by DLS and may help to elucidate the degree of aggregation.

5.4.4 Morphology of Surface-Adsorbed PCN

PCN solutions were applied to aluminum stubs, dried, and coated with gold prior to imaging by scanning electron microscopy. Representative scanning electron micrographs are shown in Figure 5.6. Figure 5.6a and 5.6b depict positively and negatively charged chi-hep PCN (with charge mixing ratios of 4.68 and 0.29), respectively. Figure 5.6c and 5.6d depict positively and negatively charged chi-ha PCN (with charge mixing ratios of 8.52 and 0.53), respectively. Figure 6e shows the chi-hep preparation at a charge mixing ratio of 0.78, at which no soluble PCN were obtained (c.f. Table 5.2). The chi-hep PCN with charge mixing ratio of 4.68 exhibit a relatively uniform preparation of particles, free from aggregates, when these are dried on a surface (Figure 5.6a). The particles seen in the SEM image are somewhat smaller than the range of sizes determined by DLS, probably

due to collapse of the PCN upon drying. In contrast, the negatively charged chi-hep particles formed at a charge mixing ratio of 0.53 (Figure 5.6b) show some individual PCN and some apparent flocculation (see inset). The negatively charged chi-ha PCN (Figure 5.6d) formed at a charge mixing ratio of 0.53 have a relatively narrow distribution of sizes in solution (see Figures 5.4 and 5.5b). However, when adsorbed to a surface and dried, these PCN show a very broad range of sizes, ranging from less than 100 nm to over 1 μm. These appear to be a mixture of PCN and larger coalesced particles. The chi-ha PCN shown in Figure 6c and the chi-hep particles shown in Figure 5.6e are mostly flocculated when adsorbed to a surface. In these two samples, flocculated clusters are clearly made up of smaller, ~100-nm particles, as seen in the insets.

Presumably, in solution the particles do not behave as hard spheres. Rather, they likely have a gel-like or solid core surrounded by a charged corona.[43] Both the core and the corona likely collapse upon drying, but the drying also is accompanied by an increase in the concentration of both the PCN and the buffer salts. The increase in buffer concentration during drying results in additional screening of the electrostatic repulsions that otherwise stabilize the PCN and expand their coronas. Thus relatively stable particles may get smaller, as seen in Figure 5.6a and some of the particles in Figures 5.6b and 5.6d. While other PCN flocculate (as seen in Figures 5.6b and 5.6c) or coalesce (as seen in Figure 5.6d) to form larger particles.

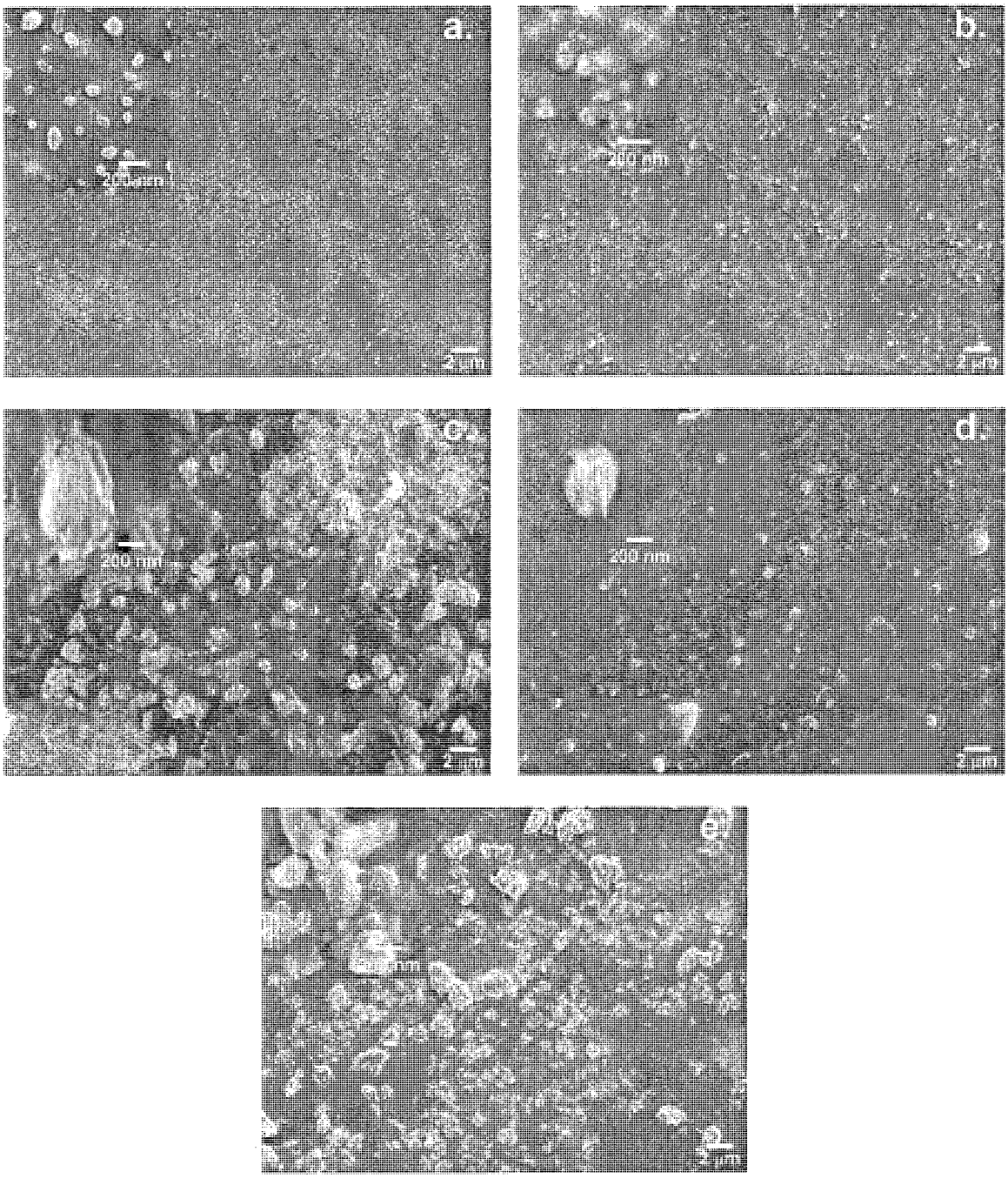

Figure 5.6. Scanning electron micrographs of positively charged chi-hep PCN (a.), negatively charged chi-hep PCN (b.), positively charged chi-ha PCN (c.), negatively charged chi-ha PCN (d.), and chi-hep particles at 0.78 charge mixing ratio showing aggregation (e.). The higher magnification inset in the upper left corner of each image shows the morphology of the PCN.

5.5 Discussion

In this work, the formation of both positively charged and negatively charged PCN was achieved for both the chi-hep and the chi-ha polyelectrolyte pairs. DLS of the PCN solutions exhibited a primary relaxation that could be attributed to the diffusion of the particles, and secondary relaxations that could be attributed to either larger aggregates, constrained diffusion of the PCN, or uncertainty in fitting the DLS data at long relaxation times. The use of the stretched exponential (equation 5.2) to interpret the DLS data suggested that there is not strong coupling of the particle dynamics. Thus we conclude that at the concentrations studied (< 1.0 mg mL^{-1}), the PCN are in the dilute regime, and that slower relaxations represent some aggregation arising from instability of the colloidal particles.

PCN from a polysaccharide system (chitosan-dextran sulfate, chi-DS) similar to our chi-hep PCN were recently studied by Schatz *et al.* They observed a decrease in PCN size as the charge mixing ratio approached 1 (over the charge mixing ratio range from about 1.2 to 20) for positively charged chi-DS nanoparticles when a high-molecular weight chitosan (350 kDa) was combined with relatively low molecular weight DS (5 or 10 kDa).[9] Also, they were not able to make negatively charged particles with 5 kDa DS or with charge mixing ratios greater than 0.3 (+/-) using 10 kDa DS. Because the heparin used in our work and the low-molecular weight DS used their work are both small strong polyanions with high negative charge density, these discrepancies warrant additional discussion.

In the work of Schatz *et al.*, the inability to form PCN using low molecular weight DS was attributed to the relative flexibility of the DS chains.[9] In their model of the PCN

formation the relatively flexible (α-1,6–linked) DS chains are capable of achieving complete charge neutralization when interacting with a chitosan molecule by conforming to the larger chitosan molecule and by forming ionic cross-links among chitosan chains. This presumably results in two populations of DS chains – those that remain in solution and those that complex almost completely with chitosan, forming insoluble hydrophobic aggregates. The flexibility of the DS may also help to explain why they observe decreasing PCN size as the charge mixing ratio approaches 1 for positively charged particles. As DS is added, it can conform to chitosan in the corona of existing PCN, causing them to collapse.

DS is a flexible, branched polysaccharide, whereas heparin is a relatively stiff (see Table 5.1), linear polysaccharide. Thus, we propose that the negatively charged chi-hep particles form by a different mechanism than the chi-DS aggregation observed by Schatz *et al.* When chitosan is added (in default) to a heparin solution (in excess), the high charge density and relative stiffness of the heparin combined with the large size of the chitosan prevents the conformational matching of the positive and negative charge groups. Thus a region of a chitosan molecule that is bound to excess heparin acquires a negative charge and strong water solubility, while the region that binds less heparin is able to form a gel-like core with similar regions of chitosan chains on other molecules, surrounded by the negatively charged corona. Over the range of charge mixing ratios investigated in this work, increasing the excess heparin causes farther collapse of the chi-hep particles, possibly by increasing the degree of ionic crosslinking in the particle cores or by increased electrostatic repulsion that limits the coalescence of primary complexes. Positively charged chi-hep PCN formed when chitosan is in excess, are probably formed

when heparin forms ionic cross-links among multiple chitosan chains. In contrast to the chi-DS complexes, additional heparin causes positively charged chi-hep PCN to grow rather than to collapse. This could be because the relatively stiff heparin prefers to form ionic crosslinks among primary chi-hep complexes, rather than inducing collapse of the corona into the PCN core.

For the weak polyelectrolyte pair, chi-ha, the conditions farther from a charge mixing ratio of 1 have a broader distribution of sizes than those closer to a charge mixing ratio of 1. (See Figure 5.4 and 5.5b). This probably indicates that the particles consist of a relatively dense hydrophobic core, in which the charges are neutralized, surrounded by a much less dense hydrophilic corona containing the excess charge. Thus as the charge mixing ratio is farther from 1, the relative size of the corona is increased.

The formulations of PCN studied here exhibit a variety of morphologies when adsorbed to surfaces. When adsorbed to surfaces and dried, the particles with sufficiently high zeta potential adsorb as discrete particles. Figure 5.6a shows a condition with the highest magnitude of zeta potential (chi-hep at charge mixing ratio of 4.68, zeta potential > 30 mV) exhibiting distinct particles adsorbed to the surface. For this and similar conditions, electrostatic repulsion prevented aggregation during adsorption. Less stable PCN may coalesce (Figure 5.6d) or flocculate (Figures 5.6b), or may aggregate almost completely before (Figure 5.6e) or during (Figures 5.6c) deposition and drying.

Reihs *et al.* studied the adsorption of a preparation of PCN using a synthetic weak polyanion-strong polycation pair by scanning electron microscopy.[44] Their PCN had similar size distributions to ours. In their work the adsorption of the neat PCN preparation and the PCN isolated by centrifugation were compared. They found that the neat PCN

solution, which had a higher polydispersity index, also had a higher propensity to coalesce when adsorbed, than the less polydisperse PCN isolated by centrifugation.[44] This was attributed to the presence of many smaller primary aggregates in the non-purified sample, which might facilitate interactions among larger PCN during adsorption.[44] We did not specifically investigate the effects of polydispersity on aggregation or coalescence, but we did observe some coalescence (Figure 5.6d) in our samples that had the narrowest size distributions. Nonetheless, the work of Reihs *et al.* suggests that controlling the purity and polydispersity of the PCN preparation may be important to controlling the morphology of adsorbed particles.

5.6 Conclusion

In this work, the formation of PCN from the chi-hep and chi-ha polyelectrolyte pairs was characterized. Both systems could form either positively charged or negatively charged PCN. The size and morphology of the particles were examined by DLS and SEM respectively. At conditions close to a charge mixing ratio of 1 the size of both positively charged and negatively charged chi-hep PCN tends to increase, and PCN tend to aggregate. For chi-ha PCN, this trend in PCN size with charge mixing ratio was not observed for the conditions investigated. These PCN provide a means of introducing nanoscale surface topographical features and nanoscale regions of varying biochemical functionality for the modification of biomaterials surfaces. The resulting surface morphology can be altered by changing the charge mixing ratio resulting in changes in the PCN stability.

5.7 Supporting Information (Appendix 2)

Details of the two methods used to interpret the DLS data, and the results of these analyses are available in the Supporting Information. This material is available free of charge via the Internet at http://pubs.acs.org.

5.8 References

1. Antonietti, M.; Conrad, J.; Thunemann, A., Polyelectrolyte-surfactant complexes - a new-type of solid, mesomorphous material. *Macromolecules* **1994,** 27, (21), 6007-6011.
2. Philipp, B.; Dautzenberg, H.; Linow, K. J.; Kotz, J.; Dawydoff, W., Poly-electrolyte complexes - recent developments and open problems. *Progress in Polymer Science* **1989,** 14, (1), 91-172.
3. Thunemann, A. F.; Muller, M.; Dautzenberg, H.; Joanny, J. F. O.; Lowne, H., Polyelectrolyte complexes. *Polyelectrolytes with Defined Molecular Architecture Ii* **2004,** 166, 113-171.
4. Tsuchida, E., Formation of Polyelectrolyte Complexes and Their Structures. *J Macromol Sci Pure Appl Chem* **1994,** A31, (1), 1-15.
5. Fredheim, G. E.; Christensen, B. E., Polyelectrolyte complexes: Interactions between lignosulfonate and chitosan. *Biomacromolecules* **2003,** 4, (2), 232-239.
6. Tsuchida, E.; Osada, Y.; Sanada, K., Interaction of poly(styrene sulfonate) with polycations carrying charges in the chain backbone. *J Polym Sci Polym Chem Ed* **1972,** 10, 3397-3404.
7. Kabanov, V.; Zezin, A., Soluble interpolymeric complexes as a new class of synthetic polyelectrolytes. *Pure Appl Chem* **1984,** 56, (3), 343-354.
8. Dautzenberg, H., Polyelectrolyte complex formation in highly aggregating systems. 1. Effect of salt: Polyelectrolyte complex formation in the presence of NaCl. *Macromolecules* **1997,** 30, (25), 7810-7815.
9. Schatz, C.; Domard, A.; Viton, C.; Pichot, C.; Delair, T., Versatile and efficient formation of colloids of biopolymer-based polyelectrolyte complexes. *Biomacromolecules* **2004,** 5, (5), 1882-1892.
10. Drogoz, A.; David, L.; Rochas, C.; Domard, A.; Delair, T., Polyelectrolyte complexes from polysaccharides: Formation and stoichiometry monitoring. *Langmuir* **2007,** 23, 10950-10958.
11. Dautzenberg, H.; Karibyants, N., Polyelectrolyte complex formation in highly aggregating systems. Effect of salt: response to subsequent addition of NaCl. *Macromolecular Chemistry and Physics* **1999,** 200, (1), 118-125.
12. Ball, V.; Winterhalter, M.; Schwinte, P.; Lavalle, P.; Voegel, J. C.; Schaaf, P., Complexation mechanism of bovine serum albumin and poly(allylamine hydrochloride). *Journal of Physical Chemistry B* **2002,** 106, (9), 2357-2364.
13. Liu, W. G.; Sun, S. J.; Cao, Z. Q.; Xin, Z.; Yao, K. D.; Lu, W. W.; Luk, K. D. K., An investigation on the physicochemical properties of chitosan/DNA polyelectrolyte complexes. *Biomaterials* **2005,** 26, (15), 2705-2711.
14. Hartig, S. M.; Greene, R. R.; Carlesso, G.; Higginbotham, J. N.; Khan, W. N.; Prokop, A.; Davidson, J. M., Kinetic analysis of nanoparticulate polyelectrolyte complex interactions with endothelial cells. *Biomaterials* **2007,** 28, (26), 3843-3855.
15. Kay, S.; Thapa, A.; Haberstroh, K. M.; Webster, T. J., Nanostructured polymer/nanophase ceramic composites enhance osteoblast and chondrocyte adhesion. *Tissue Engineering* **2002,** 8, (5), 753-761.

16. Webster, T. J.; Ergun, C.; Doremus, R. H.; Siegel, R. W.; Bizios, R., Enhanced functions of osteoblasts on nanophase ceramics. *Biomaterials* **2000,** 21, (17), 1803-1810.
17. Christenson, E. M.; Anseth, K. S.; van den Beucken, J. J. J. P.; Chan, C. K.; Ercan, B.; Jansen, J. A.; Laurencin, C. T.; Li, W.-J.; Murugan, R.; Nair, L. S.; Ramakrishna, S.; Tuan, R. S.; Webster, T. J.; Mikos, A. J., Nanobiomaterial applications in orthopedics. *J Orthop Res* **2007,** 25, 11-22.
18. Li, W.-J.; Jiang, Y. J.; Tuan, R. S., Chondrocyte phenotype in engineered fibrous matrix is regulated by fiber size. *Tissue Eng* **2006,** 12, (7), 1775-7285.
19. Silva, G. A.; Czeisler, C.; Niece, K. L.; Beniash, E.; Harrington, D. A.; Kessler, J. A.; Stupp, S. I., Selective differentiation of neural progenitor cells by high epitope density nanofibers. *Science* **2004,** 303, 1352-1355.
20. Boddohi, S.; Killingsworth, C. E.; Kipper, M. J., Polyelectrolyte multilayer assembly as a function of pH and ionic strength using the polysaccharides chitosan and heparin. *Biomacromolecules* **2008,** 9, 2021-2028.
21. Liu, X. F.; Guan, Y. L.; Yang, D. Z.; Li, Z.; De Yao, K., Antibacterial action of chitosan and carboxymethylated chitosan. *Journal of Applied Polymer Science* **2001,** 79, (7), 1324-1335.
22. Hu, S. G.; Jou, C. H.; Yang, M. C., Surface grafting of polyester fiber with chitosan and the antibacterial activity of pathogenic bacteria. *Journal of Applied Polymer Science* **2002,** 86, (12), 2977-2983.
23. Suh, J. K. F.; Matthew, H. W. T., Application of chitosan-based polysaccharide biomaterials in cartilage tissue engineering: a review. *Biomaterials* **2000,** 21, (24), 2589-2598.
24. Schatz, C.; Viton, C.; Delair, T.; Pichot, C.; Domard, A., Typical physicochemical behaviors of chitosan in aqueous solution. *Biomacromolecules* **2003,** 4, (3), 641-648.
25. Ding, W.; Lian, Q.; Samuels, R. J.; Polk, M. B., Synthesis and characterization of a novel derivative of chitosan. *Polymer* **2003,** 44, (3), 547-556.
26. Salmivirta, M.; Lidholt, K.; Lindahl, U., Heparan sulfate: A piece of information. *FASEB J.* **1996,** 10, (11), 1270-1279.
27. Lindahl, U., What else can 'heparin' do? *Haemostasis* **1999,** 29, 38-47.
28. Guimond, S.; Maccarana, M.; Olwin, B. B.; Lindahl, U.; Rapraeger, A. C., Activating and inhibitory heparin sequences for FGF-2 (basic FGF) - distinct requirements for FGF-1, FGF-2, and FGF-4. *Journal of Biological Chemistry* **1993,** 268, (32), 23906-23914.
29. Maccarana, M.; Casu, B.; Lindahl, U., Minimal Sequence in Heparin Heparan-Sulfate Required for Binding of Basic Fibroblast Growth-Factor. *J. Biol. Chem.* **1993,** 268, (32), 23898-23905.
30. Zhao, B. H.; Katagiri, T.; Toyoda, H.; Takada, T.; Yanai, T.; Fukuda, T.; Chung, U. I.; Koike, T.; Takaoka, K.; Kamijo, R., Heparin potentiates the in vivo ectopic bone formation induced by bone morphogenetic protein-2. *Journal of Biological Chemistry* **2006,** 281, (32), 23246-23253.
31. Ruppert, R.; Hoffmann, E.; Sebald, W., Human bone morphogenetic protein 2 contains a heparin-binding site which modifies its biological activity. *European Journal of Biochemistry* **1996,** 237, (1), 295-302.

32. Mccaffrey, T. A.; Falcone, D. J.; Du, B. H., Transforming Growth Factor-Beta-1 Is a Heparin-Binding Protein - Identification of Putative Heparin-Binding Regions and Isolation of Heparins with Varying Affinity for Tgf-Beta-1. *J Cell Physiol* **1992,** 152, (2), 430-440.
33. Rider, C. C., Heparin/heparan sulphate binding in the TGF-beta cytokine superfamily. *Biochem Soc Trans* **2006,** 34, 458-460.
34. Cowman, M. K.; Matsuoka, S., Experimental approaches to hyaluronan structure. *Carbohydrate Research* **2005,** 340, (5), 791-809.
35. Kasaai, M. R., Calculation of Mark-Houwink-Sakurada (MHS) equation viscometric constants for chitosan in any solvent-temperature system using experimental reported viscometric constants data. *Carbohydrate Polymers* **2007,** 68, (3), 477-488.
36. Nystrom, B.; Walderhaug, H.; Hansen, F. K., Dynamic crossover effects observed in solutions of a hydrophobically associating water-soluble polymer. *Journal of Physical Chemistry* **1993,** 97, (29), 7743-7752.
37. Kjoniksen, A. L.; Baldursdottir, S. G.; Nystrom, B., Characterization of riboflavin-photosensitized changes in aqueous solutions of alginate by dynamic light scattering. *Macromolecular Bioscience* **2004,** 4, (2), 76-83.
38. Kita, R.; Takahashi, A.; Kaibara, M.; Kubota, K., Formation of fibrin gel in fibrinogen-thrombin system: Static and dynamic light scattering study. *Biomacromolecules* **2002,** 3, (5), 1013-1020.
39. Stepanek, P., Data analysis in dynamic light scattering. In *Dynamic light scattering: the method and some applications*, Brown, W., Ed. Oxford University Press: New York, NY, 1993; pp 177-240.
40. Horkay, F.; Basser, P. J.; Hecht, A. M.; Geissler, E., Gel-like behavior in aggrecan assemblies. *Journal of Chemical Physics* **2008,** 128, (13).
41. Ngai, K. L., Dynamics of semidilute solutions of polymers and associating polymers. *Advances in Colloid and Interface Science* **1996,** 64, 1-43.
42. Finsy, R., Particle Sizing by Quasi-Elastic Light-Scattering. *Adv Colloid Interfac* **1994,** 52, 79-143.
43. Kokufuta, E.; Ogawa, K.; Doi, R.; Kikuchi, R.; Farinato, R. S., Geometrical characteristics of polyelectrolyte nanogel particles and their polyelectrolyte complexes studied by dynamic and static light scattering. *J Phys Chem B* **2007,** 111, (29), 8634-8640.
44. Reihs, T.; Muller, M.; Lunkwitz, K., Preparation and adsorption of refined polyelectrolyte complex nanoparticles. *Journal of Colloid and Interface Science* **2004,** 271, (1), 69-79.

Chapter 6

Fabrication and Characterization of Polysaccharide-based Nanostructured Surfaces Prepared with Polyelectrolyte Complex Nanoparticles

- **S. Boddohi**, J. Almodóvar, H. Zhang, P.A. Johnson, and M.J. Kipper," Fabrication and characterization of polysaccharide-based nanostructured surfaces prepared with polyelectrolyte complex nanoparticles." *Journal of colloids and surfaces B*, 2009 (submitted).

6.1 Abstract

Nanoscale chemical and topographical features have been demonstrated to influence a variety of significant responses of mammalian cells to biomaterials surfaces. Thus, an important goal for biomaterials scientists is the ability to engineer the nanoscale surface features of biologically active materials. Here we demonstrate the fabrication and characterization of polysaccharide-based nanostructured surface coatings that combine polyelectrolyte complex nanoparticles (PCNs) in polyelectrolyte multilayers (PEMs) to create surfaces with controlled nanoscale surface topography and nanoscale presentation of surface chemistry. The polysaccharides used in this work are the biomedically relevant chitosan, heparin, and hyaluronan. Nanostructured surface coatings were characterized on both modified gold substrates and tissue-culture polystyrene surfaces. PCNs were adsorbed to oppositely charged PEMs, and were also embedded within PEMs. The construction of the surface coatings was characterized by quartz crystal microbalance

with dissipation (QCM-D). The surface morphology was characterized by scanning electron microscopy (SEM) and atomic force microscopy (AFM). The chemistry of the coatings was confirmed by both X-ray photoelectron spectroscopy (XPS) and polarization modulation infra-red reflection absorption spectroscopy (PM-IRRAS). Morphologically, we found that PCNs were colloidally stable and homogeneously distributed when adsorbed on or in the PEMs. Chemical analysis confirms that the PCNs adsorbed to PEMs significantly altered the surface chemistry, indicating significant surface coverage. Furthermore, when incorporated as a sub-terminal layer within PEMs, the position of the PCNs normal to the surface can be tuned. Thus, PCNs can be used to introduce discrete nanoscale surface topographical features and varying surface chemistry into PEM surface coatings in a controlled way.

6.2 Introduction

Since the pioneering work by Decher and coworkers, who first introduced the layer-by-layer (LBL) assembly of the polyelectrolyte multilayers (PEMs),[1-4] this technology has gained attention as an attractive method of surface coating for a broad range of applications. LBL assembly is of great interest because of its simplicity and the control over coating thickness and composition that can be obtained at the nanometer length scale. PEMs are formed by the alternating adsorption of polycations and polyanions to charged surfaces. Surface charge inversion during each adsorption step limits each layer thickness and prepares the surface for the subsequent adsorption of the oppositely charged polyelectrolyte. PEMs have been used to tune the properties of surfaces and thin films for separations, catalysis, sensors, and optical and electronic devices.[5-9] LBL assembly has generated particular interest as a technique for modifying biomaterials

surfaces.[10-14] For example, PEMs containing inorganic nanoparticles have been demonstrated to improve the attachment and spreading of mesenchymal stem cells.[13] PEMs containing polysaccharides have been used to develop surface coatings that have biochemical functionality,[15, 16] and have also been used to control the delivery of therapeutic molecules.[17-19]

Many of the applications mentioned above are made possible by the incorporation of functional macromolecules or nanoparticles into PEMs. The adsorption of inorganic and organic nanoparticles during PEM formation has been studied for several systems.[20-23] These strategies have included the use of polyelectrolyte complex nanoparticles (PCNs) incorporated into PEMs.[23-25] PCNs are made by the electrostatic complexation of oppositely charged polyelectrolytes in solution. Their formation, stability, and behavior in solution and at surfaces has been studied extensively for over 30 years.[26-28] This line of research has been pursued by several research groups, primarily using synthetic polyelectrolytes.

In their native biological contexts, the components of the extracellular matrix (ECM) and the pericellular space are organized into complex assemblies with nanoscale features.[29] These nanoscale features are essential to the biochemical and biomechanical function of the tissues in which they are found. Thus, functionalization of thin films and surface coatings with nanoscale surface features for biological applications enables the investigation of the responses of biological systems to nanomaterials, and the engineering of nanoscale surface features to tune biochemical activity and biological responses.[30, 31] For example, nanoscale topographical features of surfaces have been shown to improve the adhesion of osteogenic cells[32, 33] and chondrocytes,[34] and promote the production of

bone ECM components.[35, 36] Nanoscale organization of peptide adhesion ligands and surface chemistry have also been shown to increase the proliferation and ECM production of a pre-osteoblast cell line[37] and to promote chondrocyte adhesion and proliferation.[38] In order to fully realize the potential of nanostructured surfaces for bioengineering applications, it is essential to gain an understanding of how the nanoscale features of surfaces can be manipulated and how these features influence the emergent biological properties and biological responses of cells and tissues.

Glycosaminoglycans are an important class of polysaccharides that are organized at the nanometer length scale in tissues.[29] These polysaccharides are of particular interest as scaffolds for a variety of engineered tissues and as coatings for biomedical materials. Hyaluronan is a polyanionic glycosaminoglycan that plays an important role in organizing proteins in the pericellular space and extracellular matrix of joint tissues and acts as an adhesion ligand for cell surface receptors.[29, 39, 40] Heparin is a glycosaminoglycan that acts as a strong polyanion, and is structurally similar to other glycosaminoglycans such as chondroitin sulfate and keratan sulfate. It binds to and potentiates the activity of members of several important families of growth factors, including the fibroblast growth factor family and the transforming growth factor beta superfamily.[41-43] Chitosan is a polycation that is structurally similar to glycosaminoglycans, has antimicrobial activity, and has been demonstrated to be compatible for a variety of mammalian cell types.[44-47] Because polysaccharides are organized at a variety of length scales in their native biological environments, we are interested in developing techniques to tune their nanoscale organization in order to develop bioactive surface coatings. Thus, we and others have studied the LBL technique

for the formation of nanoscale polysaccharide-based surface coatings. In particular, the oppositely-charged chitosan-heparin and chitosan-hyaluronan pairs have been studied in detail.[10, 14, 16, 48, 49] These studies have demonstrated that the thickness and composition of polysaccharide-based PEMs can be precisely tuned by altering the deposition solution conditions (e.g. solution pH and ionic strength), and that the biochemical functionalities of the polysaccharides are preserved in PEMs.

We also recently reported on the formation of PCNs using the polysaccharides, chitosan, heparin, and hyaluronan.[50] In this work, we demonstrated that both positively charged and negatively charged PCNs formed from the chitosan-heparin (chi-hep) and chitosan-hyaluronan (chi-ha) polyelectrolyte pairs can be used to introduce nanoscale topographical features on surfaces.[50] However, some PCN compositions tended to aggregate or coalesce either before or during adsorption and drying. Furthermore, PCNs that adsorbed discretely were not homogeneously distributed on surfaces. The goal of the current work is to demonstrate that chi-hep PCNs can be used to modify surfaces, and that their homogeneous distribution can be achieved by combining them with PEMs. Because of our interest in nanostructured polysaccharide-based coatings, we used the chi-ha polysaccharide pair for the PEMs and the chi-hep polysaccharide pair for the PCNs. We demonstrated formation of these nanostructured surface coatings on both modified gold and tissue-culture polystyrene (TCPS) surfaces. The coating deposition was characterized on gold surfaces by quartz-crystal microbalance with dissipation (QCM-D). The surface morphology of these nanostructured surface coatings was characterized by scanning electron microscopy (SEM) and atomic force microscopy (AFM). The chemistry of the coatings was confirmed by both X-ray photoelectron

spectroscopy (XPS) and polarization modulation infra-red reflection absorption spectroscopy (PM-IRRAS).

6.3 Materials and Methods

6.3.1 Materials

Purified chitosan (chi) (4.7% acetylated) was purchased from Biosyntech Inc. (Laval, Canada). Heparin sodium (hep) (from porcine intestinal mucosa, 12.5% sulfur) was purchased from Celsus Laboratories (Cincinnati, OH). Hyaluronic acid sodium salt (ha) was purchased from Sigma-Aldrich (St. Louis, MO). We previously determined that these three polymers had weight average molecular weights of 302 kDa (chi), 14.7 kDa (hep) and 743 kDa (ha).[50] 11-Mercaptoundecanoic acid was purchased from Sigma-Aldrich (St. Louis, MO). Glacial acetic acid and ethanol (200 proof 99.5+ %) were purchased from Acros Organics (Geel, Belgium). Sodium acetate was purchased from Fisher Scientific (Pittsburgh, PA). A Millipore Synthesis water purification unit was used to obtain 18.2 MΩ water, used for making all aqueous solutions (Millipore, Billerica, MA).

6.3.2 PCN Preparation

PCN formation is fully described in our previous work, where the size distribution and zeta potential of PCNs are also reported.[50] Chitosan and heparin solutions were prepared at concentrations of 0.9 mg mL^{-1} and 0.95 mg mL^{-1}, respectively in acetate buffer solution (pH 5, 0.1 M). PCNs were formed by the one-shot addition of the polyelectrolyte in default to the polyelectrolyte in excess, to create a total volume of 10

mL. Charge mixing ratios (n^+/n^-) of 0.29 and 4.68 were used for the anionic and cationic PCNs, respectively. The mixture was stirred for 3 hours at 800 rpm. PCNs were then centrifuged, after allowing aggregates to settle overnight, and PCNs were resuspended in 10 mL of pH 5.0, 0.1 M acetate buffer. The yield of PCNs for these two conditions found in our previous work was about 25 % by mass.[50] Thus, after resuspending in the 10 mL of acetate buffer the PCN concentration is about 0.20 to 0.25 mg mL^{-1}. Zeta potential measurements reported in our previous work for these two conditions were –20.8 ± 0.6 mV and 31.2 ± 0.6 mV for the negatively and positively charged PCNs, respectively.[50]

6.3.3 Construction of Nanostructured Surface Coatings on Modified Gold Surfaces

PEM and PCN-containing PEM surface coatings described in Table 6.1 were constructed on two different types of gold-coated substrates using similar techniques. These two types of gold-coated substrates were AT-cut piezoelectric gold-coated sensor crystals (Q-Sense, Inc. Glen Burnie, MD) and glass slides prepared by coating with an adhesion layer of chromium, followed by gold. Details of the coating procedure are given in our previous work.[10] Both types of gold surfaces were annealed for 2 hours in 250 °C to obtain a smooth surface,[51] and then modified with a self-assembled monolayer (SAM) of 11-mercaptoundecanoic acid by soaking in a 1 mM ethanolic solution for at least 20 h, followed by a brief ethanol rinse, and drying with a gentle stream of dry air.[52, 53] The SAM provides a well-characterized surface revealing carboxylic acid groups suitable for adsorption of a polycation from solution. Chitosan and hyaluronan polyelectrolyte solutions with concentrations of 0.01 M (on a repeat unit basis) were prepared at pH 5.0

in 0.2 M acetate buffer for PEM formation. Surface coatings were then constructed by alternating adsorption of polycationic chitosan, polyanionic hyaluronan, and PCNs using five-minute adsorption steps. A five-minute rinse step (water acidified to pH 4.0 using acetic acid) followed each adsorption step. Layer-by-layer assembly of the surface coatings was conducted on the QCM-D crystals in a Q-Sense E4™ quartz crystal microbalance with dissipation monitoring (QCM-D) system (Q-Sense, Inc.). The Q-Sense E4 is equipped with QSoft 401™ software for resonance frequency and dissipation data acquisition and QTools 301™ (version 2.1.6.134) analytical software. The flow rate for the PEM formation was set at 400 μl/min. Surface coatings on the gold-coated glass substrates for PM-IRRAS were constructed in a flow cell using a similar protocol.

Eight different types of nanostructured polysaccharide-based surface coatings were studied, each of them based on chi-ha PEMs. All surfaces begin with a chi-ha PEM containing six layers, denoted m_6. These surfaces are terminated with hyaluronan. Surfaces terminated with a seventh layer (of chitosan) are denoted m_7. Both the m_6 and the m_7 surfaces were then modified with either positively charged or negatively charged chi-hep PCNs. These surfaces are denoted m_6p^+ or m_7p^+, for modification with positively charged PCNs, and m_6p^- or m_7p^- for modification with negatively charged PCNs. PEMs containing PCNs in a sub-terminal layer were prepared by adding additional multilayers on top of the m_6p^+ and m_7p^- surfaces. The multilayers added on top of the PCNs begin with the polysaccharide that has a similar charge to the adsorbed PCNs. These PEM-PCN-PEM surfaces are denoted $m_6p^+m_6$ and $m_7p^-m_6$. The composition and nomenclature for these is summarized in Table 6.1.

Table 6.1. Nomenclature used to refer to different types of surface coatings.

sample name	surface condition
m_6	$(chi\text{-}ha)_3$
m_6p^-	$(chi\text{-}ha)_3\text{-}(PCN)^-$
m_6p^+	$(chi\text{-}ha)_3\text{-}(PCN)^+$
$m_6p^+m_6$	$(chi\text{-}ha)_3\text{-}(PCN)^+\text{-}(chi\text{-}ha)_3$

sample name	surface condition
m_7	$(chi\text{-}ha)_3\text{-}chi$
m_7p^+	$(chi\text{-}ha)_3\text{-}chi\text{-}(PCN)^+$
m_7p^-	$(chi\text{-}ha)_3\text{-}chi\text{-}(PCN)^-$
$m_7p^-m_6$	$(chi\text{-}ha)_3\text{-}chi\text{-}(PCN)^-\text{-}(ha\text{-}chi)_3$

QCM-D was used to characterize the coating process during PEM and PCN deposition. In QCM-D a decrease in the resonance frequency (f) of the quartz crystal is linearly correlated with the thin film mass when the film is rigid, according to the Sauerbrey equation[54]

$$\Gamma_{QCM-D} = -\frac{C}{n}\Delta f \qquad \textbf{(6.1)}$$

where Γ_{QCM-D} is the mass adsorbed per unit area, C is the mass sensitivity constant (17.7 ng cm^{-1}), and Δf_n is the measured resonant frequency shift for overtone n. For viscoelastic films, energy dissipation may become significant, requiring that the film be modeled with a complex shear modulus in order to relate the film thickness and density to the frequency shift. In such cases, the Sauerbrey model presented in equation 6.1 is not valid.[55] The dissipation factor is defined as

$$D = \frac{E_{lost}}{2\pi E_{stored}} \tag{6.2}$$

where E_{lost} is the energy dissipated during an oscillation and E_{stored} is the energy stored during the oscillation. This dissipation factor contains information about the viscoelastic response of the film. In our experiments, we monitored both the frequency shift and the dissipation factor for the first, third, fifth, seventh, ninth, and eleventh overtones.

6.3.4 Construction of Nanostructured Surface Coatings on Tissue Culture Polystyrene (TCPS)

Construction of the PEM and PCN-containing PEM surface coatings described in Table 6.1 on TCPS was performed using sterile tissue culture polystyrene 6-well Nunclon Δ surfaces (Nunc ALS, Roskilde, Denmark). Chitosan, hyaluronan, and PCNs were adsorbed from solutions prepared as indicated above on the bottom of a 6-well plate, with adsorption steps of five minutes using acidified water (pH 4) as a rinse between adsorption steps. The adsorption and rinse steps were conducted under agitation using a vortexer, to improve mass transfer. The bottoms of the 6-well TCPS surfaces were then cut in pieces suitable for characterization

6.3.5 Atomic Force Microscopy (AFM)

The surface morphology of the nanostructured coatings was investigated using a Nanosurf Easyscan 2 AFM (Fort Lee, NJ) and PPP-NCLR-50 tips from Nanosensors (Switzerland). Micrographs were obtained using tapping mode. Image analysis was

performed using the Scanning Image Probe Processor version 4.2.2.0 software. Samples prepared on the gold-coated nanosensor crystals and TCPS surfaces were both evaluated by AFM. AFM was performed at room temperature in air at a rate of one line scan per second.

6.3.6 Scanning Electron Microscopy (SEM)

The surface morphology of the nanostructured coatings was investigated by SEM using a JEOL JSM-6500F field emission scanning electron microscope (Jeol, Peabody, MA). All samples were coated with 10 nm of gold using an argon atmosphere evaporator before taking any images. Images at five different magnifications (330×, 1000×, 3300×, 1000×, and 33000×) were collected for each sample.

6.3.7 X-ray Photoelectron Spectroscopy (XPS)

XPS experiments were performed on a Physical Electronics 5800 spectrometer (Chanhassen, MN). This system has a monochromatic Al Kα X-ray source (hν = 1486.6 eV), hemispherical analyzer, and multichannel detector. A low energy (30 eV) electron gun was used for charge neutralization on the non-conducting samples. The binding energy scales for the samples were referenced to the Au1 peak at 84 eV. High resolution spectra of the N1s and S2p envelopes were acquired at analyzer pass energy of 23.5 eV, with 0.1 eV steps, and an X-ray spot size of 800 μm. XPS elemental compositions of samples were obtained using a pass energy of 187.85 and 0.8 eV steps. All XPS analyses were performed at a photoelectron takeoff angle of 45°.[56]

6.3.8 Polarization Modulation-Infrared Reflection Absorption Spectroscopy (PM-IRRAS)

PM-IRRAS was conducted using a Nicolet 8700 FT-IR spectrometer (Thermo-Electron) configured with a Tabletop Optics Module, equipped with a PEM-90 photoelastic modulator (Hinds Instruments, Hillsboro, OR), to provide a polarization of the incident infrared light, grazing angle sampling optics, a liquid N_2-cooled MCT-A detector, and a demodulator (Hinds Instruments, Hillsboro, OR) to process the polarized spectra. 1000 PM-IRRAS spectra were collected for each sample at 8 cm^{-1} resolution. The raw PM-IRRAS spectra were then corrected to remove the second-order Bessel function of the first kind (J_2) by dividing by a baseline. The baseline was determined using predefined splinepoints in regions of the spectrum in which no IR absorption peaks appear.[57]

6.4 Results and Discussion

6.4.1 Monitoring Formation of PEMs and PCN-Containing PEMs Using QCM-D

Figure 6.1 shows the frequency shift for the third, fifth, seventh, and ninth overtones for the $m_6p^+m_6$ sample. The alternating five-minute rinse and adsorption steps can be clearly seen. The first five minutes correspond to a rinse step, followed by a five-minute chitosan adsorption step. In Figure 6.1, the beginning of each of the first six polyelectrolyte adsorption steps is indicated with an up arrow (↑), and the beginning of the PCN adsorption step is indicated by the asterisk (*). The beginning of the rinse step

following each of these adsorption steps is indicated with a down arrow (↓). Notice that the normalized frequency shifts for the different overtones overlap during the rinse steps following each of the first six polyelectrolyte adsorptions. This indicates that the Sauerbrey relation is valid for determining the film mass during these rinse steps. However, during the adsorption steps the normalized frequency shifts for the different overtones do not precisely overlap, indicating that the film at this point is viscoelastic (*i.e.,* the Sauerbrey relation does not hold). After adsorption of the PCNs (indicated by the *), the normalized frequency shifts no longer overlap during the rinse steps. This indicates that adsorbed films are viscoelastic, and that the mass can no longer be precisely determined from the Sauerbrey relationship. After adsorption of the PCNs, the ratio of the change in the dissipation factor to the change in frequency ($\Delta D/\Delta f$) remains between 0.5×10^{-7} and 1.3×10^{-7} $Hz^{-1}$for the remainder of the experiment (not shown). Where the Sauerbrey model fails, a more complex model accounting for the mechanical properties of the coatings might be used to determine the adsorbed mass from the frequency shift and dissipation data, however the parameters required to describe this multiple layered system are difficult to determine with precision for these very thin films.

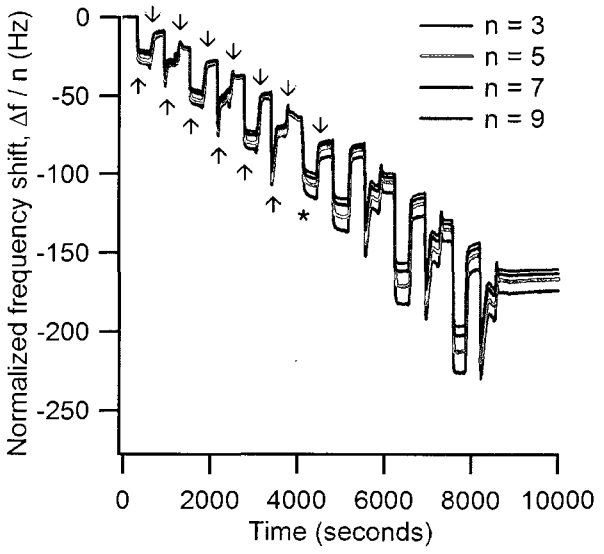

Figure 6.1. QCM-D data showing the normalized frequency shift as a function of time for the 3rd, 5th, 7th, and 9th overtones for the $m_6p^+m_6$ surface coating. The beginning of each of the first six polyelectrolyte adsorption steps is marked with an up arrow (↑), and the beginning of the PCN adsorption step is indicated by the asterisk (*). The beginning of each of the rinse steps following these adsorption steps is indicated with a down arrow (↓).

Figure 6.2 shows the normalized frequency shift for the third overtone versus time for each of the different surface coatings summarized in Table 6.2 Figure 6.2a shows the normalized frequency shift of multilayers based on hyaluronic acid (ha)-terminated (m_6) PEMs, and Figure 6.2b shows the normalized frequency shift of multilayers based on chitosan (chi)-terminated (m_7) PEMs. The mass per area for the m_6 and m_7 surface coatings can be calculated accurately from the Sauerbrey relationship. These are 1130 ng cm^{-2} and 1310 ng cm^{-2}, respectively, using the 3rd overtone. The QCM-D traces for each of the four surface coatings shown in Figure 6.2a and Figure 6.2b overlap during the adsorption of the first six layers, indicating that the coating procedure is reproducible.

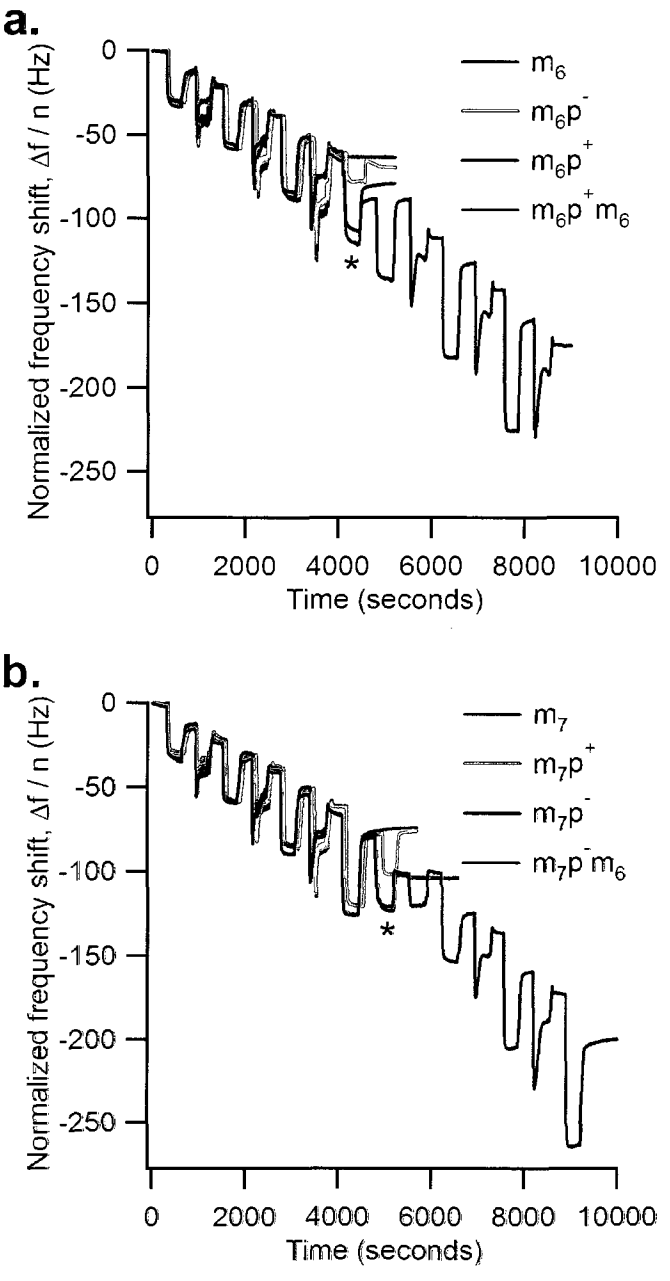

Figure 6.2. QCM-D data showing the change of normalized frequency shift as a function of time at the third overtone during the construction of eight different PEM and PEM-PCN surface coatings, with alternating five-minute rinse and adsorption intervals. Conditions based on ha-terminated (m_6) PEMs (a.). Conditions based on chi-terminated (m_7) PEMs (b.). The adsorption of PCNs is indicated by the *. The surface coatings are described in Table 6.1.

The m_6p^- and m_7p^+ conditions are cases where the PCNs have the same charge as the terminal layer of the PEMs, resulting in little adsorption of PCNs. The m_6p^+ and m_7p^- are the conditions in which positively charged PCNs were adsorbed to negatively charged surfaces and negatively charged PCNs were adsorbed to positively charged surfaces respectively. These two cases show significant frequency shifts following the PCN adsorption steps, indicating that PCNs strongly adsorb to oppositely charged surfaces. The $m_6p^+m_6$ and $m_7p^-m_6$ conditions have three chi-ha bilayers deposited on top of the PCN layer. These conditions have the greatest frequency shift corresponding to the greatest mass adsorbed among all the surfaces. We also note that during construction of the $m_6p^+m_6$ and the $m_7p^-m_6$ coatings (black traces in Figure 6.2), the frequency shifts before and after the adsorption step immediately following the PCN adsorption are very nearly equal. Since this layer has the same charge as the PCNs, it is apparent that the preceding PCN layer covers the surface uniformly and with sufficient density to electrostatically repel most of the subsequent like-charged polyelectrolyte layer.

6.4.2 Surface Morphology

Each of the eight types of surfaces represented in Table 6.1 and Figure 6.2 were imaged with atomic force microscopy (AFM). Representative 2.5 μm × 2.5 μm micrographs are shown in Figure 6.3 and Figure 6.4 for surfaces based on the m_6 PEMs and the m_7 PEMs, respectively. Figure 6.3a and Figure 6.4a show the m_6 and m_7 PEMs, respectively. Figure 6.3b and Figure 6.4b show the m_6p^- and m_7p^+ surfaces, respectively. Some surface features are observed in both of these images, indicating some surface structural changes when the surface is exposed to like-charged PCNs solutions. However,

the relatively small frequency shifts associated with the adsorption of like-charged PCNs (c.f. Figure 6.2), indicates that very few of these particles adsorb to the surfaces. This conclusion was also supported by SEM images. (See below.) This confirms that the electrostatic repulsion between the surfaces and the like-charged PCNs prevents significant PCN adsorption. Figure 6.3c and Figure 6.4c show the surface coatings with one layer of positively charged PCNs on m_6 and one layer of negatively charged PCNs on m_7, respectively (m_6p^+ and m_7p^-). QCM-D data demonstrate considerable accumulation of mass associated with the adsorption PCN onto oppositely charged surfaces (c.f. Figure 6.2). Figures 6.3d and 6.4d show the $m_6p^+m_6$ and $m_7p^-m_6$ surfaces, which have three polyelectrolyte bilayers deposited on top of the PCN layers.

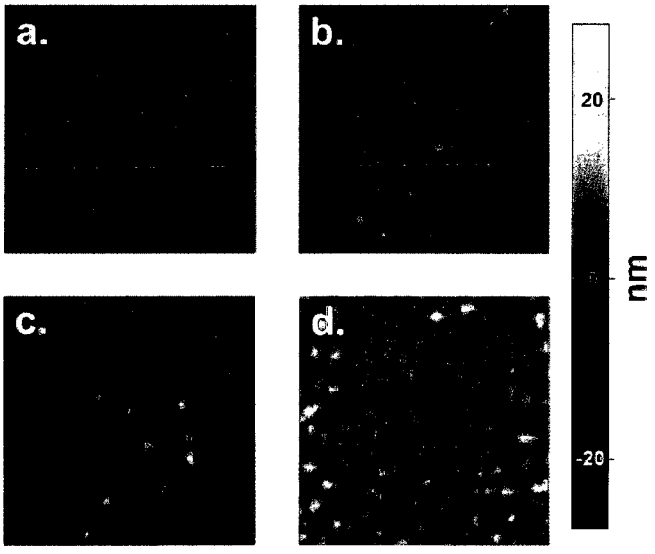

Figure 6.3. Atomic force micrographs of a chi-ha PEM (m_6) (a.), a chi-ha PEM with negatively charged chi-hep PCNs adsorbed (m_6p^-) (b.), a chi-ha PEM with positively charged chi-hep PCNs adsorbed (m_6p^+) (c.), and a chi-ha PEM with a layer of PCNs and three bilayers of chi-ha PEM adsorbed ($m_6p^+m_6$) (d.). Each AFM image is 2.5 × 2.5 μm. The color scale applies to all four images.

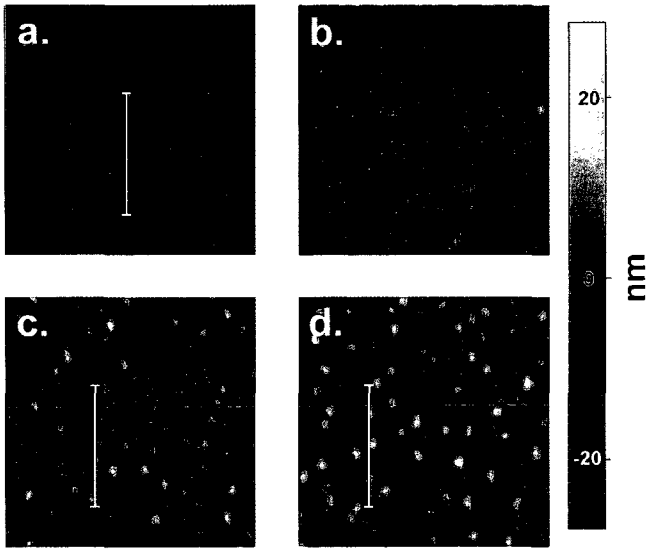

Figure 6.4. Atomic force micrographs of a chi-ha PEM (m_7) (a.), a chi-ha PEM with positively charged chi-hep PCNs adsorbed (m_7p^+) (b.), a chi-ha PEM with negatively charged chi-hep PCNs adsorbed (m_7p^-) (c.), and a chi-ha PEM with a layer of PCNs and three bilayers of chi-ha PEM adsorbed ($m_7p^-m_6$) (d.). Each AFM image is 2.5 × 2.5 μm. The color scale applies to all four images. Blue lines in a., c. and d. correspond to the line profiles shown in Figure 6.5.

Figure 6.5 shows a line profile across the m_7, m_7p^-, and $m_7p^-m_6$ surfaces. The locations of the line profiles are indicated by the blue lines in Figure 6.4. The m_7 line profile illustrates the roughness of the PEM, while the m_7p^- and $m_7p^-m_6$ line profiles show the dimensions of the adsorbed PCNs. The width of the PCNs is from 80-250 nm and their height is from 15-30 nm depending on the experimental condition. Figure 6.5 also shows that when adsorbed into or within PEMs, the adsorbed PCNs are not spherical. Rather, upon adsorption the PCNs collapse, both in the plane of the surface and in the direction normal to the surface. This morphological change during adsorption is

probably associated with water and counterion release as the PCNs form strong electrostatic interactions with the surface and potentially penetrate into the PEMs.

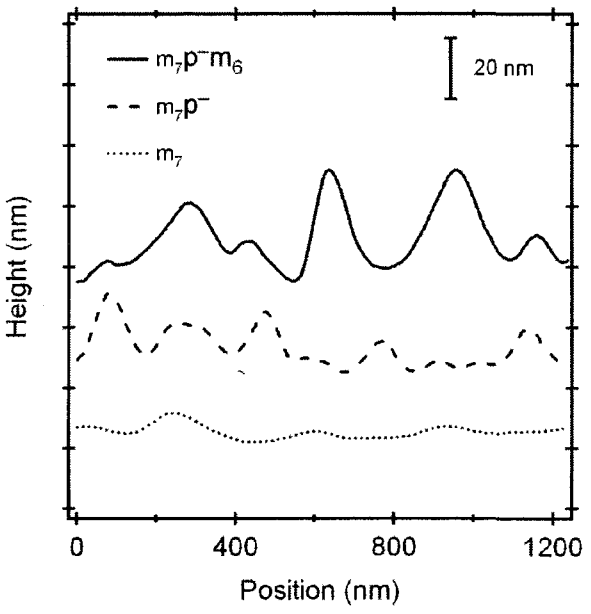

Figure 6.5. Line profile for three surface coatings obtained from AFM. The line profiles correspond to the blue lines on the images in Figure 6.4.

Surfaces were also imaged with SEM in order to evaluate the surface coverage and the coating morphology. Representative SEM images of four of the surfaces (m_6, m_6p^+, m_7p^-, and $m_6p^+m_6$) are shown in Figure 6.6. The m_6 surface shown in Figure 6.6a is relatively featureless compared to the other surfaces. When PCNs are added to PEMs (Figures 6.6b and 6.6c), uniform coverage of the entire surface is observed. This is in contrast to our observations in our previous publication, where PCNs were dried onto surfaces not modified with PEMs. In these studies PCNs did not uniformly cover the surfaces.[50] A small number of larger (~1 μm diameter) features are also observed. When PEMs are added on top of PCNs some non-spherical features are observed in the SEM

images (Figure 6.6d). It appears that the particles act as nucleation sites for additional complexation of polyelectrolytes, resulting in these small non-spherical features.

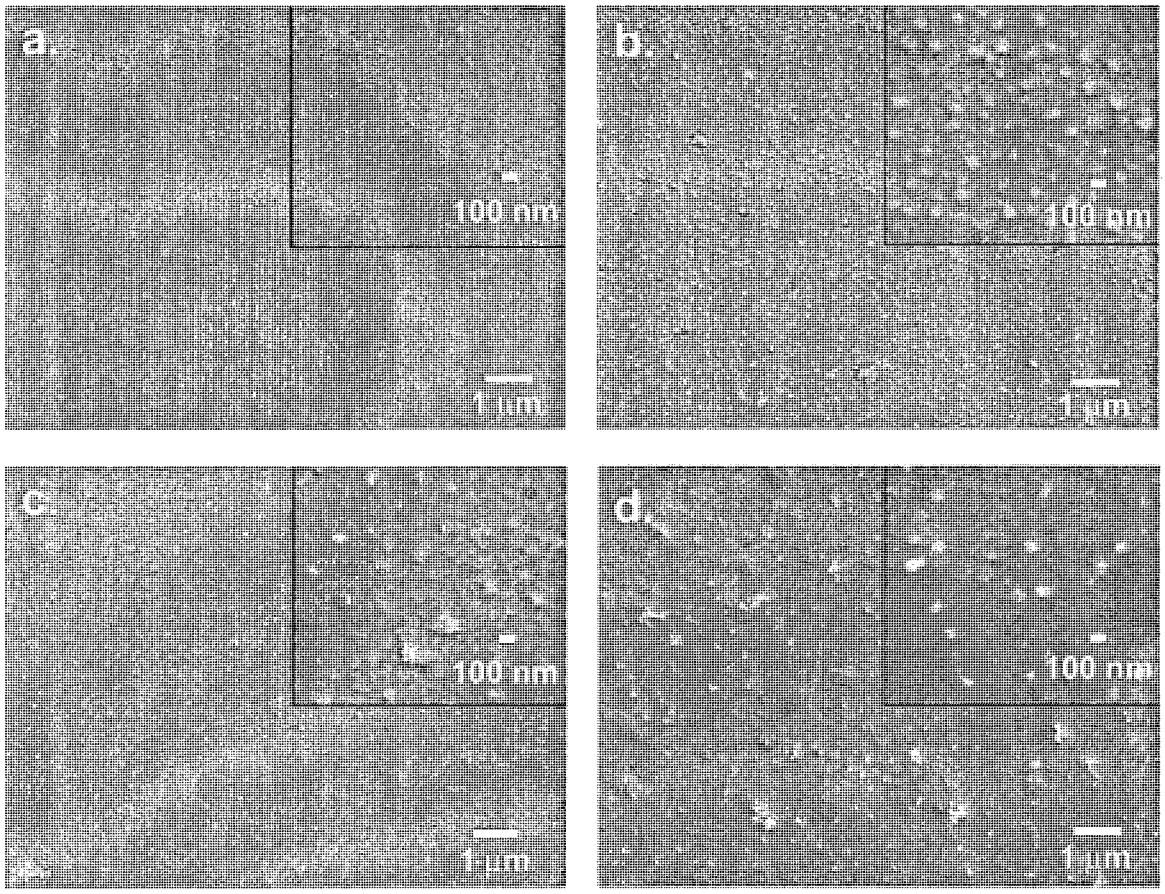

Figure 6.6. Scanning electron micrographs of m_6 (a.), m_6p^+ (b.), m_7p^- (c.), and $m_6p^+m_6$ (d.) surface coatings. The inset on the upper right corner of each image shows the surface features in higher magnification.

6.4.3 Translation of Surface Coatings to Tissue-Culture Polystyrene

In order to develop surfaces suitable for evaluating the response of mammalian cells to the nanostructured polysaccharide-based coatings described here, the polyelectrolyte multilayer assembly was also performed on tissue culture polystyrene. Surface coatings on polystyrene were prepared by exposing polystyrene surfaces to polymer, PCN, and

rinse solutions under agitation. Atomic force micrographs of the m_6 and $m_6p^+m_6$ coatings on tissue culture polystyrene are shown in Figure 6.7 The surface roughness of the polystyrene is greater than that observed on the QCM-D crystals shown in Figure 6.3 and Figure 6.4. Scanning electron micrographs of these two surfaces are shown in Figure 6.8 Figure 6.7b shows that when PCNs are added to PEM surface coatings on polystyrene they do not aggregate or coalesce, similarly to their behavior on the gold-coated substrates. However, the surface coverage on polystyrene is not as dense as on the gold-coated substrate. This is likely due to the relative charge density of the underlying substrate. The polystyrene surface may not have adsorbed as much polyelectrolyte as the modified gold-coated substrates, leading to reduced adsorption of the PCNs. Nonetheless, the micrographs of PCN-containing coatings on polystyrene (Figures 6.7b and 6.8b) demonstrate uniform, homogeneous coverage of the surface with nanoparticles.

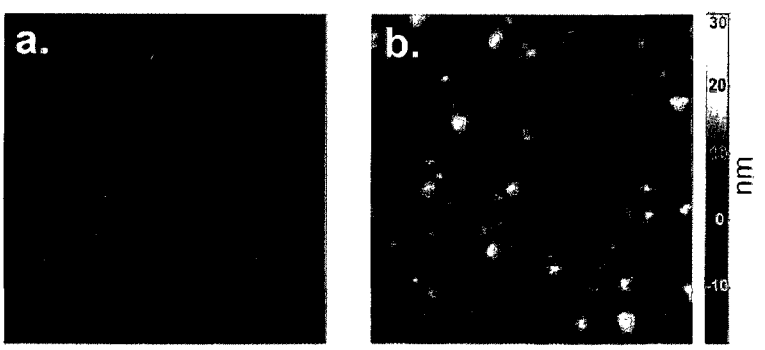

Figure 6.7. AFM image of a bare chi-ha PEM (m_6) (a.), and a PEM-PCN-PEM coating ($m_6p^+m_6$) (b.) on polystyrene. Each AFM image is 2.5 × 2.5 μm. The color scale applies to both images.

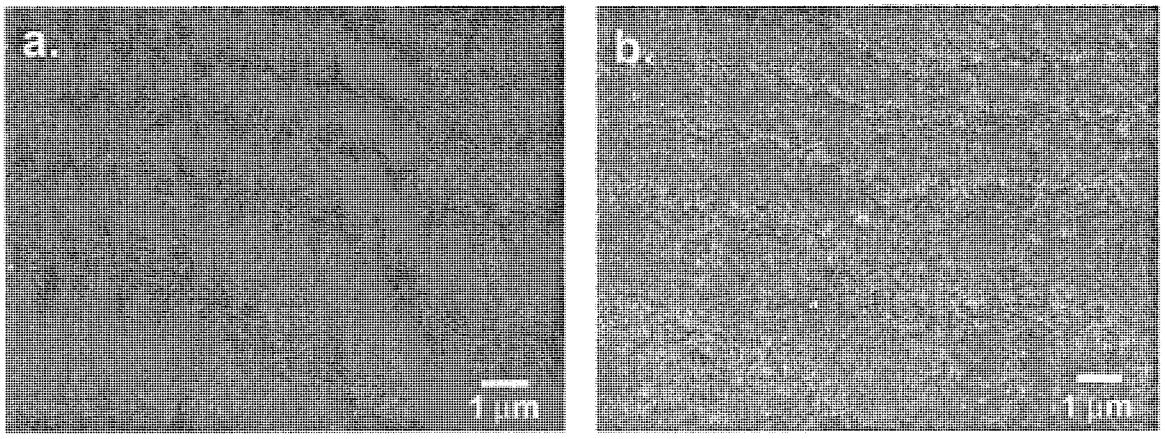

Figure 6.8. Scanning electron micrographs of m_6 (a.) and $m_6p^+m_6$ (b.) coatings on polystyrene.

6.4.4 Chemistry of Surface Coatings

The chemistry of the surface coatings was assayed with XPS and PM-IRRAS, to confirm that the features observed microscopically represent the polysaccharide-based PEMs and PCNs. Surface coatings on gold were prepared on gold-coated glass slides mounted in a flow cell, following a similar alternating rinse-adsorption protocol described for the QCM-D experiments. Atomic ratios of S to N were computed from high-resolution X-ray photoelectron spectra by finding the area of the S2p and N1s envelopes and accounting for the atom sensitivity factors, for surface coatings on both gold and polystyrene. These data are shown in Figure 6.9 Neither of the underlying substrates contains nitrogen. However, nitrogen is present in all three of the polysaccharides used in this work. Sulfur is only present in the heparin, and should therefore be detected when the PCNs are present. In the m_6 coating on gold, a very small amount of sulfur is present but no sulfur is detected for the m_6 coating on polystyrene. This small amount of sulfur observed on the gold surfaces may be from residual

physisorbed mercaptoundecanoic acid that was not completely removed from the surface prior to the PEM formation, and subsequently became oxidized. In the m_6p^+ coatings, sulfur is detected on both substrates, confirming that the features observed in the AFM and SEM images are indeed the (heparin-containing) PCNs. In $m_6p^+m_6$ surfaces the S/N ratio is reduced compared to the m_6p^+ surfaces, confirming that the multilayers are deposited on top of the particles, thereby attenuating the sulfur signal. In m_7p^- surfaces negatively charged PCNs are adsorbed onto the positively charged PEMs, meaning that heparin is the majority component in the PCNs. This is confirmed by the increased S/N ratio compared to the m_6p^+ surfaces.

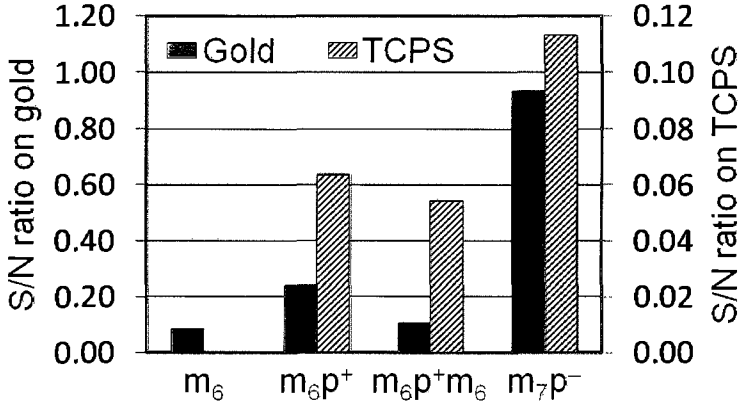

Figure 6.9. Atom ratio of sulfur to nitrogen from XPS for four different surface coatings on both gold and polystyrene substrates.

PM-IRRAS was used to study the composition of the surface coatings on gold-coated substrates. Figure 6.10 shows the corrected spectra for three of the coatings. All of the spectra have a peak at 1090 cm^{-1} corresponding to sugar modes from the polysaccharides.[58] A shoulder on this peak at 1160 cm^{-1} can be assigned to C–OH and C–N stretching modes.[58] A strong amide I peak at 1600–1700 cm^{-1} is observed from the

acetylated saccharides in chitosan and hyaluronan. A carboxylate peak at 1425 cm^{-1} arises from the carboxylic acid groups in heparin and hyaluronan.[58] The m_6p^+ and $m_6p^+m_6$ samples both exhibit a peak from 1200–1260 cm^{-1}, which is attributed to the asymmetric sulfonate stretch in heparin.[15, 59] In general, the vibrational intensities increase as more mass is added to the surface coatings.

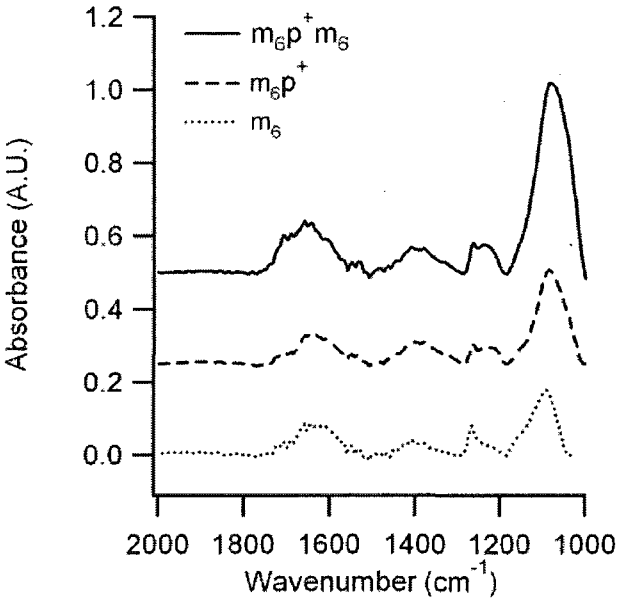

Figure 6.10. PM-IRRAS spectra of m_6-based nanostructured surface coatings on modified gold-coated glass surfaces. The m_6p^+ and $m_6p^+m_6$ spectra are vertically offset.

6.5 Conclusions

In this work, nanostructured surface coatings formed by combination of polysaccharide-based PEMs and PCNs were characterized. By adsorbing PCNs to PEMs, or including PCNs as one of the sub-terminal layers within PEMs, we demonstrate that nanoscale regions of varying surface topography can be uniformly and homogeneously introduced into PEM surface coatings. Upon adsorption, PCNs collapse significantly,

interacting strongly with the PEM surfaces. The nanoscale surface features represented by the PCNs are 15-30 nm in height and 80-250 nm in diameter. Chemical analysis by XPS and PM-IRRAS confirms the chemistry of the surfaces. Furthermore, XPS demonstrates that both positively charged and negatively charged PCNs adsorbing to oppositely charged PEMs significantly alter the surface chemistry as expected (increased sulfur for negatively charged PEMs and increased nitrogen for positively charged PEMs) indicating that the surface coverage is high. The incorporation of PCNs within PEMs enables the precise tuning of the location of the nanoparticles in the dimension normal to the surface.

This work is of particular interest for the development of biologically active nanostructured surface coatings. Heparin, and other similar sulfated glycosaminoglycans are presented in the extra cellular matrix and pericellular space of a variety of tissues. In these contexts their biochemical functionality (e.g. regulation of growth factor activity) and biomechanical function (e.g. imparting compressive strength to skeletal tissues) may depend strongly on their organization at multiple length scales, including the nanometer length scale. Thus, the ability to engineer the nanostructure of polysaccharide-based surface coatings will lead to improved understanding of the effects of nanoscale features on biological systems, and the ability to tune nanostructured surfaces to exploit emergent biological properties for bioengineering applications.

6.6 References

1. Decher, G.; Hong, J. D., Buildup of Ultrathin Multilayer Films by a Self-Assembly Process .2. Consecutive Adsorption of Anionic and Cationic Bipolar Amphiphiles and Polyelectrolytes on Charged Surfaces. *Ber. Bunsen-Ges.* **1991,** 95, (11), 1430-1434.
2. Decher, G.; Hong, J. D., Buildup of Ultrathin Multilayer Films by a Self-Assembly Process .1. Consecutive Adsorption of Anionic and Cationic Bipolar Amphiphiles on Charged Surfaces. *Macromol. Chem. Macromol. Symp.* **1991,** 46, 321-327.
3. Decher, G.; Hong, J. D.; Schmitt, J., Buildup of Ultrathin Multilayer Films by a Self-Assembly Process .3. Consecutively Alternating Adsorption of Anionic and Cationic Polyelectrolytes on Charged Surfaces. *Thin Solid Films* **1992**, 831-835.
4. Decher, G., Fuzzy nanoassemblies: Toward layered polymeric multicomposites. *Science* **1997,** 277, (5330), 1232-1237.
5. Zhang, G. J.; Song, X.; Ji, S. L.; Wang, N. X.; Liu, Z. Z., Self-assembly of inner skin hollow fiber polyelectrolyte multilayer membranes by a dynamic negative pressure layer-by-layer technique. *J. Memb. Sci.* **2008,** 325, (1), 109-116.
6. Datta, S.; Cecil, C.; Bhattacharyya, D., Functionalized membranes by layer-by-layer assembly of polyelectrolytes and *in situ* polymerization of acrylic acid for applications in enzymatic catalysis. *Ind. Eng. Chem. Res.* **2008,** 47, (14), 4586-4597.
7. Carballo, R. R.; Orto, V. C.; Hurst, J. A.; Spiaggi, A.; Bonazzola, C.; Rezzano, I. N., Covalently attached metalloporphyrins in LBL self-assembled redox polyelectrolyte thin films. *Electrochim. Acta* **2008,** 53, (16), 5215-5219.
8. Zhao, W.; Xu, J. J.; Chen, H. Y., Electrochemical biosensors based on layer-by-layer assemblies. *Electroanalysis* **2006,** 18, (18), 1737-1748.
9. Hammond, P. T., Form and function in multilayer assembly: New applications at the nanoscale. *Advanced Materials* **2004,** 16, (15), 1271-1293.
10. Boddohi, S.; Killingsworth, C. E.; Kipper, M. J., Polyelectrolyte multilayer assembly as a function of pH and ionic strength using the polysaccharides chitosan and heparin. *Biomacromolecules* **2008,** 9, 2021-2028.
11. Houska, M.; Brynda, E., Interactions of proteins with polyelectrolytes at solid/liquid interfaces: Sequential adsorption of albumin and heparin. *Journal of Colloid and Interface Science* **1997,** 188, (2), 243-250.
12. Kommireddy, D. S.; Ichinose, I.; Lvov, Y. M.; Mills, D. K., Nanoparticle Multilayers: Surface Modification for Cell Attachment and Growth. *Journal of Biomedical Nanotechnology* **2005,** 1, (3), 286-290.
13. Kommireddy, D. S.; Sriram, S. M.; Lvov, Y. M.; Mills, D. K., Stem cell attachment to layer-by-layer assembled TiO2 nanoparticle thin films. *Biomaterials* **2006,** 27, (24), 4296-4303.
14. Kujawa, P.; Moraille, P.; Sanchez, J.; Badia, A.; Winnik, F. M., Effect of molecular weight on the exponential growth and morphology of hyaluronan/chitosan multilayers: A surface plasmon resonance spectroscopy and atomic force microscopy investigation. *Journal of the American Chemical Society* **2005,** 127, (25), 9224-9234.

15. Serizawa, T.; Yamaguchi, M.; Akashi, M., Alternating bioactivity of polymeric layer-by-layer assemblies: Anticoagulation vs procoagulation of human blood. *Biomacromolecules* **2002,** 3, (4), 724-731.
16. Thierry, B.; Winnik, F. M.; Merhi, Y.; Silver, J.; Tabrizian, M., Bioactive coatings of endovascular stents based on polyelectrolyte multilayers. *Biomacromolecules* **2003,** 4, (6), 1564-1571.
17. Qiu, X.; Leporatti, S.; Donath, E.; Mohwald, H., Studies on the Drug Release Properties of Polysaccharide Multilayers Encapsulated Ibuprofen Microparticles. *Langmuir* **2001,** 17, (17), 5375-5380.
18. Schneider, A.; Vodouhe, C.; Richert, L.; Francius, G.; Le Guen, E.; Schaaf, P.; Voegel, J. C.; Frisch, B.; Picart, C., Multifunctional polyelectrolyte multilayer films: Combining mechanical resistance, biodegradability, and bioactivity. *Biomacromolecules* **2007,** 8, (1), 139-145.
19. Wood, K. C.; Chuang, H. F.; Batten, R. D.; Lynn, D. M.; Hammond, P. T., Controlling interlayer diffusion to achieve sustained, multiagent delivery from layer-by-layer thin films. *Proc. Natl. Acad. Sci. U. S. A.* **2006,** 103, (27), 10207-10212.
20. Grigoriev, D.; Gorin, D.; Sukhorukov, G. B.; Yashchenok, A.; Maltseva, E.; Mohwald, H., Polyelectrolyte/magnetite nanoparticle multilayers: Preparation and structure characterization. *Langmuir* **2007,** 23, (24), 12388-12396.
21. Li, Q.; Quinn, J. F.; Wang, Y. J.; Caruso, F., Preparation of nanoporous polyelectrolyte multilayer films via nanoparticle templating. *Chemistry of Materials* **2006,** 18, (23), 5480-5485.
22. Bogdanovic, G.; Sennerfors, T.; Zhmud, B.; Tiberg, F., Formation and structure of polyelectrolyte and nanoparticle multilayers: Effect of particle characteristics. *Journal of Colloid and Interface Science* **2002,** 255, (1), 44-51.
23. Reihs, T.; Muller, M.; Lunkwitz, K., Preparation and adsorption of refined polyelectrolyte complex nanoparticles. *Journal of Colloid and Interface Science* **2004,** 271, (1), 69-79.
24. Guo, Y.; Geng, W.; Sun, J., Layer-by-Layer Deposition of Polyelectrolyte-Polyelectrolyte Complexes for Multilayer Film Fabrication. *Langmuir* **2009,** 25, (2), 1004-1010.
25. Schuetz, P.; Caruso, F., Multilayer thin films based on polyelectrolyte-complex nanoparticles. *Colloids Surf., A* **2002,** 207, (1-3), 33-40.
26. Tsuchida, E.; Osada, Y.; Sanada, K., Interaction of poly(styrene sulfonate) with polycations carrying charges in the chain backbone. *J Polym Sci Polym Chem Ed* **1972,** 10, 3397-3404.
27. Kabanov, V.; Zezin, A., Soluble interpolymeric complexes as a new class of synthetic polyelectrolytes. *Pure Appl Chem* **1984,** 56, (3), 343-354.
28. Thunemann, A. F.; Muller, M.; Dautzenberg, H.; Joanny, J. F. O.; Lowne, H., Polyelectrolyte complexes. *Polyelectrolytes with Defined Molecular Architecture Ii* **2004,** 166, 113-171.
29. Dudhia, J., Aggrecan, aging and assembly in articular cartilage. *Cellular and Molecular Life Sciences* **2005,** 62, (19-20), 2241-2256.

30. Mendelsohn, J. D.; Yang, S. Y.; Hiller, J.; Hochbaum, A. I.; Rubner, M. F., Rational design of cytophilic and cytophobic polyelectrolyte multilayer thin films. *Biomacromolecules* **2003,** 4, (1), 96-106.
31. Chluba, J.; Voegel, J. C.; Decher, G.; Erbacher, P.; Schaaf, P.; Ogier, J., Peptide hormone covalently bound to polyelectrolytes and embedded into multilayer architectures conserving full biological activity. *Biomacromolecules* **2001,** 2, (3), 800-805.
32. Riehle, M. O.; Dalby, M. J.; Johnstone, H.; MacIntosh, A.; Affrossman, S., Cell behaviour of rat calvaria bone cells on surfaces with random nanometric features. *Mat Sci Eng C-Bio S* **2003,** 23, (3), 337-340.
33. Webster, T. J.; Siegel, R. W.; Bizios, R., Osteoblast adhesion on nanophase ceramics. *Biomaterials* **1999,** 20, (13), 1221-1227.
34. Kay, S.; Thapa, A.; Haberstroh, K. M.; Webster, T. J., Nanostructured polymer/nanophase ceramic composites enhance osteoblast and chondrocyte adhesion. *Tissue Engineering* **2002,** 8, (5), 753-761.
35. Webster, T. J.; Ergun, C.; Doremus, R. H.; Siegel, R. W.; Bizios, R., Enhanced functions of osteoblasts on nanophase ceramics. *Biomaterials* **2000,** 21, (17), 1803-1810.
36. de Oliveira, P. T.; Nanci, A., Nanotexturing of titanium-based surfaces upregulates expression of bone sialoprotein and osteopontin by cultured osteogenic cells. *Biomaterials* **2004,** 25, (3), 403-413.
37. Lee, K. Y.; Alsberg, E.; Hsiong, S.; Comisar, W.; Linderman, J.; Ziff, R.; Mooney, D., Nanoscale adhesion ligand organization regulates osteoblast proliferation and differentiation. *Nano Lett* **2004,** 4, (8), 1501-1506.
38. Olmedilla, M. P.; Garcia-Giralt, N.; Pradas, M. M.; Ruiz, P. B.; Ribelles, J. L. G.; Palou, E. C.; Garcia, J. C. M., Response of human chondrocytes to a non-uniform distribution of hydrophilic domains on poly (ethyl acrylate-co-hydroxyethyl methacrylate) copolymers. *Biomaterials* **2006,** 27, (7), 1003-1012.
39. Lapcik, L.; Lapcik, L.; De Smedt, S.; Demeester, J.; Chabrecek, P., Hyaluronan: Preparation, structure, properties, and applications. *Chem. Rev.* **1998,** 98, (8), 2663-2684.
40. Cowman, M. K.; Matsuoka, S., Experimental approaches to hyaluronan structure. *Carbohydrate Research* **2005,** 340, (5), 791-809.
41. Salmivirta, M.; Lidholt, K.; Lindahl, U., Heparan sulfate: A piece of information. *FASEB J.* **1996,** 10, (11), 1270-1279.
42. Guimond, S.; Maccarana, M.; Olwin, B. B.; Lindahl, U.; Rapraeger, A. C., Activating and inhibitory heparin sequences for FGF-2 (basic FGF) - distinct requirements for FGF-1, FGF-2, and FGF-4. *Journal of Biological Chemistry* **1993,** 268, (32), 23906-23914.
43. Zhao, B. H.; Katagiri, T.; Toyoda, H.; Takada, T.; Yanai, T.; Fukuda, T.; Chung, U. I.; Koike, T.; Takaoka, K.; Kamijo, R., Heparin potentiates the in vivo ectopic bone formation induced by bone morphogenetic protein-2. *Journal of Biological Chemistry* **2006,** 281, (32), 23246-23253.
44. Hu, S. G.; Jou, C. H.; Yang, M. C., Surface grafting of polyester fiber with chitosan and the antibacterial activity of pathogenic bacteria. *Journal of Applied Polymer Science* **2002,** 86, (12), 2977-2983.

45. Suh, J. K. F.; Matthew, H. W. T., Application of chitosan-based polysaccharide biomaterials in cartilage tissue engineering: a review. *Biomaterials* **2000,** 21, (24), 2589-2598.
46. Li, J. L.; Pan, J. L.; Zhang, L. G.; Guo, X. J.; Yu, Y. T., Culture of primary rat hepatocytes within porous chitosan scaffolds. *Journal of Biomedical Materials Research Part A* **2003,** 67A, (3), 938-943.
47. Liu, X. F.; Guan, Y. L.; Yang, D. Z.; Li, Z.; De Yao, K., Antibacterial action of chitosan and carboxymethylated chitosan. *Journal of Applied Polymer Science* **2001,** 79, (7), 1324-1335.
48. Fu, J. H.; Ji, J.; Yuan, W. Y.; Shen, J. C., Construction of anti-adhesive and antibacterial multilayer films via layer-by-layer assembly of heparin and chitosan. *Biomaterials* **2005,** 26, (33), 6684-6692.
49. Richert, L.; Lavalle, P.; Payan, E.; Shu, X. Z.; Prestwich, G. D.; Stoltz, J. F.; Schaaf, P.; Voegel, J. C.; Picart, C., Layer by layer buildup of polysaccharide films: Physical chemistry and cellular adhesion aspects. *Langmuir* **2004,** 20, (2), 448-458.
50. Boddohi, S.; Moore, N.; Johnson, P. A.; Kipper, M. J., Polysaccharide-based polyelectrolyte complex nanoparticles from chitosan, heparin, and hyaluronan. *Biomacromolecules* **2009,** 10, 1402-1409.
51. Jordan, C. E.; Frey, B. L.; Kornguth, S.; Corn, R. M., Characterization of poly-L-Lysine adsorption onto alkanethiol-modified gold surfaces with polarization-modulation Fourier-transform infrared-spectroscopy and surface-plasmon resonance measurements. *Langmuir* **1994,** 10, (10), 3642-3648.
52. Bain, C. D.; Evall, J.; Whitesides, G. M., Formation of monolayers by the coadsorption of thiols on gold - variation in the head group, tail group, and solvent. *Journal of the American Chemical Society* **1989,** 111, (18), 7155-7164.
53. Bain, C. D.; Troughton, E. B.; Tao, Y. T.; Evall, J.; Whitesides, G. M.; Nuzzo, R. G., Formation of monolayer films by the spontaneous assembly of organic thiols from solution onto gold. *Journal of the American Chemical Society* **1989,** 111, (1), 321-335.
54. Sauerbrey, G., Verwendung Von Schwingquarzen Zur Wagung Dunner Schichten Und Zur Mikrowagung. *Zeitschrift Fur Physik* **1959,** 155, (2), 206-222.
55. Voinova, M. V.; Rodahl, M.; Jonson, M.; Kasemo, B., Viscoelastic acoustic response of layered polymer films at fluid-solid interfaces: Continuum mechanics approach. *Phys. Scr.* **1999,** 59, (5), 391-396.
56. McCurdy, P. R.; Sturgess, L. J.; Kohli, S.; Fisher, E. R., Investigation of the PECVD TiO2-Si(100) interface. *Applied Surface Science* **2004,** 233, (1-4), 69-79.
57. Methivier, C.; Beccard, B.; Pradier, C. M., *In situ* analysis of a mercaptoundecanoic acid layer on gold in liquid phase, by PM-IRAS. Evidence for chemical changes with the solvent. *Langmuir* **2003,** 19, (21), 8807-8812.
58. Barth, A.; Zscherp, C., What vibrations tell us about proteins. *Quarterly Reviews of Biophysics* **2002,** 35, (4), 369-430.
59. Amarasekara, A. S.; Opoku, G.; Qiu, X. D.; Doctor, V., Effect of oversulfation on the chemical and biological properties of chondroitin-6-sulfate. *Carbohydrate Polymers* **2007,** 68, (1), 116-121.

Chapter 7

Conclusions

7.1 Conclusions

The work reported in this dissertation has contributed to understanding the physical chemistry and polyelectrolyte behavior of an important class of biological macromolecules in different nanostructures, including polyelectrolyte multilayers (PEMs), polyelectrolyte complex nanoparticle (PCNs), and PCN-containing PEMs of various compositions. These polyelectrolytes were chosen based on their biocompatibility and biological functionality. Engineering nanostructured polyelectrolytes could provide valuable tools to characterize biological responses governed by biochemical and biomechanical functionalities organized at the nanoscale.

The objectives accomplished by this work are:

Objective 1. Engineer polysaccahride-based PEMs using chitosan, heparin, and hyaluronan by varying the processing conditions.

Objective 2. Experimental investigation of the solution behavior of polysaccharides.

Objective 3. Develop a method to make and tune PCNs in different charge mixing ratios with two different systems: chitosan-heparin (chi-hep) and chitosan-hyaluronan (chi-ha).

Objective 4. Tailor morphology and composition of different surface coatings with PEMs and PCNs.

For Objective 1, results demonstrate the formation of chi-hep PEMs and thickness obtained at different values of pH ranging from 4.6 to 5.8 in 0.1, 0.2, 0.5 M buffer by *in situ* Fourier-transform surface plasmon resonance (FT-SPR). Oppositely charged polyelectrolytes were successfully deposited on modified gold surfaces. We confirmed that the layer-by-layer (LBL) technique can be used to tune the nanoscale structure of chi-hep PEMs by controlling pH and ionic strength. The thickness of the PEMs increased with increasing pH in all three ionic strengths. Buffer ionic strength changed the range of thickness accessible in all conditions. At 0.2 M buffer, a broader range of thickness was observed, and at 0.5 M buffer, a narrower range of thickness was obtained, due to the screening of the electrostatic interactions. Ellipsometry data also confirmed the trend for thickness increase for different conditions. X-ray photoelectron spectroscopy (XPS) provided information about the sulfur and nitrogen content of the films. The relative amount of these two atoms was then used to determine the PEM composition. While the pH of the buffer solution provided a means of controlling the PEM thickness, the composition of the PEMs was more sensitive to buffer ionic strength. High resolution XPS spectra also provided information about how the amine groups from chitosan interact with the sulfate groups from heparin. Chi-ha PEMs were also reproducibly constructed at different values of pH ranging from 4.6 to 5.8 in 0.1, 0.2, 0.5 M buffer by *in situ* FT-SPR. Comparison of these PEM formation experiments to the solution conformation of the polyelectrolytes (studied in Chapter 4) reveals how the solution properties affect both solution conformation and PEM assembly.

For Objective 2, the conformation of individual polyelectrolytes was characterized in solution. In Chapter 4, some physical properties of chitosan, heparin, and hyaluronan were evaluated. Conformation of the polyelectrolytes in solution was characterized by determining the hydrodynamic radius (R_H) and Mark-Houwink exponent (a), at pH ranging from 4.6 to 5.8 and 0.1, 0.2, and 0.5 M buffer ionic strength. The average hydrodynamic radius for chitosan was 33 nm and average for a was 0.85, which suggests that chitosan behaves as a flexible coil in solution. Heparin had an average R_H of 3.7 nm and average a of 1.0 which verifies that heparin has a stiff coil shape. For HA, the average R_H and a were 62 nm and 0.64 respectively, which indicates that HA behaves more like a large random coil in solution. In this objective, we also concluded that for chi-hep and chi-ha systems at reduced solution ionic strength, pH has a stronger influence over the complexation at surfaces, independent of the solution conformation, while at high ionic strength, the electrostatic screening tends to reduce the influence of electrostatic interactions in both individual polymer chains in solution and between oppositely charged polymer chains at surfaces.

For Objective 3, oppositely charged polyelectrolytes were electrostatically complexed in solution in different charge mixing ratios (n^+/n^-) ranging from 0.08 to 19.2. Two systems of PCNs were studied in this dissertation; chi-hep and chi-ha. A reproducible method was designed for making these PCNs based on the one-shot addition method. The size distributions of the PCN preparations were measured by dynamic light scattering. The zeta potential for each condition was also measured for characterizing the colloidal stability of the PCNs in solution. Results ranged from -18.7 to 31.2 mV. For chi-hep PCNs, mean size for hydrodynamic radius increased when charge mixing ratios

approached 1:1. The mean hydrodynamic radius determined from dynamic light scattering was in the range of 170 to 318 nm for both positively charged and negatively charged particles for both polyelectrolyte pairs studied.

Morphology of PCNs was also investigated by scanning electron microscopy by adsorbing the PCNs to metal surfaces. When deposited and dried on surfaces, PCNs are distributed non-homogeneously on the surface, and in conditions further from the 1:1 ratio, particles were more colloidally stable than close to the 1:1 ratio. Aggregates were observed on conditions with mixing ratios near 1:1 point.

For Objective 4, the combination of PCNs in PEMs is described. In Chapter 5, we showed that PCNs could be adsorbed to surfaces, but that the nanoscale features could not be accurately controlled, because the adsorption sometimes lead to aggregation and non-uniform surface coverage. In Chapter 6, we combined PCNs with PEMs as a surface coating to provide more uniform control over the geometry and composition at the nanoscale. Eight different types of surface coatings were characterized. The goal of this chapter was to make chi-ha PEMs as a multilayer surface and decorate the surfaces with chi-hep PCNs. PCNs were successfully deposited on PEMs and quartz crystal microbalance with dissipation experiments were used to characterize the adsorption. Atomic force microscopy and scanning electron microscopy were used to describe the topographic features of PEMs with like-charged and oppositely charged PCNs adsorbed. We also characterized surfaces with PCNs embedded in the PEMs. The nanostructured features introduced by adsorption of the PCNs were approximately 15-30 nm in height and 80-250 nm in diameter. The adsorption of both positively and negatively charged

PCNs was confirmed by XPS and polarization modulation infrared reflection absorption spectroscopy.

We comprehensively investigated the engineering of nanostructured polysaccharides. The assembly of nanostructures from three biomedically relevant, naturally derived polysaccharides was studied at different processing conditions. We demonstrated that the physical chemistry of these polysaccharides can be used to tune the composition, morphology, and size of different nanostructures of polysaccharide complexes on surfaces and in solution. Development of reproducible methods of engineering these nanostructures can be a successful route toward application of nanoscale polysaccharides for a variety of biomaterials. Tuning the nanostructure of polysaccharide-based materials will enable detailed studies of their biological activities and developments of new materials for tissue engineering and drug delivery.

7.2 Possible Future Studies

Future studies in this field should include development of a theoretical model for PEM assembly and PCN formation in different processing conditions for polysaccharide-based polyelectrolytes. We have already investigated these phenomena experimentally, and obtained detailed information about PEM and PCN physical chemistry, shape, size, morphology, and composition. We have investigated how these characteristics are influenced by buffer ionic strength and pH. Other researchers have investigated the effects of polyelectrolyte molecular weight. This information could be used to develop and validate detailed models of the electrostatic interactions that govern polyelectrolyte complexation. Such models should include effects due to counterion interactions and

charge screening. For example, the Debye length for electrostatic screening could be used as a predictor of how solution properties influence polyelectrolyte complexation. This might require investigation of a broader range of solution conditions (ion type, ionic strength, solvent quality, etc.), and polyelectrolyte chemistry (pK_a, charge density, flexibility, etc.). Such theoretical models might provide detailed predictions about complex formation, and might provide a framework for interpreting future experimental results.

Models of polyelectrolyte complexation should also account for the kinetics of different complexation mechanisms. Particularly during formation of PCN, there are likely multiple phenomena occurring simultaneously (e.g. nucleation of primary complexes, aggregation of these complexes to form nanoparticles, and rearrangement of polymer chains within nanoparticles). The relative rates of these processes may have a large effect on the final structure of individual nanoparticles and the final distribution of nanoparticle size and composition. *In situ* scattering methods could be used to monitor the PCN formation process to parameterize models of the PCN formation with the necessary rate coefficients.

In this work, both *in situ* and *ex situ* techniques were used to characterize the formation of PEMs. However, all of the *ex situ* experiments (XPS, SEM, ellipsometry, and AFM) were performed on films that had been dried. Comparison of these *ex situ* characterizations to the *in situ* characterizations has raised some questions, particularly about the structure of the PCN-containing PEMs. It is not clear whether the PCNs in the PEMs are close enough together to influence the adsorption of neighboring PCNs in the hydrated state, and the collapse of PCNs is due to adsorption to the PEMs or due to

drying. *In situ* AFM experiments conducted in a liquid cell could provide valuable information about how the PCNs are interacting with the surface and with neighboring PCNs in the hydrated state.

Finally, as indicated in Chapter 2, researchers are just beginning to understand how the nanostructure of polysaccharide-based materials influences the response of biological systems to these materials. Future experimental investigations can build on this work by using PEMs and PCNs to precisely tune the composition and morphology of polysaccharides at the nanometer length scale, to study how these features influence cell and tissue responses. These materials might be used to stabilize deliver therapeutic molecules (drugs, proteins, and DNA) with controlled release profiles from surfaces. They might also be used to develop nanostructured materials which features that mimic the features of biological nanostructures.

Appendix 1

Supporting Information for:

Polyelectrolyte Multilayer Assembly as a Function of pH and Ionic Strength Using the Polysaccharides Chitosan and Heparin

PEM Composition from XPS Spectra

The ratio of sulfur to nitrogen in pure heparin is assumed to be 0.751:0.249 (according to the supplier's analysis). The fraction of the nitrogen in the multilayer associated with heparin, $x_{N,Heparin}$, is computed from[1]

$$x_{N,Heparin} = \left(\frac{S_{PEM}}{S_{PEM} + N_{PEM}}\right)\left(\frac{1}{S_{Heparin}}\right)N_{Heparin} \qquad \textbf{(S.1)}$$

where S_{PEM} and N_{PEM} are the atom fractions of sulfur and nitrogen in the PEM, respectively, on a sulfur plus nitrogen basis. S_{PEM} includes only the contribution from the peak centered at 169 eV, to eliminate the contribution from sulfur in the MUA SAM (the peak centered at 164.8 eV). $S_{Heparin}$ and $N_{Heparin}$ are the atom fractions of sulfur and nitrogen in heparin (0.751 and 0.249), respectively, on a total sulfur plus nitrogen basis.

[1] The first term on the right-hand side of equation 1 is equal to $\frac{S/N}{S/N+1}$, where *S/N* is the sulfur to nitrogen atom ratio reported in Table 3.3 of the manuscript.

The balance of the nitrogen is associated with chitosan; so the fraction of nitrogen associated with chitosan in the multilayer, $x_{N,Chitosan}$ is then

$$x_{N,Chitosan} = N_{PEM} - x_{N,Heparin} \quad \textbf{(S.2)}$$

Where N_{PEM} is the fraction of nitrogen in the PEM (on a sulfur plus nitrogen basis). The ratio of heparin to chitosan in the PEM can then be computed on a saccharide basis, recognizing that there is one nitrogen per saccharide residue in chitosan and one nitrogen for every two saccharide residues in heparin (Figure 3.1). Thus,

$$\frac{Heparin}{Chitosan} = \frac{2x_{N,Heparin}}{x_{N,Chitosan}} \quad \textbf{(S.3)}$$

This ratio of heparin to chitosan is reported in Table 3.3 of the manuscript.

Appendix 2

Supporting Information for:

Polysaccharide-based Polyelectrolyte Complex Nanoparticles from Chitosan, Heparin, and Hyaluronan

The dynamic light scattering instrument measures the intensity autocorrelation function, $g^{(2)}(\tau)$, of the scattered radiation.

$$g^{(2)}(\tau) = \frac{\langle I(t) * I(t+\tau) \rangle}{\langle I(t)^2 \rangle} \qquad \textbf{(SI.1)}$$

From the intensity autocorrelation function, the electric field autocorrelation function, $g^{(1)}(\tau)$, can be obtained according to the Seigert relationship.[1]

$$g^{(1)}(\tau) = \left| \frac{g^{(2)}(\tau) - 1}{B} \right|^{0.5} \qquad \textbf{(SI.2)}$$

where B is a parameter that depends upon the number of coherence volumes in the sample and can be obtained from the limit of $g^{(2)}(\tau)$ as τ approaches 0. DLS correlation functions were analyzed by two separate methods that are commonly used to interpret light scattering of polymer solutions and colloids.

First, the regularization algorithm in the Dynamics software package (Wyatt, Version 6.10.1.2) was used to determine relaxation rates, Γ_i, corresponding to the diffusion of nanoparticles (and, potentially, other modes of relaxation in the samples). The regularization algorithm is a regression method for obtaining a distribution of relaxation rates that fit the field autocorrelation function to a superposition of multiple relaxations according to

$$g^{(1)}(\tau) = \sum_i w_i \exp(-\Gamma_i \tau)] \qquad \textbf{(SI.3)}$$

The relative intensity weight of the i^{th} relaxation rate, Γ_i, is w_i. ($\Sigma_i w_i = 1.$) The regularization algorithm makes no assumptions regarding the shape of the distribution of relaxation rates. For quasi-elastic light scattering from single particles the Γ_i are related to an observed translational diffusion coefficient for particles, D_i, by the scattering vector, q ($q = (4\pi n_0/\lambda)\sin(\theta/2)$),

$$\Gamma_i = D_i q^2 \qquad \textbf{(SI.4)}$$

where n_0 is the refractive index of dispersant, λ is the wavelength of the scattered radiation in a vacuum, and θ is the scattering angle (90°). Finally the hydrodynamic radii (R_H) of the particles corresponding to each relaxation rate is calculated using the Stokes-Einstein relationship.

$$R_{H,i} = \frac{k_B T}{6\pi\eta D_i} \qquad \textbf{(SI.5)}$$

The use of equation SI.3 is particularly useful when samples are multimodal and meaningful information can be extracted from the presence of multiple relaxation rates. However, use of equation SI.3 is an ill-posed problem in that the number of relaxation rates required to accurately describe the system is not known, so the solution is only unique when there are no experimental uncertainties in the data and there are no rounding errors in the fitting algorithm.[1] This may result in peaks in the distribution of relaxation rates that have no physical significance. In our experiments, five replicate measurements were made for each sample. For each sample, the distribution of relaxation rates contained a primary peak (present in all five replicate measurements and generally accounting for > 90% of the total distribution) that was attributed to the diffusion of the PCN. Peaks in the relaxation rate distribution that represented faster or slower rates generally accounted for less than 10 % of the distribution of relaxation rates for all samples. These secondary peaks were often present, but did not appear in all five replicate measurements for any of the formulations.

Second, field autocorrelation functions, $g^{(1)}(\tau)$, were also fit by regression using a modified Levenberg-Marquardt algorithm to a function containing a "fast" single exponential followed by a "slow" stretched exponential (Williams-Watts equation) of the form.

$$g^{(1)}(\tau) = A\exp(\Gamma_f \tau) + (1-A)\exp\left[-(\Gamma_s \tau)^{\beta}\right] \qquad \textbf{(SI.6)}$$

In equation SI.6 Γ_f and Γ_s represent the characteristic fast and slow relaxation rates, respectively, and the parameter β is a measure of the breadth of the distribution of

relaxation rates for the stretched exponential component. The fitting was performed using the function fitting operation in the Igor Pro software package with the default convergence criterion (< 0.1 % change in χ^2 between successive iterations). Equation SI.6 has been found to be a good description of DLS for amphiphillic polymers in aqueous solutions in general, and for polysaccharides in particular, which are capable of interparticle interactions that result in a coupling of the individual particle dynamics to the surroundings.[1-6] In the semidilute regime, the values of A and β both decrease as the coupling among individual particles' motions becomes stronger, approaching 0 at the gel point, where the autocorrelation function is no longer described by equation SI.6.[4, 6] Thus, A and β are measures of the relative strength of particle-particle interactions.

There are important differences between these two methods for interpreting the DLS data which make these two models complementary. While the regularization method (equation SI.3) requires a large number of adjustable parameters (two parameters for each of an unknown number relaxation rates), equation SI.6 describes the field autocorrelation function with only four adjustable parameters. Typically, each of the relaxation rates obtained from equation SI.3 is assigned to a diffusive mode, corresponding to a particle size, while equation SI.6 can be used to provide a different interpretation of slower relaxations (e.g., particle-particle interactions). If equation SI.6 reveals significant coupling among particles' relaxations, the slower relaxation modes observed using equation SI.3 can be interpreted differently. Finally, equation SI.6 is not capable of effectively dealing with multimodal distributions; it assumes that there is only one characteristic diffusive mode in the sample.

The results from the model fit to equation SI.6 for the chi-hep and chi-ha nanoparticle formulations are shown in Tables SI.1 and SI.2, respectively.

Table SI.1. Parameters from fits to equation SI.6 for chi-hep PCN at each charge mixing ratio.

Charge mixing ratio (+/-)	A^a	Γ_f $(s^{-1})^a$	β^a
17.55	0.68	216	0.41
10.53	0.62	205	0.45
4.68	0.66	192	0.57
2.73	0.65	163	0.46
1.75	0.62	152	0.43
0.78	-	-	-
0.50	0.43	191	0.64
0.29	0.58	251	0.58
0.13	0.60	272	0.47
0.08	0.73	287	0.45

[a]The uncertainties on the parameter Γ_f are all less than 2 % of the parameter value, and the uncertainties on the values of A and β are all less than 6 % of the parameter value.

Table SI.2. Parameters from fits to equation SI.6, for chi-ha PCN at each charge mixing ratio.

Charge mixing ratio (+/-)	A^a	Γ_f $(s^{-1})^a$	β^a
19.2	-	-	-
8.52	0.80	171	0.35
3.19	0.87	213	0.44
1.4	-	-	-
0.53	0.88	258	0.41
0.23	0.77	249	0.25

[a]The uncertainties on the parameter Γ_f are all less than 2 % of the parameter value, and the uncertainties on the values of A and β are all less than 6 % of the parameter value.

References

1. Stepanek, P., Dynamic light scattering: The method and some applications. In Brown; Wyn, Eds. Oxford university press Inc.: New York, **1993**.
2. Nystrom, B.; Walderhaug, H.; Hansen, F. K., Dynamic crossover effects observed in solutions of a hydrophobically associating water-soluble polymer. *Journal of Physical Chemistry* **1993,** 97, (29), 7743-7752.
3. Kjoniksen, A. L.; Baldursdottir, S. G.; Nystrom, B., Characterization of riboflavin-photosensitized changes in aqueous solutions of alginate by dynamic light scattering. *Macromolecular Bioscience* **2004,** 4, (2), 76-83.
4. Kita, R.; Takahashi, A.; Kaibara, M.; Kubota, K., Formation of fibrin gel in fibrinogen-thrombin system: Static and dynamic light scattering study. *Biomacromolecules* **2002,** 3, (5), 1013-1020.
5. Horkay, F.; Basser, P. J.; Hecht, A. M.; Geissler, E., Gel-like behavior in aggrecan assemblies. *Journal of Chemical Physics* **2008,** 128, (13).
6. Ngai, K. L., Dynamics of semidilute solutions of polymers and associating polymers. *Advances in Colloid and Interface Science* **1996,** 64, 1-43.

Biographical Sketch

Soheil Boddohi was born in Tehran, Iran in August 19, 1983. He earned his B.S. in June 2006 in chemical engineering from Sharif University of Technology. He worked on improving refinery design for flare gas pollution prevention for his B.S. theses. Soheil also worked as a process engineer intern in Sadre Sanat Consulting Company from May 2004 – July 2004. Soheil joined the Department of Chemical and Biological Engineering at Colorado State University as a Graduate Research Assistant, in August 2006. Here, he earned his Ph.D. in chemical engineering, awarded in December 2009.

Journal Publications

- **S. Boddohi**, M.J. Kipper, "Engineering nanoassemblies of polysaccharides." *Advanced Materials*, 2009 (Submitted).
- **S. Boddohi**, J. Almodóvar, H. Zhang, P.A. Johnson, and M.J. Kipper," Fabrication and characterization of polysaccharide-based nanostructured surfaces prepared with polyelectrolyte complex nanoparticles." *Journal of colloids and surfaces B*, 2009 (submitted).
- H.J. Park, J.T. McConnell, **S. Boddohi**, M.J. Kipper, and P.A. Johnson, " Synthesis and characterization of Glucose Oxidase (EC1.1.3.4) immobilized on three different size magnetic nanoparticles for applications in biocatalysis." *Journal of Molecular Catalysis B: Enzymatic*, 2009 (Submitted).
- **S. Boddohi**, N. Moore, P.A. Johnson, M.J. Kipper, "Size and composition of polysaccharide-based polyelectrolyte complex nanoparticles at different charge molar ratios." *Biomacromolecules,* 10, 1402-1409, 2009
- **S. Boddohi**, C.E. Killingsworth, M.J. Kipper, "Polyelectrolyte multilayer assembly as a function of pH and ionic strength using the polysaccharides chitosan and heparin." *Biomacromolecules,* 9, 2021-2028, 2008.

Proceedings Papers

- **S. Boddohi**, J. Almodóvar, H. Zhang, P.A. Johnson, and M.J. Kipper, "Nanoassembly of polysaccharide based polyelectrolytes: Tuning morphology and size" *Proceedings of the 38th Annual Biochemical Engineering Symposium*, 50-56, 2009

- **S. Boddohi**, S. Yonemura, M.J. Kipper, "Polysaccharides with tailored nanostructures for biomedical applications." *Polymer Preprints,* 50(1), 331-332 2009.

Conference Presentation (* denotes speaker)

- **S. Boddohi***, J. Almodovar, P.A. Johnson, M.J. Kipper, "Nanostructured polysaccharide-based surface coatings: Tailored morphology and chemistry." *Annual AICHE meeting*, Nashville, TN, November 9, 2009.

- **S. Boddohi***, J. Almodovar, P.A. Johnson, M.J. Kipper, "Nanoassembly of polysaccharide-based polyelectrolytes: Tuning morphology and size." *38th Annual Biochemical Engineering Symposium*, Pingree Park, CO, May 23, 2009

- **S. Boddohi***, M.J. Kipper, "Exploring the size and composition of polysaccharide-based polyelectrolyte complex nanoparticles at different charge molar ratios." *Annual AICHE meeting*, Philadelphia, PA, November 20, 2008.

- C. Killingsworth*, **S. Boddohi**, and M.J. Kipper, "Tuning Polyelectrolyte Behavior of Polysaccharides at Surfaces and in Solution," *2008 AIChE Rocky Mountain Regional Conference*, Socorro, NM, March 8, 2008.

- **S. Boddohi***, S. Yonemura, M.J. Kipper, "Characterization of polyelectrolyte behavior of the polysaccharides chitosan, heparin, and hyaluronan, by light scattering and viscometry". *National APS meeting*, New Orleans, LA, March 10, 2008

- **S. Boddohi***, C. Killingsworth, and M.J. Kipper, "Engineering polyelectrolyte multilayer structure at the nanometer length scale by tuning polymer solution conformation". *National APS meeting*, New Orleans, LA, March 13, 2008

- **S. Boddohi***, C. Killingsworth, and M.J. Kipper, "Nanostructured Glycosaminoglycan-based Polyelectrolyte Multilayers using the Polyanion Heparin and the Polycation Chitosan." *Annual AIChE Meeting*, Salt Lake City, UT, November 7, 2007.

- C. E. Killingsworth*, **S. Boddohi**, and M.J. Kipper, "Properties of Charged Polysaccharides in Solution by Gel Permeation Chromatography." *Annual AIChE Meeting*, Salt Lake City, UT, November 5, 2007.

- **S. Boddohi*** and M.J. Kipper, "pH-Dependent Thickness Behavior of Nanostructured Polyelectrolyte Multilayers using Heparin and Chitosan." *2007 Joint ACS/AIChE Rocky Mountain Regional Meeting*, Denver, CO, August 31, 2007.

Academic Experience

- **2009 Teaching Assistant,** "Process Control and Instrumentation" Department of Chemical and Biological Engineering, Colorado State University.
- **2008 Teaching Assistant,** "Mass Transfer and Separation Laboratory" Department of Chemical and Biological Engineering, Colorado State University.
- **2008 Teaching Assistant**, "Thermodynamic Process Analysis" Department of Chemical and Biological Engineering, Colorado State University.
- **2007 Teaching Assistant,** "Mass Transfer and Separation Laboratory" Department of Chemical and Biological Engineering, Colorado State University.
- **2007 Teaching Assistant**, "Introduction to Chemical Process Fundamentals and Design" Department of Chemical and Biological Engineering, Colorado State University.